

# ANALYSIS OF SPATIAL PATTERNS IN THE PROBLEM OF BIOLOGICAL INVASION

by

WENXIN ZHANG

A thesis submitted to  
The University of Birmingham  
for the degree of  
DOCTOR OF PHILOSOPHY

School of Mathematics  
College of Engineering and Physical Sciences  
The University of Birmingham  
May 2021

UNIVERSITY OF  
BIRMINGHAM

**University of Birmingham Research Archive**

**e-theses repository**

This unpublished thesis/dissertation is copyright of the author and/or third parties. The intellectual property rights of the author or third parties in respect of this work are as defined by The Copyright Designs and Patents Act 1988 or as modified by any successor legislation.

Any use made of information contained in this thesis/dissertation must be in accordance with that legislation and must be properly acknowledged. Further distribution or reproduction in any format is prohibited without the permission of the copyright holder.

## **Abstract**

Biological invasion of alien species usually has an adverse impact on ecology as alien species are often regarded as harmful species to the local ecosystems. A comprehensive understanding of spatial patterns of species spread during biological invasion is needed for efficient monitoring and control of harmful alien pests. Various growth-dispersal-type models of population dynamics predict that invasive species spread can follow two qualitatively different scenarios: propagation of a continuous population front and ‘no-front’ patchy invasion. Distinguishing between those two types of spatial pattern is important as patchy invasion may require a different approach to monitoring and control. However, a mathematical theory of patchy invasion is still missing and it remains unclear which parameter values in the underlying model result in the formation of patchy spatial patterns and how much this dynamical regime is different from the continuous front propagation.

In this thesis we address the problem of spatial patterns recognition in biological invasion in terms of two biologically meaningful mathematical models. We employ several topological characteristics of spatial pattern to investigate various spatial density distributions. The topology of continuous front and patchy spatial structures will be carefully compared and conclusions about sensitivity and ‘topological stability’ of those spatial patterns will be derived.

## LIST OF PUBLICATIONS

1. N.B.Petrovskaya, S.V. Petrovskii, W. Zhang. *Patchy, not Patchy, or How Much Patchy? Classification of Spatial Patterns Appearing in a Model of Biological Invasion*. Math. Model. Nat. Phenom., 2017, vol.12, pp. 208-225
2. N.B.Petrovskaya, W. Zhang. *Accurate Recognition of Spatial Patterns Arising in Spatio-Temporal Dynamics of Invasive Species*. in: M.Aguiar, C.Braumann, B.Kooi, A.Pugliese, N.Stollenwerk, E.Venturino (eds.), Current Trends in Dynamical Systems in Biology and Natural Sciences, SEMA-SIMAI Springer Series 21, 2020, pp.19-43.
3. N.B.Petrovskaya, W. Zhang. *When Seeing Is Not Believing: Comparative Study of Various Spatial Distributions of Invasive Species*. Journal of Theoretical Biology, 2020, 488: 110141

# CONTENTS

|          |   |           |
|----------|---|-----------|
| <b>1</b> | <b>Introduction</b>   | <b>1</b>  |
| <b>2</b> | <b>Non-spatial models of biological invasion</b>                                  | <b>12</b> |
| 2.1      | Continuous-time models . . . . .  | 12        |
| 2.1.1    | Logistic growth . . . . .   | 14        |
| 2.1.2    | The Allee effect . . . . .  | 16        |
| 2.1.3    | Continuous-time models: multiple species system . . . . .                         | 18        |
| 2.2      | Discrete-time models . . . . .  | 23        |
| 2.2.1    | General multiple species models . . . . .   | 25        |
| 2.2.2    | Multiple species models affected by the Allee effect . . . . .                    | 27        |
| <b>3</b> | <b>Spatial patterns of biological invasion of stage-structured species</b>        | <b>32</b> |
| 3.1      | Integro-difference model with Allee effect . . . . .                              | 32        |
| 3.2      | Classification of dispersal kernels . . . . .                                     | 34        |
| 3.3      | Initial conditions and boundary conditions . . . . .                              | 36        |
| 3.4      | Numerical simulation: the FFT method . . . . .                                    | 37        |
| 3.5      | Numerical validation . . . . .  | 40        |
| <b>4</b> | <b>Simulation results for stage-structured population with short-distance and</b> |           |

|   |            |
|---|------------|
| <b>long-distance dispersal</b>  | <b>46</b>  |
| 4.1 Simulation results for the Gaussian dispersal kernel . . . . .                | 49         |
| 4.2 Simulation results for Cauchy dispersal kernel . . . . .                      | 51         |
| <b>5 Classifications of spatial patterns</b>                                      | <b>56</b>  |
| 5.1 Structure of parametric plane . . . . .                                       | 57         |
| 5.2 Topological indices . . . . .   | 59         |
| 5.2.1 The number of objects . . . . .   | 60         |
| 5.2.2 The fragmentation rate and the density of objects . . . . .                 | 62         |
| <b>6 Sensitivity of spatial patterns to the parameters of monitoring protocol</b> | <b>69</b>  |
| 6.1 Sensitivity of spatial patterns to the cutoff value . . . . .                 | 69         |
| 6.2 Reconstruction of spatial patterns from sparse data . . . . .                 | 73         |
| <b>7 Spatial patterns arising in reaction-diffusion models</b>                    | <b>81</b>  |
| 7.1 Model . . . . .   | 82         |
| 7.2 Numerical approach . . . . .  | 85         |
| 7.3 Stability analysis . . . . .  | 86         |
| 7.4 Topological indices of spatial patterns . . . . .                             | 90         |
| 7.4.1 Number of objects and density of objects . . . . .                          | 90         |
| 7.4.2 The Morisita index and the fragmentation rate . . . . .                     | 90         |
| 7.5 Topological stability . . . . .   | 94         |
| 7.6 Topological stability of invasion regimes . . . . .                           | 98         |
| 7.7 Topological indices of field data: gypsy moth in the United States . . . . .  | 103        |
| <b>8 Conclusion and discussion</b>  | <b>110</b> |

|                        |     |
|------------------------|-----|
| Appendix: Matlab codes | 116 |
| List of References     | 121 |

## CHAPTER 1

# INTRODUCTION

When living creatures are brought to a new environment where they are not native, they can begin to propagate and disperse. This phenomenon is called biological invasion, and the species are called alien (exotic) species, or invasive species. An invasive species can be an animal, plant or fungus, all of which usually spread quickly after being introduced because of the absence of natural enemies in the new environment. Biological invasion is regarded as one of the major threats to ecosystems around the world [93, 96] as it often has a significant negative effect on agriculture, forestry, fishery, etc., with direct and indirect economic losses being in the order of hundreds of billions of dollars [90, 73]. It is therefore essential to understand the underlying mechanism of biological invasion as this can enable harmful invasive species to be effectively managed and controlled.

One example of biological invasion is the Japanese beetle (*Popillia japonica*) in North America. This species is native to Japan and is not very destructive in its own country as it has natural predators that control its propagation. However, in North America it is a harmful invasive species for about 200 species of plants, such as rose bushes, grapes, birch trees, linden trees, and many others [39]. The ways that the Japanese beetle disperses includes flying and



human-assisted dispersal.

The Japanese beetle was firstly discovered in the United States (US) in a nursery near Riverton, New Jersey in 1916 when just only a dozen were found. By 1920, the infested area was estimated to be 120 km<sup>2</sup> and the infested area increased to 700 km<sup>2</sup> in 1922. In the summer of 1923, the infested area by the Japanese beetle was estimated to be 1,800km<sup>2</sup> and the beetles inflicted a lot of damage on the local forestry and agriculture [11]. In less than 30 years, the Japanese beetle invaded the whole of the eastern US (see Fig. 1.1), while it started to spread into Canada by the late 1930s [39]. As of 2015, only nine western US states were considered free of Japanese beetles [91].

Another example is the muskrat (*Ondatra zibethicus*) (Fig. 1.2). The muskrat is a native species in the US, and was introduced to Europe and Asia as an invasive species. These animals mostly inhabit wetlands where they have an important effect on the ecology of wetlands because they contribute to the abundance of the plant species by selectively removing their preferred plant types [29]. The muskrat is also a resource of food and fur for humans so it is not always

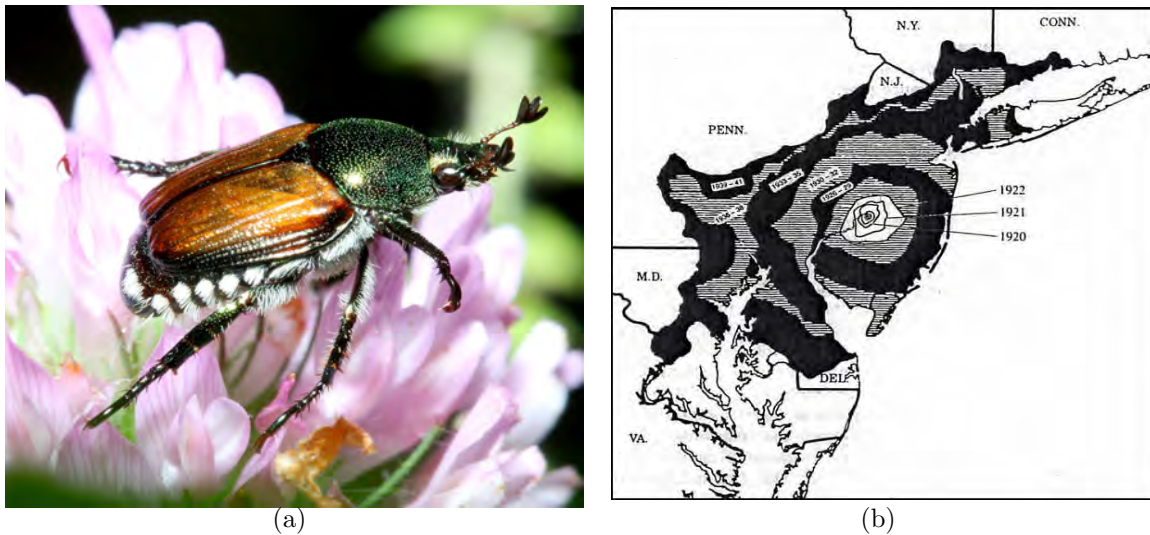


Figure 1.1: (a) Photograph of Japanese beetle and (b) Maps of Japanese beetle distribution in the US [39]

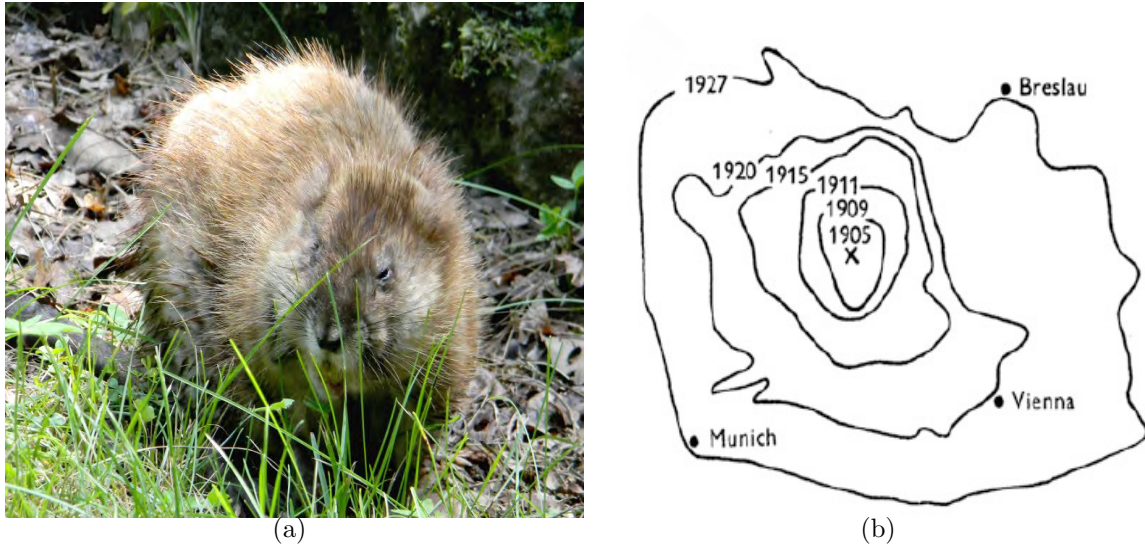


Figure 1.2: (a) Photograph of a muskrat; (b) Maps of muskrat invasion in eastern Europe [39].

considered a harmful invasive species. However, in some European countries, such as Belgium, France, and the Netherlands, the muskrat is regarded as an invasive pest, as its burrowing damages the dams and dykes that are used to prevent flooding in these low-lying countries [58]. Muskrats were brought to Dobrisch in Bohemia by Prince Colloredo-Mansfeld in 1905. Between 1905 and 1914, the radius of expansion amounted to between four and 30 km yearly and by the end of this period, the whole of Bohemia was colonised by the muskrat. By 1914, the total number of muskrats in Bohemia was estimated at two million. Further, in 1923 and 1924, the muskrat migration in Bavaria was said to have increased by 50–70 km annually [51].

There are four clearly distinguishable stages in biological invasion: introduction, establishment, spread and impact [85, 79]. At the introduction stage, non-native species are introduced locally and this transport is often as a result of human activity rather than natural forces. If the transport of individuals is caused by natural forces, then the movement is called dispersal. Introduction can occur deliberately or accidentally. For instance, horticultural trade and the pet trade are examples of deliberate introduction and it is estimated that approximately 60%

of naturalised plants in the US were deliberately introduced [47]. Meanwhile, accidental introduction can occur through seed contaminants, shipping materials and ballast water discharge. Once a species has been introduced to a new environment, it will become established locally if it survives, but the establishment of species is not always successful. Indeed, only 10% of introduced species become established [96, 97]. The next stage is spread; if the species survive the establishment stage, the individuals start propagating and spreading. The propagation rate and spread speed of different species vary according to their species traits. The final stage is impact. Biological invasions usually have an adverse impact on ecosystems, e.g. native species may be driven to extinction which may result in considerable economic losses [73]. Therefore, corresponding measures should be taken to control the alien species.

Because of its negative economic and ecological impact, biological invasion has been a focus of intense research for several decades. It is necessary to have a comprehensive understanding of the biological invasion in order to efficiently control and manage the alien species. Common research approaches include data collection, statistical analysis of the data, and mathematical modelling. The latter approach is especially useful as, given the spatial and temporal scales of biological invasion, it can offer considerable savings in the resource required to carefully investigate this phenomenon, while various biological hypotheses can be tested at relatively low cost to reveal the underlying mechanisms of biological invasion [22, 85]. Therefore, there is a need to set up appropriate mathematical models to simulate biological invasion where in our work we are mostly interested in the spatial spread of invasive species.

In 1937, Fisher proposed a diffusion-reaction equation to describe the spatial spread of the mutation among the population [14], this diffusion-reaction equation is known as the Fisher's equation. The Fisher's equation can also be used to describe the process of biological invasion

and conventional studies on biological invasion by Skellam [87], Andow et al. [5], and Dwyer [10] were based on Fisher's results.

Reaction-diffusion models are very popular in the study of biological invasion and a variety of reaction-diffusion models have been comprehensively studied. The KISS (Kierstead, Slobodkin and Skellam) models with linear growth and Fickian diffusion have been used to study the red tide outbreaks [30]. The Fisher's equation with logistic growth and Fickian diffusion [14] has a simple travelling wave solution. In a different context, a single-species PDE of reaction-diffusion type where nonlinear function describing the reaction term has properties consistent with the Allee effect (i.e., a sigmoidal shape), the equation is known as Nagumo equation [55].

Although reaction-diffusion models are useful for studying the spatial population dynamics of alien species, they have some defects in modelling biological invasion. Firstly, reaction-diffusion models are not appropriate for long-distance dispersal as the dispersal is reduced to diffusion so that only short-distance dispersal is considered [81]. In addition, in reaction-diffusion models, it is assumed that population has overlapping generations which means that the population size grows continuously. However, in the real world many species are stage-structured, births occur at regular times, known as breeding seasons. For stage-structured species, another mathematical model based on integro-difference equation was developed by Kot and Schaffer [33], Anderson [4], and Neubert et al. [57].

When the spread stage of biological invasion is investigated, the crucial question concerns the spatial patterns that arise when the invasive species propagates into the space. The seminal results in the theory of biological invasion obtained in [14], [32] and [87] have stated the existence of a continuous population front which separates the invaded area behind the front from the non-invaded area. Their results indicate that a travelling population front exists (Fig. 1.3)

during the biological invasion. The travelling population front is defined as a gradient in the population density which separates the invaded and non-invaded area. In the realistic 2-D case, such a front forms a continuous boundary that separates the invaded and non-invaded areas [5].

Propagation of a population front was a paradigm of biological invasion for several decades [14, 32, 87]. More recently, however, there has been a growing understanding that the invading species can proliferate into space by creating isolated patches or colonies but without forming any continuous population front [67, 86]; see Fig. 1.4. Patchy invasion, as this invasion scenario was eventually named, is a phenomenon of considerable theoretical and practical importance; it has been observed in several field studies [8, 40, 42, 46] and in a variety of different mathematical models [37, 50, 86] including PDEs [24, 53] and, recently, integral-difference equations [77]. However, despite the intense study of patchy invasion in recent years, many questions remain open and a comprehensive understanding is lacking. The mathematical theory of patchy

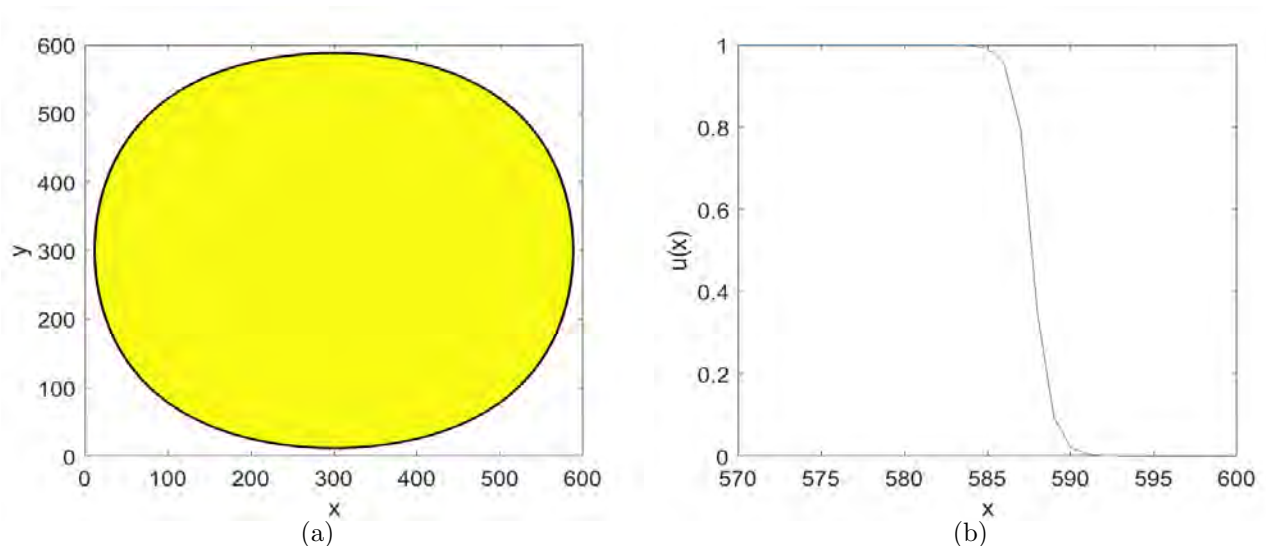


Figure 1.3: (a) Example of a continuous population front in a 2D domain obtained in numerical simulations using a single-species diffusion-reaction model with logistic growth. (b) Cross-sectional version of the population front  $u(x)$  in the  $x$  direction.

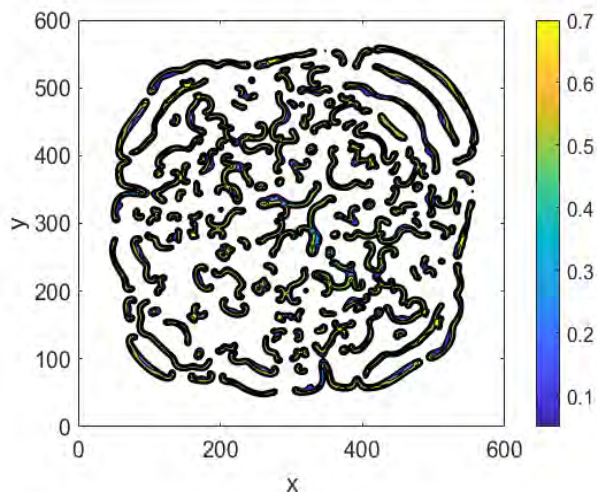


Figure 1.4: Patchy spatial distribution of the density of invasive species obtained as a result of numerical solution of the mathematical model of biological invasion.

invasion is not well developed and the appearance of patchy structures cannot be predicted in advance even in mathematical models that are used to simulate the spatio-temporal dynamics of invasive species. The situation is further exacerbated by the fact that the formation of patchy structures in the wake of a continuous front is possible for many invasion regimes that are generated in simulations, as seen in [24, 64].

Patchy invasion can be attributed to several factors, one of which is that it can occur in particular landscapes such as small islands [98]. Moreover, it can also occur as a result of the influence of predators [50, 67], pathogens [24, 68, 69], or multi-species interactions [8, 54]. In particular, in this thesis we will focus specifically on the patchy invasion arising as a result of inter-species interactions.

One issue that we aim to investigate is whether the scenario of patchy invasion is robust with respect to the mathematical and computational model employed to simulate the spatio-temporal dynamics of the invasive species. Although the previous studies [50, 24, 77] have demonstrated that patchy spatial distribution of the invasive species is not an artifact of a

specific modelling framework, it is still unclear how sensitive the spatial pattern is, e.g. patchy or not, to the dispersal properties of the interacting species. Namely, it is well-known that spread speed can be affected by the properties of the dispersal kernel [4, 33] when integro-difference equations are employed to simulate biological invasion; yet it is still unclear how much the definition of a dispersal kernel may affect the spatial pattern of the invasive species, so this issue will be examined in detail in this work. In particular, one goal of our study is to reveal the effect of the long-distance dispersal (described by fat-tailed dispersal kernels) on the spatial pattern and spread speed of the invasive species.

Another goal of our study is to quantify the patchiness itself. Understanding the topological properties of spatial patterns of alien species spread during biological invasion is a problem of considerable theoretical and practical importance [39, 71]. The question of distinguishing between continuous front and patchy spatial distributions is of particular interest as it is closely related to the problem of monitoring and control of invasive species. On the one hand, timely recognition of patchy invasion regimes is important as its monitoring may require more careful resource allocation than the monitoring of continuous front spatial distributions. The grid of sampling locations used in discontinuous spatial patterns monitoring must be fine enough to capture sufficient information about the population distribution (e.g. see [63, 62]). It has been argued in [63] that patches with the non-zero population density will be partially or completely missed if the distance between sampling locations is greater than the patch size. On the other hand, once a discontinuous spatial pattern has been accurately identified, its control may only require practitioners to deal with the areas occupied by separate density patches and more targeted means of control may therefore be applied to prevent the spatial spread of invasive species.

The importance of accurate classification and quantification of ecological patterns have been acknowledged by scientists since long ago [16, 23] and developing reliable and efficient methods for analysing spatial pattern remains an important stream of research in ecology. Various approaches have been developed in recent decades [43, 78] yet the question of accurate recognition of spatial patterns is still far away from a definitive solution. Given the wealth of spatial patterns arising in the problem of biological invasion, it is difficult to elaborate universal criteria to compare spatial distributions to each other and make conclusions about their similarity. Consider, for example, spatial patterns in Fig. 1.5. Is the spatial pattern in Fig. 1.5b similar to the spatial distribution in Fig. 1.5a because the pattern in Fig. 1.5b has similar patchy structure behind the front? On the other hand, is the pattern of Fig. 1.5b topologically closer to the spatial distribution of Fig. 1.5c because both of them are continuous fronts? In this example, there may be a range of opinions about pattern similarity, while any conclusions that are suggested after a visual inspection of the patterns in Fig. 1.5 will be subjective since it is only based on human perception and aesthetic preferences. More rigorous methods should take into account some problem-specific criteria to decide whether or not two spatial distributions are similar to each other. The simplest example of such criteria is to state that two patterns are similar if both of them are patchy (or continuous front). Comparison between two patterns then becomes straightforward as it is now based on counting the number of objects in the image of spatial distribution. Any continuous front is considered as a single object, while a ‘no front’ patchy structure can be thought of as several separate objects in the spatial domain. However, given that continuous front spatial pattern may have a complex patchy spatial structure behind the front (cf. Fig. 1.5a and 1.5b) more careful analysis of topological properties may be required to conclude about the similarity of patchy



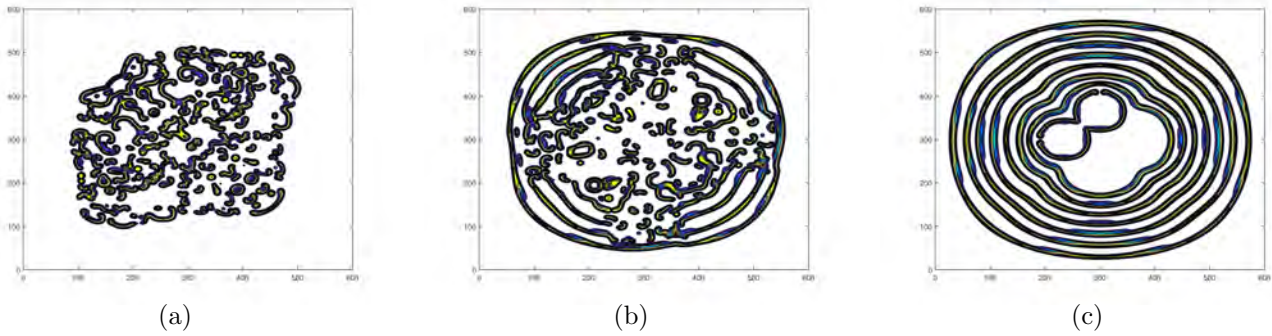


Figure 1.5: Examples of spatial distributions in a spatial domain where  $x \in [0, 600]$  and  $y \in [0, 600]$ . The regions of non-zero population density are shown in black. Are these spatial patterns similar or different? (a) Patchy spatial distribution of the density of invasive species obtained as a result of numerical solution of the mathematical model of biological invasion; (b) Continuous front density distribution obtained from the same model. The spatial pattern has patchy structure behind the front. (c) Continuous front density distribution with quasi-regular oscillations behind the front.

and continuous front density distributions or, indeed, about the similarity of two continuous fronts.

In our work we provide primary topological analysis of spatial patterns arising in the problem of biological invasion; see also [64, 65, 66]. The aim is to understand whether reliable criteria for classification and comparison can be elaborated for spatial patterns that arise in various models of biological invasion. Therefore, the basic topological indices of spatial patterns (including the number of objects, the fragmentation rate, etc.) will be analysed for a variety of spatial distributions arising to ascertain whether the spatial pattern type can be recognised correctly by using any of the quantities above.

Given the objectives of this thesis, this work will focus on two mathematical models of biological invasion. The first model is given by two coupled integro-difference equations used to simulate a predator-prey interaction where the prey is thought of as an invasive species. The model allows for consideration of both short-distance dispersal and long-distance dispersal [77] and the effect of the long-distance dispersal on the formation of patchy spatial patterns will be investigated. In this thesis, it will be demonstrated that patchy invasion can be observed for

species spread by both short-distance dispersal and long-distance dispersal. We then introduce a topological classification of spatial patterns and investigate what factors will influence the formation of topologically different spatial patterns. Finally, we introduce some topological indices to classify those spatial patterns.

The second model that we investigate is a diffusion-reaction model used to simulate the biological invasion of the gypsy moth in the North America. The employment of a reaction-diffusion model to simulate the spatio-temporal dynamics of biological invasion has previously been studied in [24]. The model allows for generating spatial distributions that are visually very close to each other, yet some of those distributions are continuous fronts while the others are patchy spatial patterns. Hence we want to understand whether a slight increment in the model parameters results in a slight increment in topological indices (i.e. the production of spatial patterns with similar topological properties). If the above is true then reliable criteria for classification and comparison can be elaborated for spatial patterns arising in the model. However, if spatial patterns of biological invasion are not ‘topologically stable’ in the sense above and the spatial patterns obtained for closed values of system parameters may have a very different topological structure then practitioners should take into account the ‘topological volatility’ of spatial patterns of biological invasion in further design of monitoring and control protocols.

The thesis is organized as follows. In Chapter 2, we discuss non-spatial models of biological invasion and analyse the stability of steady states. In Chapter 3-6 we introduce integro-difference equations to simulate the spatial patterns that arises in biological invasion and analyse these spatial distributions. In chapter 7 we study a model given by partial differential equations to simulate the biological invasion of the gypsy moth which have overlapping generations.

## CHAPTER 2

# NON-SPATIAL MODELS OF BIOLOGICAL INVASION

Although biological invasion is a spatio-temporal phenomenon, non-spatial models should be studied as a foundation before the more complicated spatio-temporal models are investigated. Non-spatial models can show us how the population size changes over time.

In nature, some species have overlapping generations so that continuous-time models can be used to describe their population dynamics. For the other species who do not have overlapping generations, their reproduction only takes place during a particular time of each year, and in this case, the population dynamics can be described by discrete-time models.

### 2.1 Continuous-time models

We consider a species  $N$  whose population size at time  $t$  is described by  $N(t)$ . After a small time interval  $\Delta t$ , the change of population over this time interval can be written as:

$$\Delta N(t, \Delta t) = N(t + \Delta t) - N(t) = B(t, \Delta t) - D(t, \Delta t) + M(t, \Delta t), \quad (2.1)$$

where  $B(t, \Delta t)$  denotes the number of births between time  $t$  and  $t + \Delta t$ ,  $D(t, \Delta t)$  denotes the number of deaths in the same time interval, and  $M(t, \Delta t)$  is the number of individuals that joined or left during this period [39]. For convenience, it is assumed there is no migration so that  $M(t) \equiv 0$  for any  $t$ .

Now we consider that species  $N$  has overlapping generation and its population grows continuously in time. We assume that  $\Delta t$  is sufficiently small, so that

$$B(t, \Delta t) \approx bN(t)\Delta t, \quad D(t, \Delta t) \approx dN(t)\Delta t, \quad (2.2)$$

where  $b$  is the reproductive rate of an individual and  $d$  is the probability of an individual dying.

We assume that both  $b$  and  $d$  are constants, therefore equation (2.1) can be rewritten as

$$\Delta N(t, \Delta t) = (b - d)N(t)\Delta t = F(N)\Delta t = f(N)N(t)\Delta t. \quad (2.3)$$

$F(N) = (b - d)N(t)$  is called the intrinsic growth rate and the  $f(N) = b - d$  is called the per capita growth rate of population.

We divide through equation (2.3) by  $\Delta t$ , and take the limit  $\Delta t \rightarrow 0$  to obtain

$$\frac{\Delta N(t, \Delta t)}{\Delta t} = \frac{N(t + \Delta t) - N(t)}{\Delta t} \approx \frac{dN(t)}{dt} = (b - d)N(t). \quad (2.4)$$

This equation (2.4) can be solved with an initial condition  $N(0) = N_0$ , and the solution is obtained by integrating both sides of (2.4),

$$N(t) = N_0 e^{(b-d)t}. \quad (2.5)$$

If the death rate is greater than the birth rate, i.e.,  $b < d$ , then the population density will decrease exponentially with time and finally extinct. If the death rate is less than the birth rate, i.e.  $b > d$ , then the population density will grow exponentially, which is not realistic.

### 2.1.1 Logistic growth

In the above, the per capita growth rate  $r = b - d$  is a constant, which means it is density-independent. However, in the real world, there are many factors regulating the growth of population, such as food, water, habitat and other environmental features, so in most cases the per capita growth rate is density-dependent. When the population density is very high, the death rate will also be very high; the species then reaches its maximum population density, which is known as the carrying capacity.

We now consider the case when the per capita growth rate decreases linearly with population density, and the carrying capacity takes the value of  $K$ . We have

$$\frac{1}{N} \frac{dN}{dt} = f(N) = r \left(1 - \frac{N}{K}\right). \quad (2.6)$$

In this model, the growth rate decreases to zero when the population density reaches the carrying capacity  $K$ . Equation (2.6) is known as the logistic equation. The growth rate of population density is described by a quadratic function of the population density:

$$\frac{dN}{dt} = F(N) = rN \left(1 - \frac{N}{K}\right). \quad (2.7)$$

The solution to equation (2.7) is

$$N(t) = \frac{K}{1 + \left(\frac{K}{N_0} - 1\right)e^{-rt}}. \quad (2.8)$$

and this model has an S-shaped growth curve (see Fig. 2.1). It can be seen that when the population density  $N(t)$  reaches the carrying capacity  $K$ , the growth rate is  $\frac{dN}{dt} = 0$ , and the population density no longer changes.

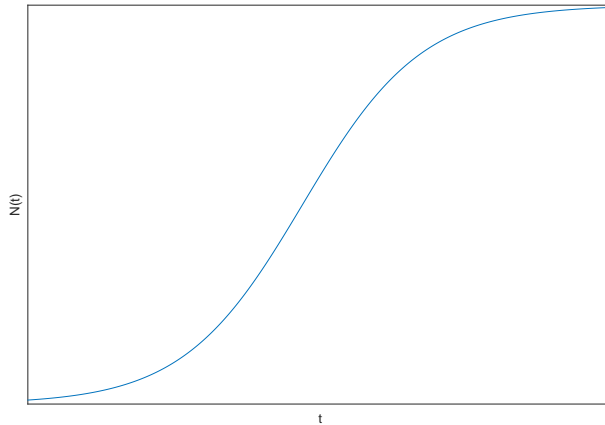


Figure 2.1: Growth curve of the logistic model

We have to emphasize that the per capita growth rate does not have to be linear. The logistic model is the simplest model to give the property that per capita growth rate decreases with respect to density. More generally, the per capita growth rate function  $f(N)$  can have other forms which satisfy the following:

$$\frac{df(N)}{dN} < 0 \quad \text{and} \quad f(K) = 0 \quad (2.9)$$

### 2.1.2 The Allee effect

However, the per capita growth rate does not always decrease as population density increases. In the 1930s, Warder Clyde Allee found that the population size of goldfish increases more quickly when there are more goldfish in the tank [1]. This phenomenon is called the Allee effect. The reason for this phenomenon is that individuals cooperate within the species, working together to defend against predators, find mates, and search for resources. Therefore, the per capita growth function  $f(N)$  is not monotonic if the species  $N$  is affected by the Allee effect, but rather increases for small density and decreases for large density. The Allee effect can be classified into two types, the strong Allee effect and the weak Allee effect. The difference between the two mechanisms is, whether the growth rate is positive or negative when population when density is low. For the strong Allee effect, the growth rate  $F(N)$  has the following conditions:

$$F(N) < 0 \text{ for } 0 < N < c \text{ and } N > K, \quad (2.10)$$

$$F(N) > 0 \text{ for } c < N < K, \quad (2.11)$$

where  $c$  is called the critical density, more generally, the threshold density under which the species could not survive. The relationship between growth rate and population density for strong Allee effect is shown in Fig. 2.2(a). For example, if the initial density is less than  $c$ , then the growth rate is negative, which will result in the population density decreasing. As a result, the density is always less than  $c$ , the growth rate is always negative as well. Finally, the population density decreases to zero. However, if the initial density is larger than  $c$ , the population density will keep increasing until it reaches the carrying capacity  $K$ .

For the weak Allee effect, there is no such threshold density, so the corresponding growth rate is positive when density is low,

$$F(N) > 0 \text{ for } 0 < N < K, \quad (2.12)$$

$$F(N) < 0 \text{ for } N > K. \quad (2.13)$$

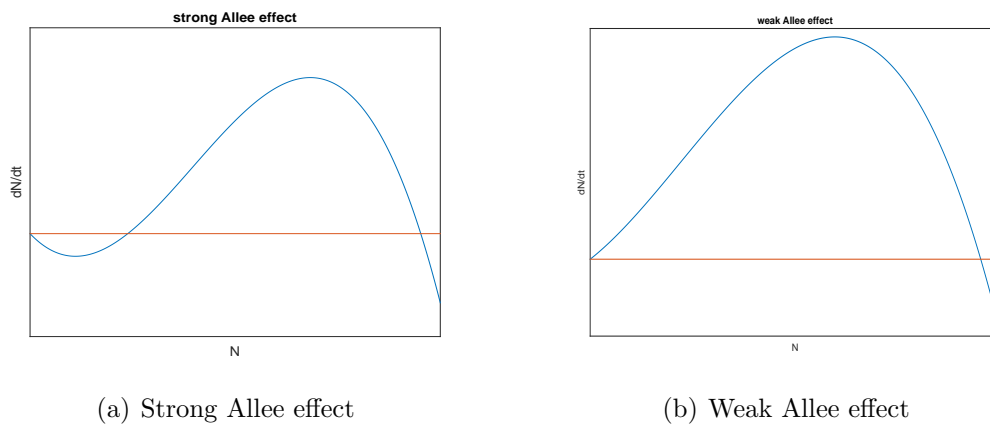


Figure 2.2: Growth rate of species influenced by (a) the strong Allee effect and (b) weak Allee effect

The relationship between growth rate and population density for the weak Allee effect is shown in Fig. 2.2(b).

One simple example of the Allee effect is given by the growth rate function described by a cubic polynomial with respect to  $N$ :

$$\frac{dN}{dt} = aN(N - c)\left(1 - \frac{N}{K}\right). \quad (2.14)$$

Equation (2.14) represents the strong Allee effect when  $0 < c < K$ , and represents the weak Allee effect when  $-K < c < 0$ . When  $c < -K$ , there is no Allee effect.



### 2.1.3 Continuous-time models: multiple species system

We now investigate a more sophisticated model as interaction between species will be required to model biological invasion in our further study.

There is usually more than one species in an ecosystem, and those species interact with each other in various ways. The relationship of the species involved in the food chain could be predation (e.g., wolves and rabbits), competition (e.g., wolves and foxes), or mutualism (e.g., rhinoceros and horn-bill). This section will study two-species models which can reveal some basic mechanisms of interacting species. Let  $N(t)$  be the density of species  $N$  and  $P(t)$  be the density of species  $P$ , then the growth rate of the two species can be described by:

$$\frac{dN}{dt} = F(N, P), \quad (2.15)$$

$$\frac{dP}{dt} = G(N, P), \quad (2.16)$$

where  $F(N, P)$  is the growth rate of species  $N$ , and  $G(N, P)$  is the growth rate of species  $P$ . Model (2.15)-(2.16) can describe various relationships between the species.

**Competition:** Competition occurs due to limited resources, such as food, water, and territory. Therefore, an increase in the density of species  $P$  will result in a decrease in the growth rate of species  $N$ :

$$\frac{\partial F}{\partial P} < 0, \quad \frac{\partial G}{\partial F} < 0. \quad (2.17)$$

**Mutualism:** Mutualism is the relationship in which different species benefit from each other, which can be described by

$$\frac{\partial F}{\partial P} > 0, \quad \frac{\partial G}{\partial F} > 0. \quad (2.18)$$

**Predation:** Prey is the food of the predator. Thus, an increase in the density of prey  $N$  will lead to an increase in the growth rate of predator  $P$ , while an increase in predator density will result in a decrease in the growth rate of prey:

$$\frac{\partial F}{\partial P} < 0, \quad \frac{\partial G}{\partial F} > 0. \quad (2.19)$$

If the growth rate is equal to 0, the population densities will not change with time. In this case, the system is said to be in a steady state, that is:

$$\frac{dN}{dt} = F(N^*, P^*) = 0 \quad (2.20)$$

$$\frac{dP}{dt} = G(N^*, P^*) = 0, \quad (2.21)$$

where  $N^*$  and  $P^*$  are the population densities when the system is in equilibrium.

The question remains that how a community in a steady state responds to perturbations?

We consider at time  $t$ , the density is

$$N(t) = N^* + n(t), \quad (2.22)$$

where  $n(t)$  is sufficiently small. The steady state is said to be stable if the perturbed community tends to return to the steady state, so that

$$n(t) \rightarrow 0 \text{ as } t \rightarrow \infty, \quad (2.23)$$

otherwise unstable.

We apply the Taylor series expansion

$$\frac{d(N^* + n)}{dt} = \frac{dn}{dt} = F(N^* + n, P^* + p) \quad (2.24)$$

$$= F(N^*, P^*) + F_N(N^*, P^*)n + F_P(N^*, P^*)p + \dots \quad (2.25)$$

$$\approx F_N(N^*, P^*)n + F_P(N^*, P^*)p, \quad (2.26)$$

and

$$\frac{d(P^* + p)}{dt} = \frac{dp}{dt} = G(N^* + n, P^* + p) \quad (2.27)$$

$$= F(N^*, P^*) + G_N(N^*, P^*)n + G_P(N^*, P^*)p + \dots \quad (2.28)$$

$$\approx G_N(N^*, P^*)n + G_P(N^*, P^*)p, \quad (2.29)$$

Combining (2.26) and (2.29) we have

$$\frac{d}{dt} \begin{pmatrix} n \\ p \end{pmatrix} = \begin{pmatrix} F_N(N^*, P^*) & F_P(N^*, P^*) \\ G_N(N^*, P^*) & G_P(N^*, P^*) \end{pmatrix} \begin{pmatrix} n \\ p \end{pmatrix}, \quad (2.30)$$

where

$$J = \begin{pmatrix} f_N(N^*, P^*) & f_P(N^*, P^*) \\ g_N(N^*, P^*) & g_P(N^*, P^*) \end{pmatrix} = \begin{pmatrix} a_{11} & a_{12} \\ a_{21} & a_{22} \end{pmatrix} \quad (2.31)$$

is known as the Jacobian matrix of system (2.15)-(2.16). The system is stable if  $n(t) \rightarrow 0$  and  $p(t) \rightarrow 0$  as  $t \rightarrow \infty$ . For the system of linear ordinary differential equations  $\mathbf{y}' = \mathbf{J}\mathbf{y}$ , the solution has the form  $\mathbf{y} = \mathbf{x}e^{\lambda t}$ . Hence  $\mathbf{y}' = \lambda \mathbf{x}e^{\lambda t} = \mathbf{J}\mathbf{x}e^{\lambda t}$  or  $\lambda \mathbf{x} = \mathbf{J}\mathbf{x}$ , where  $\lambda$  is the eigenvalue and  $\mathbf{x}$  is the corresponding eigenvector. The eigenvalues of matrix  $\mathbf{J}$  can be found

by solving

$$\det(\mathbf{J} - \lambda\mathbf{I}) = \begin{vmatrix} a_{11} - \lambda & a_{12} \\ a_{21} & a_{22} - \lambda \end{vmatrix} = 0 \quad (2.32)$$

or

$$\lambda^2 - (a_{11} + a_{22})\lambda + a_{11}a_{22} - a_{12}a_{21} = 0 \quad (2.33)$$

The behaviour of the species is determined by the eigenvalues [34]:






| <b>Eigenvalues</b>               | <b>Fixed point</b> | <b>Flow</b>   |
|----------------------------------|--------------------|---|
| complex with positive real parts | unstable focus     |    |
| complex with negative real parts | stable focus       |    |
| real and positive                | unstable node      |   |
| real and negative                | stable node        |  |
| one positive and one negative    | saddle point       |  |

Figure 2.3: Basic types of stationary points. The classification of stationary points is taken from [34]

We consider an example given by

$$\frac{du(t)}{dt} = \gamma u(u - \beta)(1 - u) - uv, \quad (2.34)$$

$$\frac{dv(t)}{dt} = uv - mv. \quad (2.35)$$

There are four steady states:  $s_1 = (0, 0)$ ,  $s_2 = (1, 0)$ ,  $s_3 = (\beta, 0)$ , and  $s_4 = (m, \gamma(m - \beta)(1 - m))$ .

We notice that  $s_1$ ,  $s_2$  and  $s_3$  always exist while  $s_4$  is feasible for  $m < 1$  and  $\beta < m$ . We need to know the stability of these steady states which depends on the eigenvalues of the corresponding

Jacobian matrix

$$J = \begin{pmatrix} \gamma[-3u^2 + 2(\beta + 1)u - \beta] - v & -u \\ v & u - m \end{pmatrix}. \quad (2.36)$$

The eigenvalues are given by

$$\lambda_{1,2} = \frac{1}{2} \left( tr(\mathbf{J}) \mp \sqrt{tr(\mathbf{J})^2 - 4det(\mathbf{J})} \right), \quad (2.37)$$

where  $tr(\mathbf{J})$  and  $det(\mathbf{J})$  are the trace and the determinant of the Jacobian matrix  $\mathbf{J}$ .

Then we can obtain four pairs of eigenvalues computed at steady states  $s_1$ ,  $s_2$ ,  $s_3$  and  $s_4$  respectively. The stability analysis reveals that  $s_1$  is always stable,  $s_2$  is stable for  $m > 1$  and  $\beta < 1$ , and the steady state  $s_3$  would only be stable when  $\beta < m$  and  $\beta > 1$ . The eigenvalues  $\lambda_1$  and  $\lambda_2$  computed at the coexistence state  $s_4$  are given by (2.37) where  $tr(\mathbf{J}) = \gamma m(1 - 2m + \beta)$  and  $det(\mathbf{J}) = m\gamma(m - \beta)(1 - m)$ . Let us introduce function  $F(\beta)$  as

$$F(\beta) \equiv tr(\mathbf{J})^2 - 4det(\mathbf{J}) = \gamma^2 m^2 (\beta - 2m + 1)^2 - 4\gamma m (\beta - m)(m - 1).$$

To find sub-domains in the parametric plane  $(m, \beta)$  where the eigenvalues  $\lambda_{1,2}$  are complex numbers we factorize  $F(\beta) = (\beta - \beta_1(m))(\beta - \beta_2(m))$ . We have

$$\beta_{1,2}(m) = 2m - 1 + \frac{2(m - 1)}{\gamma m} \left( 1 \mp \sqrt{\gamma m + 1} \right).$$

The structure of the parameter plane  $(m, \beta)$  is shown in Fig. 2.4 where the curves  $\beta_1(m)$  and  $\beta_2(m)$  are shown for  $m > 0$  and  $\beta > 0$  as two dashed lines in the figure. We have  $\beta_1(m) > \beta_2(m)$  for  $0 < m < 1$  and  $\beta_1(m) < \beta_2(m)$  for  $m > 1$ . Thus  $F(\beta) < 0$  in sub-domains where  $m < 1$ ,  $\beta_2(m) < \beta < \beta_1(m)$  and  $m > 1$ ,  $\beta_1(m) < \beta < \beta_2(m)$ , respectively. The eigenvalues  $\lambda_{1,2}$  are

complex numbers in those sub-domains and temporal dynamics is oscillatory. Further analysis reveals that the coexistence state  $s_4$  is unstable when  $\text{tr}(J) > 0$  i.e.  $\beta > 2m - 1$ .

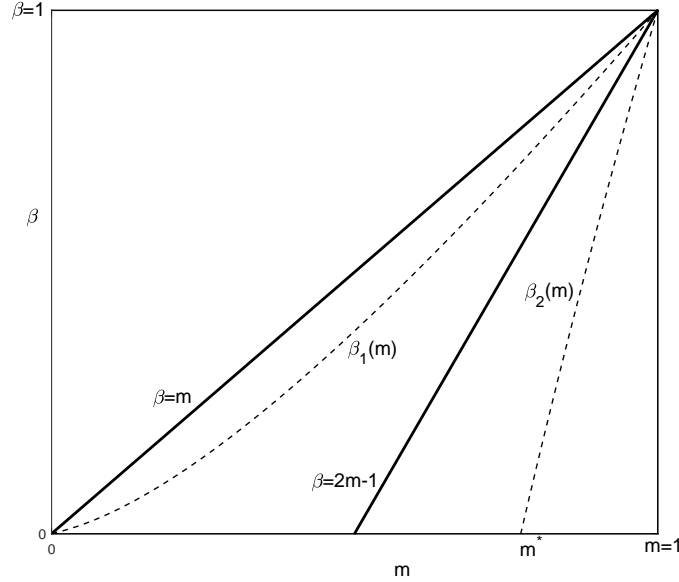


Figure 2.4: Parameter plane of  $\beta$  and  $m$  for system (2.34)-(2.35). The extinction state is stable when  $\beta > \gamma$ , and the coexistence state is stable when  $\beta < 2m - 1$ .

Let us note that  $\beta_1(m) > 0$  for  $m > 0$  and the only positive root  $m^* > 0$  of function  $\beta_2(m)$  is given by

$$m^* = \frac{\gamma - 1 + \sqrt{2\gamma + 1}}{2\gamma}.$$

Thus, the location of root  $m^*$  and therefore the size of the domain  $\beta_2(m) < \beta < \beta_1(m)$  depends on parameter  $\gamma$  where the asymptotic limits are  $m^*(\gamma) \rightarrow 1$  as  $\gamma \rightarrow 0$  and  $m^*(\gamma) \rightarrow 1/2$  as  $\gamma \rightarrow \infty$ .

## 2.2 Discrete-time models

Partial differential equations are very popular in modelling the biological invasion of species whose population has overlapping generations. If the reproduction occurs during a particular period of each year, then we consider discrete-time models described by difference equations.

For discrete-time models, the stability analysis is different from that in continuous models.

For convenience, we scale the time step  $\Delta t$  to be 1. So the population density at time  $t$  can be described by  $N_t$ . Let us suppose that the population density at time step  $t + 1$  only depends on the population density in the previous time step  $t$ , i.e.,

$$N_t = F(N_{t-1}), t \geq 1. \quad (2.38)$$

In this general discrete-time model, the steady states are determined by  $N_{t+1} = N_t$ . The steady state,  $N^*$ , is characterised by

$$N^* = F(N^*). \quad (2.39)$$

Once the population density reaches the steady state at some moment  $N_t = N^*$ , the population density remains the same in the next time step,

$$N_{t+1} = F(N_t) = F(N^*) = N^*, \quad (2.40)$$

and hence remains the same in the following time steps.

To investigate the stability, we consider a small perturbation of  $N^*$ ,  $N_t = N^* + n_t$ . So we

have

$$n_{t+1} = N_{t+1} - N^* \quad (2.41)$$

$$= F(N^* + n_t) - N^* \quad (2.42)$$

$$\approx F(N^*) + F'(N^*)n_t - N^* \quad (2.43)$$

$$= F'(N^*)n_t. \quad (2.44)$$

Taking absolute values on both sides of (2.44),

$$|n_{t+1}| = |F'(N^*)||n_t|. \quad (2.45)$$

Therefore, the steady state is stable if  $|F'(N^*)| < 1$ , otherwise unstable.

### 2.2.1 General multiple species models

For multiple species models,

$$N_{t+1} = F(N_t, P_t), \quad (2.46)$$

$$P_{t+1} = G(N_t, P_t). \quad (2.47)$$

The steady states,  $N^*$  and  $P^*$  are determined by  $N^* = F(N^*, P^*)$  and  $P^* = G(N^*, P^*)$ . Now consider small perturbations to steady states at time  $t$ ,  $N_t = N^* + n_t$  and  $P_t = P^* + p_t$ . We



apply Taylor expansions,

$$n_{t+1} = N_{t+1} - N^* \quad (2.48)$$

$$= F(N_t, P_t) - F(N^*, P^*) \quad (2.49)$$

$$= F(N^* + n_t, P^* + p_t) - F(N^*, P^*) \quad (2.50)$$

$$= F(N^*, P^*) + F_N(N^*, P^*)n_t + F_P(N^*, P^*)p_t + \dots - F(N^*, P^*) \quad (2.51)$$

$$\approx F_N(N^*, P^*)n_t + F_P(N^*, P^*)p_t, \quad (2.52)$$

and similarly

$$p_{t+1} = G_N(N^*, P^*)n_t + G_P(N^*, P^*)p_t. \quad (2.53)$$

Combining (2.52) and (2.53) we obtain

$$\begin{pmatrix} n_{t+1} \\ p_{t+1} \end{pmatrix} = \begin{pmatrix} F_N(N^*, P^*) & F_P(N^*, P^*) \\ G_N(N^*, P^*) & G_P(N^*, P^*) \end{pmatrix} \begin{pmatrix} n_t \\ p_t \end{pmatrix}, \quad (2.54)$$

then we will demonstrate the stability of steady states is determined by the eigenvalues of the Jacobian matrix of the system,

$$J = \begin{pmatrix} F_N(N^*, P^*) & F_P(N^*, P^*) \\ G_N(N^*, P^*) & G_P(N^*, P^*) \end{pmatrix} = \begin{pmatrix} a_{11} & a_{12} \\ a_{21} & a_{22} \end{pmatrix}. \quad (2.55)$$

Then the eigenvalues can be obtained by solving

$$\lambda^2 - (a_{11} + a_{22})\lambda + a_{11}a_{22} - a_{21}a_{12} = 0 \quad (2.56)$$

or

$$\lambda^2 - \text{Tr}(J)\lambda + \det(J) = 0. \quad (2.57)$$

To analyse the stability of the steady states, we have to introduce a theorem, the detailed proof is discussed in [2].

**Theorem 2.2.1** *Let  $X(t+1) = AX(t)$  where  $X(t) = (x_1(t), x_2(t), \dots, x_k(t))^T$ . And Let  $A$  be a  $k \times k$  matrix. We have  $\lim_{t \rightarrow \infty} X(t) = 0$  iff  $\rho(A) < 1$  where  $\rho(A) = \max_{i \in \{1, 2, \dots, k\}} \{|\lambda_i|\}$ .*

Therefore, we have

$$\begin{pmatrix} n_{t+1} \\ p_{t+1} \end{pmatrix} \rightarrow \begin{pmatrix} 0 \\ 0 \end{pmatrix} \text{ as } t \rightarrow \infty \text{ iff } |\lambda_1| < 1 \text{ and } |\lambda_2| < 1. \quad (2.58)$$

## 2.2.2 Multiple species models affected by the Allee effect

We now consider the predator-prey system where the prey density at the moment  $t$  is described by  $N_t$ , and the predator density is described by  $P_t$ . It is assumed that the prey is affected by a strong Allee effect. As mentioned previously, for the strong Allee effect, (i) there exist a threshold density under which the population goes to extinction; (ii) the correlation between the capita growth rate and population density is positive.

The growth function of prey influence by the strong Allee effect can be written as

$$F_1(N) = \frac{A(N_t)^2}{1 + B^2(N_t)^2}, \quad (2.59)$$

where  $A$  is the intrinsic growth rate and  $1/B$  is the density for which its per capita growth rate reaches its maximum [50]. Then we take into account the effect of predator. Predation leads

to the a decrease in prey. We assume the prey decreases exponentially as a result of predation.

Then at time step  $t$ , the function  $F(N, P)$  can be chosen as

$$F(N, P) = \frac{A(N_t)^2}{1 + B^2(N_t)^2} \exp(-\kappa P_t), \quad (2.60)$$

where  $\kappa$  is the predator efficiency.

We assume that the predator is a specialist predator. A specialist species can only thrive when its prey exists, so the predator cannot survive without the prey. The predator growth rate is assumed to be proportional to the rate at which the predators and the prey meet. Then function  $G(N, P)$  can be chosen as

$$G(N, P) = \delta N_t P_t, \quad (2.61)$$

where  $\delta$  is the predator growth rate.

Combining (2.60)-(2.61) with (2.46)-(2.47) we obtain

$$N_{t+1} = \frac{A(N_t)^2}{1 + B^2(N_t)^2} \exp(-\kappa P_t), \quad (2.62)$$

$$P_{t+1} = \delta N_t P_t. \quad (2.63)$$

For convenience, (2.62)-(2.63) is non-dimensionalised by scaling

$$N'_t = \delta N_t \text{ and } P'_t = \kappa P_t, \quad (2.64)$$

then equation (2.62) and (2.63) can be transformed to (the “ $r$ ” has been dropped here)

$$N_{t+1} = \frac{a(N_t)^2}{1 + b(N_t)^2} \exp(-P_t), \quad (2.65)$$

$$P_{t+1} = N_t P_t, \quad (2.66)$$

where  $a = A/\delta$  and  $b = (B/\delta)^2$ .

The steady states can be found by solving  $N_{t+1} = N_t$  and  $P_{t+1} = P_t$  and we can obtain four steady states,  $(0, 0)$ ,  $(N_1^*, 0)$ ,  $(N_2^*, 0)$  and  $(N^*, P^*)$ , where

$$N_1^* = \frac{a - \sqrt{a^2 - 4b}}{2b}, N_2^* = \frac{a + \sqrt{a^2 - 4b}}{2b} \quad (2.67)$$

$$(N^*, P^*) = (1, \ln(\frac{a}{b+1})). \quad (2.68)$$

The prey-only states  $(N_1^*, 0)$  and  $(N_2^*, 0)$  are only valid for  $a > 2\sqrt{b}$ . For the coexistence state  $(N^*, P^*)$ , population can not be negative so  $a > b + 1$  is required.

The Jacobian matrix of system (2.65) and (2.66) is given by

$$J = \begin{bmatrix} \frac{2an^*}{(1+b(n^*)^2)^2} & -\frac{a(n^*)^2}{1+b(n^*)^2} \exp(-p^*) \\ p^* & n^* \end{bmatrix}, \quad (2.69)$$

From Theorem 2.2.1, the steady states are stable if  $-1 < \lambda < 1$ .

If  $(n^*, p^*) = (0, 0)$ , then the eigenvalue of the Jacobian matrix (2.69) is 0. It can be concluded that this extinction state is always stable.

If  $(n^*, p^*) = (N_1^*, 0)$  or  $(N_2^*, 0)$ , the Jacobian matrix (2.69) becomes

$$\begin{bmatrix} \frac{2aN_i^*}{(1+b(N_i^*)^2)^2} & -\frac{a(N_i^*)^2}{1+b(N_i^*)^2} \\ 0 & N_i^* \end{bmatrix}, i = 1, 2. \quad (2.70)$$

There are two eigenvalues of matrix (2.70),  $\lambda_1 = \frac{2aN_i^*}{(1+b(N_i^*)^2)^2}$  and  $\lambda_2 = N_i^*$ . For equilibrium  $(N_1^*, 0)$ ,  $\lambda_1 > 1$  hence unstable. For  $(N_2^*, 0)$ , the equilibrium is stable on condition that  $2 < a < b + 1$ .

If  $(n^*, p^*) = (N^*, P^*)$ , then the Jacobian matrix (2.69) turns to

$$\begin{bmatrix} \frac{2}{1+b} & -1 \\ \ln\left(\frac{a}{b+1}\right) & 1 \end{bmatrix}, \quad (2.71)$$

so that the steady state of coexistence is stable if  $a < a_{cr} = (b + 1) \exp\left(\frac{b-1}{b+1}\right)$ .

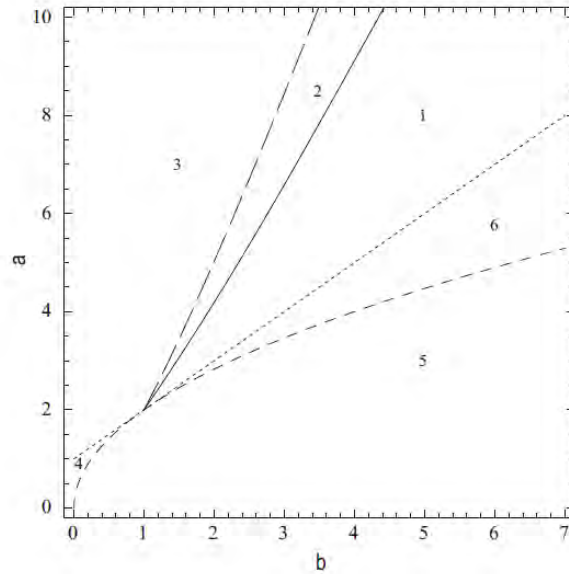


Figure 2.5: Parameter plane of  $a$  and  $b$  [76].

All of these constraints above divide the parameter plane  $(b, a)$  into six domains (see

Fig. 2.5). The straight dotted line represents  $a = b + 1$ , and the solid curve represents  $a = a_{cr}$ . The short dashed curve corresponds to  $a = 2\sqrt{b}$ . The long dashed curve is obtained numerically. The coexistence state is stable for parameters from domain 1. The coexistence equilibrium loses stability and population dynamics oscillates for parameters inside domain 2. When crossing the long dashed curve, the only attractor is the extinction state in the domain 3 [76].

Through the stability analysis of the steady states in the non-spatial models, we are able to understand the population dynamics for various parameters, e.g, we will be aware whether an alien species will invade successfully and whether a native species can survive when an alien species is introduced as their predator or competitor.

## CHAPTER 3

# SPATIAL PATTERNS OF BIOLOGICAL INVASION OF STAGE-STRUCTURED SPECIES

In the previous chapter we have introduced two non-spatial models to simulate the biological invasion, however, biological invasion is a spatio-temporal phenomenon. The spatial pattern of invasive species change with time.

This chapter will introduce a spatio-temporal model which describes biological invasion of stage-structured species [77]. This model is described by two kernel-based integro-difference equations. In this chapter we introduce two different dispersal kernels—the Gaussian kernel can be used to simulate the short-distance dispersals while the Cauchy kernel can be used to simulation long-distance dispersals.

### **3.1 Integro-difference model with Allee effect**

We follow the work in [76, 77]. We consider both predator and prey are stage-structured and have a similar life cycle. We denote the prey density located at position  $\mathbf{r} = (x, y)$  in generation  $t$  by  $N_t(\mathbf{r})$  and predator density by  $P_t(\mathbf{r})$ . During the reaction stage, the two species

reproduce and interact with each other. Then their densities change to

$$\widetilde{N}_t(\mathbf{r}) = f(N_t(\mathbf{r}), P_t(\mathbf{r})), \quad (3.1)$$

$$\widetilde{P}_t(\mathbf{r}) = g(N_t(\mathbf{r}), P_t(\mathbf{r})), \quad (3.2)$$

where functions  $\widetilde{N}_t$  and  $\widetilde{P}_t$  are the population densities after reproduction. Once the reaction stage is completed, the species starts dispersing. The population density species  $N$  and  $P$  in generation  $t + 1$  is given by:

$$N_{t+1}(\mathbf{r}) = \int_{\Omega} \widetilde{N}_t(\mathbf{r}') k_N(\mathbf{r}, \mathbf{r}') d\mathbf{r}', \quad (3.3)$$

$$P_{t+1}(\mathbf{r}) = \int_{\Omega} \widetilde{P}_t(\mathbf{r}') k_P(\mathbf{r}, \mathbf{r}') d\mathbf{r}', \quad (3.4)$$

where  $\Omega$  is the dispersal domain. The dispersal kernels  $k_N$  and  $k_P$  give the probability densities of an individual moving from position  $\mathbf{r}'$  to position  $\mathbf{r}$  after dispersal. We assume that the probability of the movement only depends on the distance between two positions, i.e.,  $k_i(\mathbf{r}, \mathbf{r}') = k_i(|\mathbf{r} - \mathbf{r}'|)$ ,  $i = N, P$ .

Then we substitute equations (3.1)–(3.2) into (3.3)–(3.4) to obtain the integro-difference equations

$$N_{t+1}(\mathbf{r}) = \int_{\Omega} f(N_t(\mathbf{r}'), P_t(\mathbf{r}')) k_N(\mathbf{r}, \mathbf{r}') d\mathbf{r}', \quad (3.5)$$

$$P_{t+1}(\mathbf{r}) = \int_{\Omega} g(N_t(\mathbf{r}'), P_t(\mathbf{r}')) k_P(\mathbf{r}, \mathbf{r}') d\mathbf{r}'. \quad (3.6)$$

For the model (3.5)–(3.6) we consider that the density of prey  $N$  is influenced by the strong



Allee effect and function  $f$  is chosen the same as in (2.60),

$$f = \frac{A(N_t)^2}{1 + B^2(N_t)^2} \exp(-\kappa P_t), \quad (3.7)$$

where  $\kappa$  is the predator efficiency.

Species P is considered a specialist predator, and function  $g$  is chosen the same as in (2.61),

$$g = \delta N_t P_t, \quad (3.8)$$

where  $\delta$  is the predator growth rate.

Therefore, using (2.64), (3.7) and (3.8) can be transformed to

$$f(N_t, P_t) = \frac{a(N_t)^2}{1 + b(N_t)^2} \exp(-P_t), \quad (3.9)$$

$$g(N_t, P_t) = N_t P_t, \quad (3.10)$$

where  $a = A/\delta$  and  $b = (B/\delta)^2$ .

## 3.2 Classification of dispersal kernels

Dispersal is a process that an individual or multiple individuals move from one location to another location. If the transport of a species to another location is caused by natural forces (e.g., the spread of seeds by the wind) and the new location is far away from the species' main range, it is called long-distance dispersal [39].

We consider two types of dispersal kernels. One is the Gaussian dispersal kernel with a thin tail which corresponds to high frequency of short-distance travel. The other is the Cauchy

dispersal kernel with a fat tail which corresponds to a higher rate of long-distance travel.

The short-distance dispersal can be described by the Gaussian kernel

$$k_i(|\mathbf{r} - \mathbf{r}'|) = \frac{1}{2\pi\alpha_i^2} \exp\left(-\frac{|\mathbf{r} - \mathbf{r}'|^2}{2\alpha_i^2}\right), i = N, P, \quad (3.11)$$

where parameter  $\alpha_i$  quantifies the scale of the dispersal. This corresponds to normal distribution so that larger  $\alpha_i$  corresponds to wider boundaries of the invasive area, hence the dispersal has a faster spread speed.

It has been shown that long-distance dispersal will take place if the probability distribution of the movement over the distance  $d$  has a power-law tail [31, 92]:

$$k(d) \sim d^{-\mu}, 1 < \mu < 3, \quad (3.12)$$

for one-dimensional space. Therefore, the corresponding two-dimensional expression is

$$k(\mathbf{d}) \sim |\mathbf{d}|^{-(\mu+1)}, \quad (3.13)$$

Here we consider two types of Cauchy kernels which describes the long dispersal,

$$k_i(|\mathbf{r} - \mathbf{r}'|) = \frac{\beta_i}{\pi(\beta_i + |\mathbf{r} - \mathbf{r}'|)^3}, \quad (3.14)$$

where  $\beta_i > 0, i = N, P$ , and

$$k_i(|\mathbf{r} - \mathbf{r}'|) = \frac{\gamma_i}{2\pi(\gamma_i^2 + |\mathbf{r} - \mathbf{r}'|^2)^{3/2}}, \quad (3.15)$$

where  $\gamma_i > 0, i = N, P$ . Equation (3.14) and (3.15) is called Cauchy kernel type I and Cauchy kernel type II. Obviously, (3.14) and (3.15) have the same power-law tail.

### 3.3 Initial conditions and boundary conditions

The problem (3.5)-(3.6) must be complemented by initial conditions. We consider two initial conditions:

The first is the symmetrical initial condition. Both prey and predator are located at the centre of the dispersal domain:

$$N_0(x, y) = \begin{cases} N_2^*, & \text{for } -1 \leq x \leq 1 \text{ and } -1 \leq y \leq 1, \\ 0, & \text{otherwise,} \end{cases} \quad (3.16)$$

$$P_0(x, y) = \begin{cases} P^*, & \text{for } -0.1 \leq x \leq 0.1 \text{ and } -1 \leq y \leq 1, \\ 0, & \text{otherwise.} \end{cases} \quad (3.17)$$

The second is asymmetrical initial condition. In this case, the prey is still located in the same region as (3.16) while the predator is located in an acentric region:

$$N_0(x, y) = \begin{cases} N_2^*, & \text{for } -1 \leq x \leq 1 \text{ and } -1 \leq y \leq 1, \\ 0, & \text{otherwise,} \end{cases} \quad (3.18)$$

$$P_0(x, y) = \begin{cases} P^*, & \text{for } -1 \leq x \leq 0.2 \text{ and } -0.9 \leq y \leq 0.4, \\ 0, & \text{otherwise.} \end{cases} \quad (3.19)$$

The system (3.5)-(3.6) are integrals that can be solved numerically given initial conditions. In this condition, we have to consider a computational domain  $\Omega$ . This computational domain

should be chosen carefully in order to make the computational error sufficiently small since a certain number of individuals leave the computational domain  $\Omega$  at each time step. Therefore, a large enough domain  $\Omega$  should be chosen to ensure that few individuals will leave the domain during the observation period.

### 3.4 Numerical simulation: the FFT method

The simplest and most straightforward way to solve the problem (3.5)-(3.6) would be numerical integration such as Newton-Cotes method. However, this approach is very computationally expensive so an alternative numerical technique will be used that is provided the Fast Fourier Transform (FFT) method.

The Fourier transform of the function  $f(x)$  is described by,

$$\hat{f}(s) = \int_{-\infty}^{\infty} f(x)e^{-2\pi isx} dx, \quad (3.20)$$

and the inverse Fourier transform is

$$f(x) = \int_{-\infty}^{\infty} \hat{f}(s)e^{2\pi isx} ds. \quad (3.21)$$

The convolution of function  $f(x)$  and  $g(x)$  is defined as

$$h(x) = f * g(x) = \int_{-\infty}^{\infty} f(x - y)g(y)dy. \quad (3.22)$$

The **convolution theorem** states that the Fourier transform of the convolution is equal to

the product of the Fourier transforms  $\hat{f}(s)$  and  $\hat{g}(s)$  [61],

$$\hat{h}(s) = \widehat{f * g}(s) = \hat{f}(s)\hat{g}(s). \quad (3.23)$$

Therefore, let  $F^{-1}$  be the inverse Fourier transform operator, we have

$$h(x) = F^{-1}(\hat{f}(s)\hat{g}(s)). \quad (3.24)$$

The system (3.5)-(3.6) can only be solved numerically. So we consider the discrete Fourier transform (DFT) of function  $f$ ,  $g$  and  $k$ . We discretise  $f(x)$  over the computational interval  $(a, b)$ ,

$$f_k = f(x_k), \quad g_k = g(x_k), \quad x_k = a + hk, \quad k = 0, 1, \dots, N - 1, \quad (3.25)$$

where  $h = \frac{b-a}{N-1}$  is the step size. The discrete Fourier transform of the sequence  $[f_k]$  is

$$F_s = \sum_{k=0}^{N-1} f_k e^{-2i\pi sk/N}, \quad (3.26)$$

and the corresponding inverse transform is

$$f_k = \sum_{s=0}^{N-1} F_s e^{2i\pi sk/N}. \quad (3.27)$$

The discrete Fourier transform is periodic, shown as follows:

$$F_{s+N} = \sum_{k=0}^{N-1} f_k e^{-2i\pi(s+N)k/N} = \sum_{k=0}^{N-1} f_k e^{-2i\pi sk/N} e^{-2\pi ik} = F_s, \quad (3.28)$$

and

$$F_s = \sum_{k=0}^{N-1} f_k e^{-2i\pi s k/N} \quad (3.29)$$

$$= \sum_{k=0}^{N/2-1} f_{2k} e^{-2i\pi s(2k)/N} + \sum_{k=0}^{N/2-1} f_{2k+1} e^{-2i\pi s(2k+1)/N} \quad (3.30)$$

$$= \sum_{k=0}^{N/2-1} f_{2k} e^{-2i\pi s k/(N/2)} + e^{-\frac{2\pi i s}{N}} \sum_{k=0}^{N/2-1} f_{2k+1} e^{-2i\pi s(k+1)/(N/2)} \quad (3.31)$$

$$= E_s + e^{-\frac{2\pi i s}{N}} O_s \quad (3.32)$$

Notice that  $E_s$  denotes the sum of the even components of  $F_s$ , while  $O_s$  denotes the sum of the odd components of  $F_s$ . Thanks to the periodicity of the discrete Fourier transform, we have

$$E_{s+\frac{N}{2}} = E_s, \text{ and } O_{s+\frac{N}{2}} = O_s \text{ if } N \text{ is even.} \quad (3.33)$$

Thus  $F_s$  can be rewritten as

$$F_s = \begin{cases} E_s + e^{-\frac{2\pi i}{N}s} O_s & \text{for } 0 \leq s < N/2, \\ E_{s-N/2} + e^{-\frac{2\pi i}{N}s} O_{s-N/2} & \text{for } N/2 \leq s < N. \end{cases} \quad (3.34)$$

We notice that

$$e^{-\frac{2\pi i}{N}(s+N/2)} = e^{-\frac{2\pi i s}{N} - \pi i} \quad (3.35)$$

$$= e^{-\pi i} e^{-\frac{2\pi i s}{N}} \quad (3.36)$$

$$= -e^{-\frac{2\pi i s}{N}}. \quad (3.37)$$

$F_s$  can be rewritten as

$$F_s = E_s + e^{\frac{-2\pi is}{N}} O_s, \quad (3.38)$$

$$F_{s+\frac{N}{2}} = E_s - e^{\frac{-2\pi is}{N}} O_s. \quad (3.39)$$

Thus, a size- $N$  DFT can be represented as two size- $N/2$  DFTs. This process was developed by Danielson and Lanczos in 1942, which is known as Danielson-Lanczos Lemma [74]. If  $N$  takes values of  $N = 2^s$ ,  $s$  is any positive integer. The number of computations for (3.26) can be reduced from  $O(N^2)$  to  $O(N \log_2 N)$ , by using a **Fast Fourier transform** (FFT) [74]. The convolution theorem is also valid for discrete Fourier transform. If we apply the FFT to two-dimensional integration (3.5), the number of computations is  $O(N^2 \log_2 N)$  while the corresponding number for the trapezoidal rule is  $O(N^4)$ .

### 3.5 Numerical validation

As there is no analytical solution to the problem, we need to choose the numerical methods carefully to ensure the accuracy of the solutions. And the only way to validate the solution is to compare the results of two numerical methods. As a grid is refined they must converge to the same answer. Thus, this section will compare the results of FFT with those obtained in numerical solution by the trapezoidal rule.

At the beginning, let us recall the computation of an integral by the trapezoidal rule. Consider a definite integral:

$$I = \int_a^b f(x) dx. \quad (3.40)$$

In order to obtain the numerical value of integral (3.40) , we divide the interval  $(a, b)$  into  $n$  subintervals of equal length  $h = (b - a)/n$  so that there are  $n + 1$  grid nodes on the interval,

$$x_0 = a, \quad x_i = x_0 + hi, \quad i = 1, 2, \dots, n. \quad (3.41)$$

If in each subinterval  $(x_{i-1}, x_i)$  we approximate the integrand by the a linear equation connecting  $f(x_{i-1})$  and  $f(x_i)$ , the integral on each subinterval  $(x_{i-1}, x_i)$  can be approximated by  $h \frac{f(x_{i-1})+f(x_i)}{2}$ , then the integral (3.40) can be approximated by

$$\int_a^b f(x)dx \approx \frac{h}{2} \sum_{i=1}^n (f(x_{i-1}) + f(x_i)), \quad (3.42)$$

which is known as the **trapezoidal rule** [6]. The error of the trapezoidal rule is

$$\text{error} = \frac{nh^3}{12} f''(\xi), \quad a \leq \xi \leq b. \quad (3.43)$$

Now that we have two numerical methods at hand, then we can investigate the accuracy of the FFT method. For doing it we introduce the numerical error for a specific problem.

We consider one-dimensional integro-difference equations for single species

$$N_t(x) = \int_{\Omega} k(x, y) f(N_{t-1}(y)) dy, \quad (3.44)$$

$$f(N) = rN \exp(-N), \quad (3.45)$$

$$k(x, y) = \frac{1}{\sqrt{2\pi\alpha^2}} \exp\left(-\frac{(x - y)^2}{2\alpha^2}\right), \quad (3.46)$$



with the initial condition

$$N_0(x) = \frac{1}{\sqrt{2\pi\alpha_0^2}} \exp\left(-\frac{(y - \mu)^2}{2\alpha_0^2}\right). \quad (3.47)$$

The system (3.44)-(3.47) can not be solved analytically. Hence we use the trapezoidal rule to obtain the numerical solution. As there is no analytical solution to the problem, the computational error cannot be directly calculated.

In this case, we consider an ‘exact’ solution obtained by the trapezoidal rule on a very fine grid of  $K_f = 2^{13} + 1 = 8193$  nodes and denote it  $N^{exact}(x)$ . Then we perform the trapezoidal rule on coarse grids of  $K = 2^s + 1, s = 1, 2, \dots, 12$  nodes. All the grids are considered uniform, so for any node  $x_i$  located on the coarse grid, there is a node  $x_j$  with the same value on the fine grid. Therefore the solution error can be obtained by

$$e_i = |N^{exact}(t, x_i) - \tilde{N}(t, x_i)|, i = 1, 2 \dots K. \quad (3.48)$$

And the error norm is given by

$$\|e\| = \max_{i=1,2,\dots,K} e_i. \quad (3.49)$$

The error norm is computed when  $K = 2^s + 1, s = 4, 5, \dots, 12$ , and they are plotted in Fig. 3.1. Then we use the FFT to compute the solutions on the same grids described above, and their error norm is the same as shown in Fig. 3.1. Besides, the solutions obtained by the FFT is very close to the solution obtained by the trapezoidal rule when they are computed on the same grid ( the absolute difference between them is less than  $10^{-10}$ ).

Therefore, it can be concluded that the two methods have the same accuracy. Moreover, it is observed that the error norm is approximately  $10^{-15}$  when  $K > 1025$  which is sufficiently small to conclude that the solution has very good accuracy.

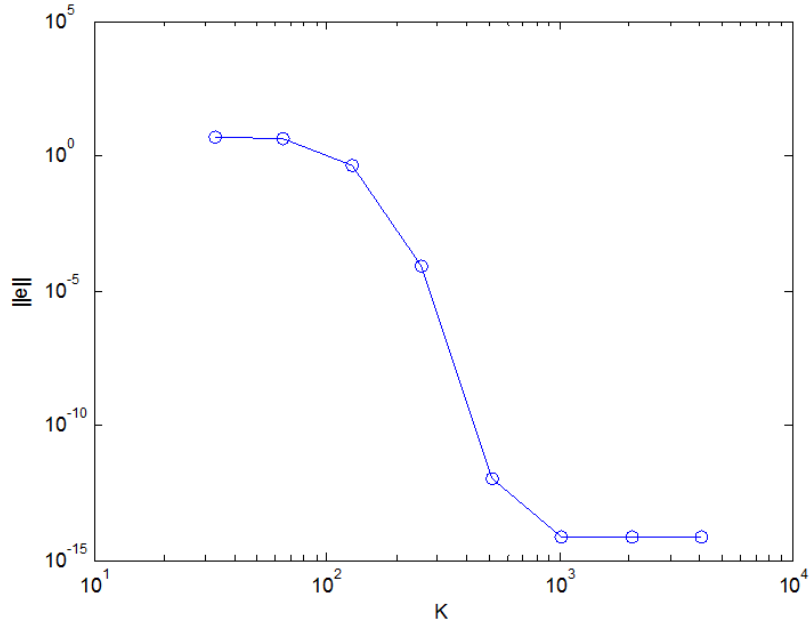


Figure 3.1: The plot of error norms for different number of grid nodes. Parameters are  $\alpha_0 = 1.0$ ,  $\mu = 0$ ,  $\alpha = 0.1$ ,  $t = 20$ ,  $L = 15$ ,  $r = 7.0$ .

Now we consider a system of two interacting species  $N$  and  $P$  which is given by

$$N_{t+1}(x) = \int_{\Omega} k(x, y) f(N_t(y), P_t(y)) dy, \quad (3.50)$$

$$P_{t+1}(x) = \int_{\Omega} k(x, y) g(N_t(y), P_t(y)) dy, \quad (3.51)$$

where

$$f(N_t, P_t) = \frac{a(N_t)^2}{1 + b(N_t)^2} \cdot \exp(-P_t), \quad (3.52)$$

$$g(N_t, P_t) = N_t P_t, \quad (3.53)$$

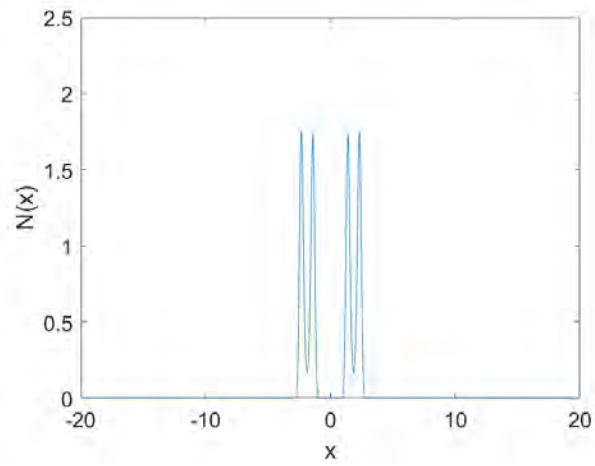
with the initial condition:

$$N_0(x) = \frac{a + \sqrt{(a^2 - 4b)}}{2b} \text{ or } -1 \leq x \leq 1 \text{ and } N_0(x, y) = 0 \text{ otherwise,} \quad (3.54)$$

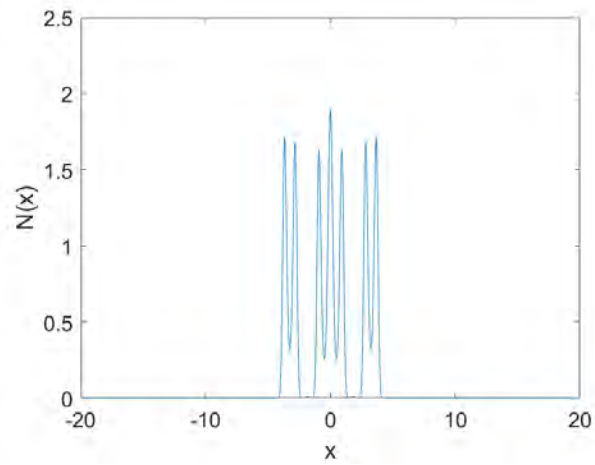
$$P_0(x) = \ln\left(\frac{a}{b+1}\right) \text{ for } 0.1 \leq x \leq 0.1 \text{ and } P_0(x) = 0 \text{ otherwise.} \quad (3.55)$$

Taking  $a = 4.5$  and  $b = 1.0$ , we can obtain the following results by FFT method:

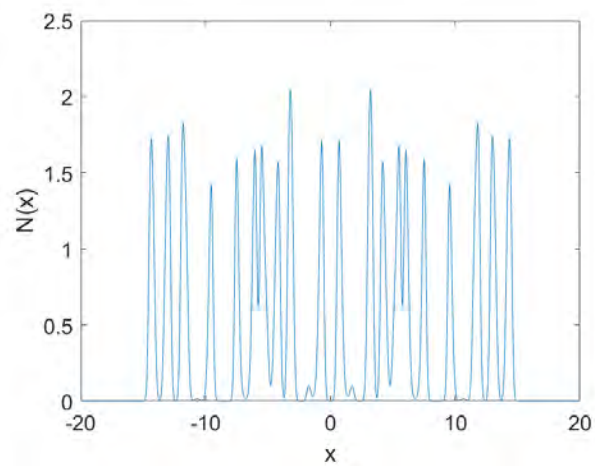
This chapter introduced a system of kernel-based integro-difference equations that describes biological invasion of stage-structured species. Both short-distance dispersal and long-distance dispersal are considered in this model. This model cannot be solved analytically, therefore we employ numerical methods to solve this problem. We introduced the FFT method in section 3.4 as it is much more efficient than numerical integration. Then in section 3.5 we validate the FFT method and the results show that the numerical solution converges as we refine a computational grid. Now that we are certain about the accuracy of our numerical approach we can move to simulation of more sophisticated 2-D problem.



(a)



(b)



(c)

Figure 3.2: The density distribution of species  $N$  at time (a)  $t = 20$ , (b)  $t = 40$  and (c)  $t = 200$ ; parameters are  $a = 4.5$ ,  $b = 1$ ,  $\alpha_N = 0.1$ ,  $\alpha_P = 0.125$ ,  $L = 20$ .

## CHAPTER 4

# SIMULATION RESULTS FOR STAGE-STRUCTURED POPULATION WITH SHORT-DISTANCE AND LONG-DISTANCE DISPERSAL

In chapter 3 we have demonstrated that the FFT method can be used to solve the integro-difference equations accurately and efficiently. This chapter will solve the the two-dimensional system (3.5)-(3.10) at different parameter values and show some typical spatial patterns. We will investigate short distance and long distance dispersal in the two-dimensional case in this chapter. Some spatial distributions have a population front while some spatial patterns do not have, the latter is called patchy distribution. Simulation results in this chapter show that patchy invasion can be observed in the short distance dispersal as well as in the long distance dispersal.

Now we apply the FFT to solving the two dimensional system (3.5)-(3.10)

$$N_{t+1}(\mathbf{r}) = \int_{\Omega} f(N_t(\mathbf{r}'), P_t(\mathbf{r}')) k_N(\mathbf{r}, \mathbf{r}') d\mathbf{r}',$$
$$P_{t+1}(\mathbf{r}) = \int_{\Omega} g(N_t(\mathbf{r}'), P_t(\mathbf{r}')) k_P(\mathbf{r}, \mathbf{r}') d\mathbf{r}',$$

where

$$f(N_t, P_t) = \frac{a(N_t)^2}{1 + b(N_t)^2} \exp(-P_t),$$

$$g(N_t, P_t) = N_t P_t.$$

Firstly we choose a dispersal domain  $\Omega = [-L, L] \times [-L, L]$  and discretise the domain by  $K \times K$  grids nodes uniformly, so that

$$x_{k+1} = x_k + \Delta, \quad x_1 = -L, \quad x_K = L, \quad \text{and} \quad y_{k+1} = y_k + \Delta, \quad y_1 = -L, \quad y_K = L, \quad (4.1)$$

where  $\Delta = 2L/(K - 1)$  is the lattice spacing.

When implementing numerical methods, it is important to be careful about the computational errors. It is therefore necessary to choose a sufficiently large number of grid nodes  $K$  to ensure that the lattice spacing  $\Delta$  is small enough.

The computational domain  $\Omega$  should be large enough so that few individuals are moving out of the domain during the observation period (up to  $t=200$ ), i.e., the population front must be sufficiently far from the domain boundary. We performed simulations up to  $t = 200$  to eliminate the impact of initial conditions on the spatio-temporal dynamics. For a Gaussian kernel that decays rapidly,  $L = 20$  is sufficiently large to guarantee that the population is not close to the domain boundary at time  $t = 200$  in our test cases provided with certain parameters and initial conditions as specified in (3.16)-(3.17), where we have  $N_2^* = \frac{a + \sqrt{a^2 - 4b}}{2b}$ ,  $P^* = \ln(\frac{a}{b+1})$ . In this thesis we choose  $2^{10} \times 2^{10}$  nodes which can ensure that computational errors are small enough, i.e. if we further refine the grid, then the computational error does not drop down significantly. For Cauchy kernels which have fatter tails, the spread speed of the population is

much faster so we have to choose a larger domain in order to be able to make our computation up to time  $t = 200$  and guarantee that the population has not approach the domain boundary yet, therefore we take  $L = 80$  and  $2^{12} \times 2^{12}$  nodes.

From the analysis of the non-spatial system in Fig. 2.5, it is known that for parameters  $(a, b)$  from domain 1, the population dynamics tend to be non-oscillatory continuous front (the density is constant behind the front); in domain 2, the population dynamics are oscillatory; in domain 3, the only attractor is extinction state. Now we are interested in whether these conclusions are the same when we deal with two-dimensional system (3.5)-(3.10).

Due to the property of dispersal kernels (3.11), (3.14) and (3.15) the population density is greater than zero anywhere in the domain at any time  $t > 0$ . However, far away from the population front the density values are very low and can be neglected. In the population density distributions figures Fig. 4.1, Fig. 4.4, Fig. 4.6 and Fig. 4.7, the areas marked in white colour implies the population density is zero. But it does not mean that of density is strictly zero in the white areas. Hence, a ‘cutoff’ is applied to low densities, see (4.2). The chosen cutoff value for these figures is 0.05 (this choice of the cutoff value is further justified in Chapter 6, which means that densities below this value are treated as zero.

The modified population distribution  $\hat{N}$  is given below:

$$\hat{N}(x, y) = N(x, y) \quad \text{for } N > C, \quad \hat{N}(x, y) = 0 \quad \text{for } N \leq C, \quad (4.2)$$

where  $C$  is the cutoff value. In this chapter, we choose  $C = 0.05$ , which is approximately 1% of the maximum density value  $N_{max}$ , further discussion of the cutoff value will be provided in Chapter 6.

## 4.1 Simulation results for the Gaussian dispersal kernel

In this section we solve the problem (3.5)-(3.10) with Gaussian kernel (3.11) and parameters  $\alpha_N$  and  $\alpha_P$  have been chosen the same as in [77], where  $\alpha_N = 0.1$ ,  $\alpha_P = 0.125$ . We vary parameters  $a$  and  $b$  in the domains 1, 2, and 3 in Fig. 2.5 and obtain the following conclusions.

For parameters from domain 1 of Fig. 2.5, the population density behind the front is constant, which is identical to non-spatial model (2.65)-(2.66). An example is shown in Fig. 4.1 where it is observed that the prey population is distributed in a circle at time  $t = 50$ ,  $t = 100$ ,  $t = 150$  and  $t = 200$ . Fig. 4.2 gives a cross-section view of prey distribution when  $x = 0$ . Fig. 4.3(a) records the corresponding radius at time  $t = 50$ ,  $t = 100$ ,  $t = 150$  and  $t = 200$ , and it is known that the spread speed of prey and predator are constants (the speed of predator are not presented here) [39]. The propagation speed has been evaluated in our numerical simulation as follows: from  $t = 50$  to  $t = 200$ , the radius of prey distribution increases by  $6.7969 - 2.7734 = 4.0235$ , so the spreading speed is  $v_{prey} = (6.7969 - 2.7734)/(200 - 50) = 0.0268$ . Therefore, it can be predicted where the population front is located at each moment. Moreover, once the species density arrives at the constant value and this value does not change any longer. Thus, the spatial distribution of prey and predator is possible to predict at any time without complicated computation.

For the parameters from domain 2 of Fig. 2.5, the spatial density distribution behind the front oscillates, which is the same as the non-spatial model (2.65)-(2.66). Fig. 4.4 shows an example of oscillatory distribution for  $a = 6.0$  and  $b = 2.4$  and Fig. 4.5 is the cross-sectional view of it. Although the spreading speed of prey appears to be constant (see Fig. 4.3(b)), we cannot predict the exact spatial shape of the density distribution at any moment of time.

For parameters in domain 3, the population density distributions are more complicated.



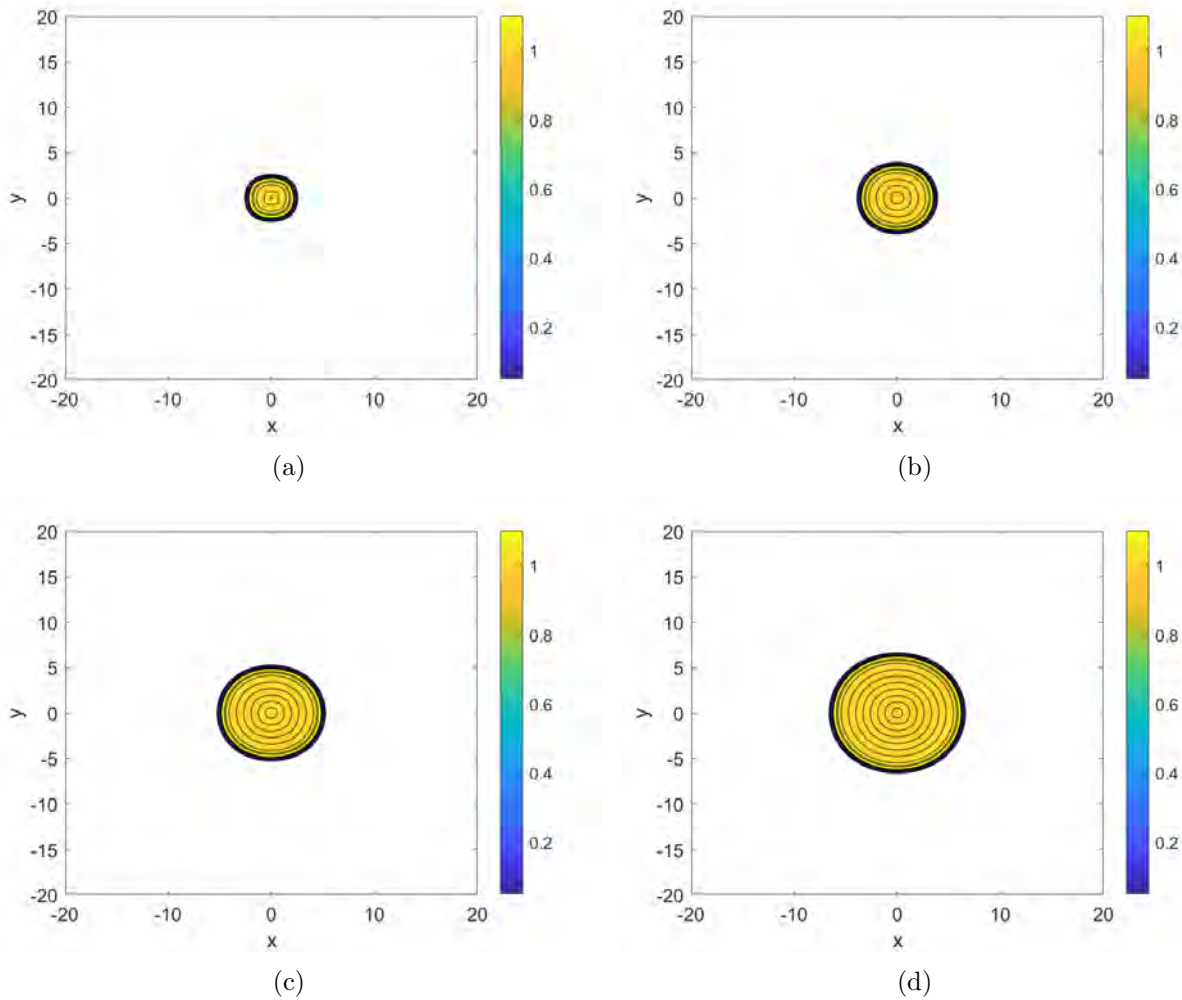


Figure 4.1: Examples of spatial distributions of the prey species in a spatial domain where  $x \in [-20, 20]$  and  $y \in [-20, 20]$  at time (a)  $t = 50$ , (b)  $t = 100$ , (c)  $t = 150$  and (d)  $t = 200$  respectively. Parameters are  $\alpha_N = 0.1$ ,  $\alpha_P = 0.125$ ,  $a = 4.0$  and  $b = 2.4$ . Initial conditions are given by (3.16)-(3.17).

Some examples are shown in Fig. 4.6. Fig. 4.6(a) and Fig. 4.6(c) are examples of patchy invasion, so called because they do not have a continuous population front which separates the invaded and non-invaded areas. The spatial patterns in Fig. 4.6(b), and Fig. 4.6(d)-Fig. 4.6(f) have continuous fronts, yet their topology are different. In Fig. 4.6(b) and Fig. 4.6(d), the population fronts are concave, whereas the distributions in Fig. 4.6(e) and Fig. 4.6(f) have convex continuous fronts.

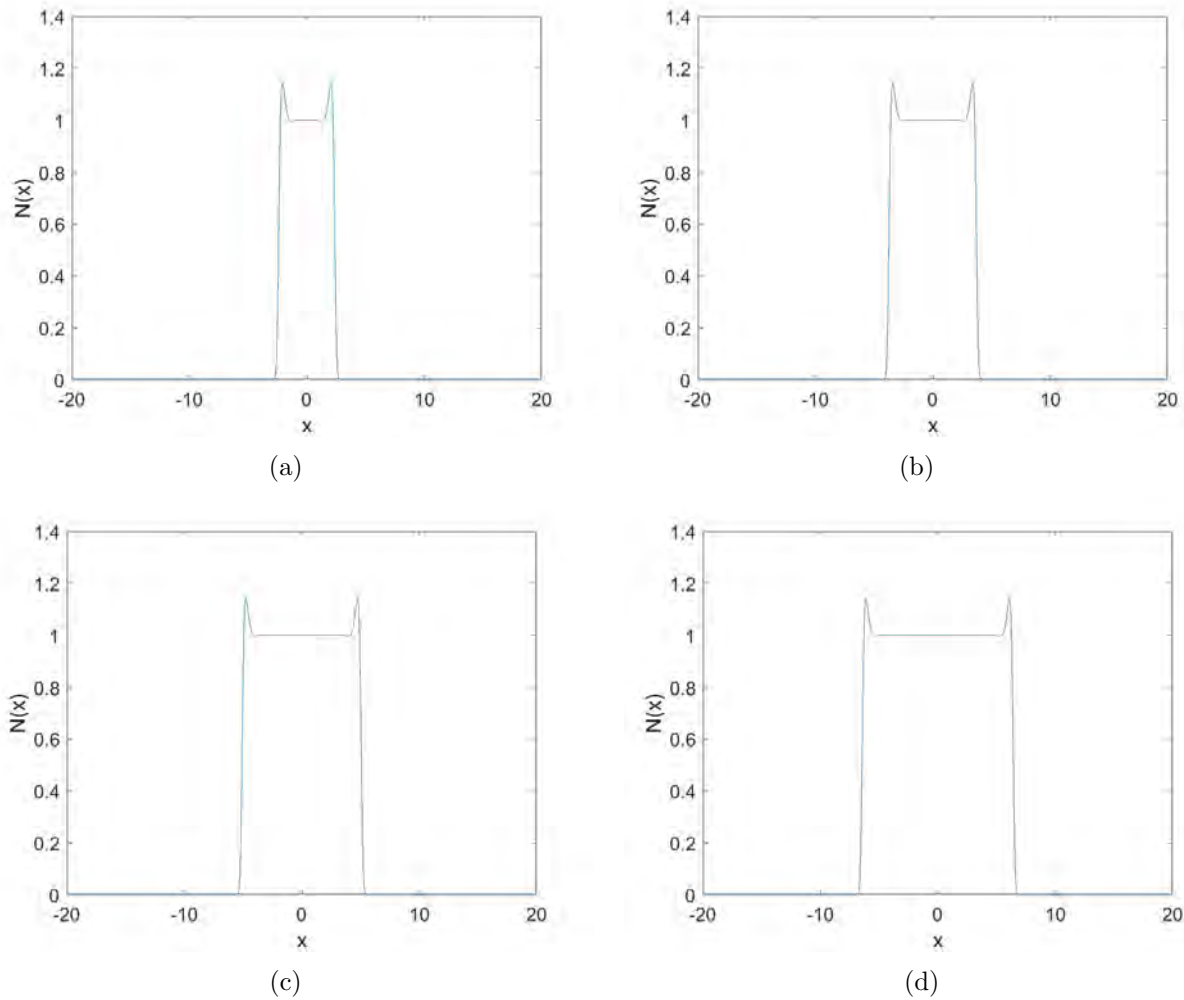


Figure 4.2: A cross-sectional view of Fig. 4.1 at  $y = 0$ .

## 4.2 Simulation results for Cauchy dispersal kernel

When long-distance dispersal frequently occurs during the invasion, the Cauchy kernels that have fat tails are considered as such dispersal kernels can be used to simulate long-distance dispersal [77]. We performed numerical simulations for Cauchy kernel type I (3.14) where  $\beta_N = 0.0488$  and  $\beta_P = 0.098$  at different time steps and the results are shown in Fig. 4.7. This shows that patchy invasion can also occur for long-distance dispersal.

We simulated various invasion regimes in this chapter and obtained various spatial patterns. We have shown that, in a certain parameter range, the invasion takes place by a somewhat

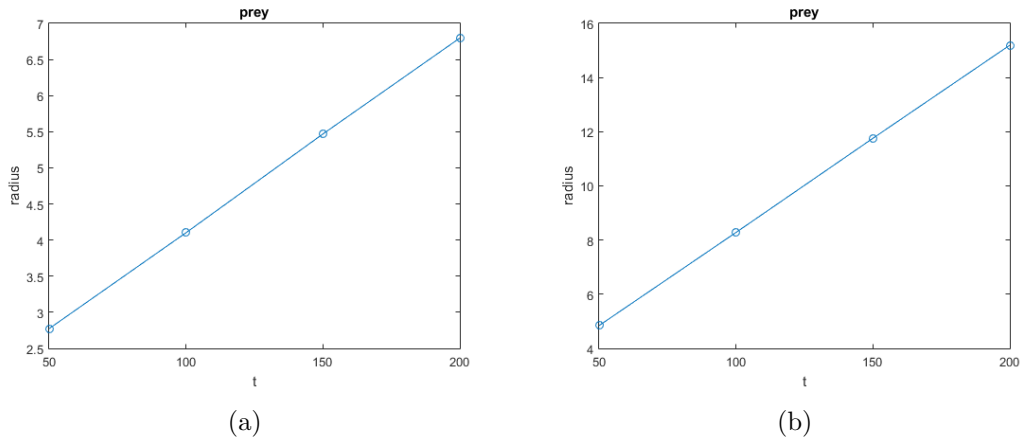


Figure 4.3: Radius of prey density distribution at time  $t=50, 100, 150$  and  $t=200$  respectively. Parameters are (a)  $a = 4.0, b = 2.4$  and (b)  $a = 6.0, b = 2.4$ .

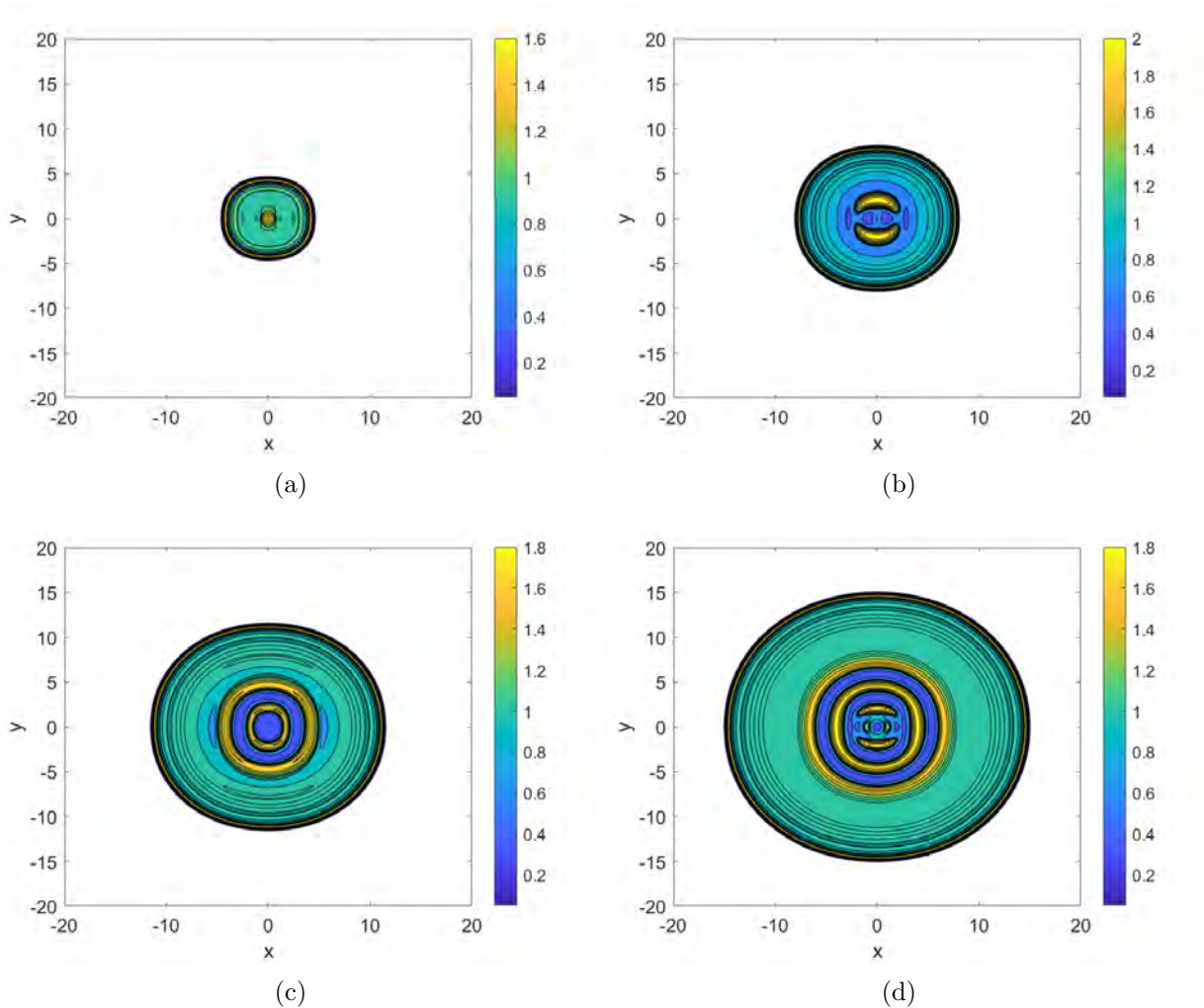
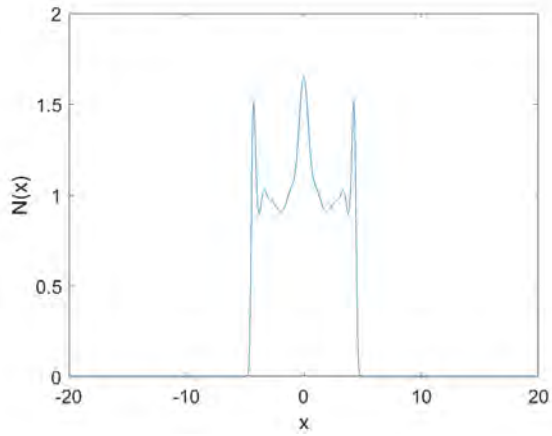
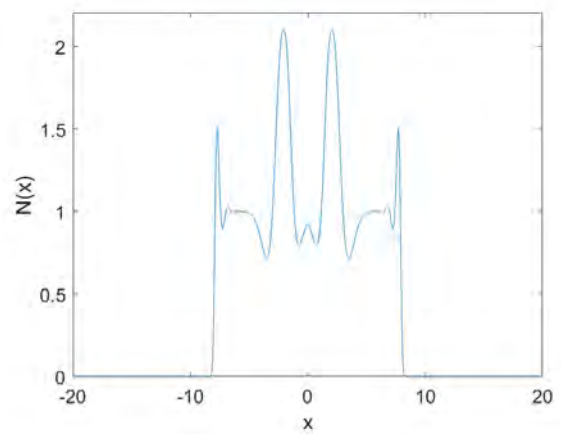


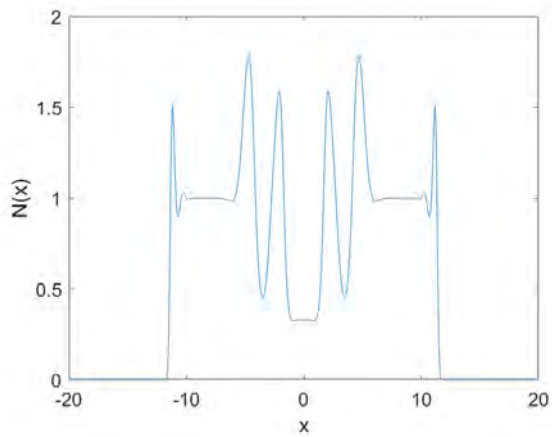
Figure 4.4: Examples of spatial distributions in a spatial domain where  $x \in [-20, 20]$  and  $y \in [-20, 20]$ . Contour plots of prey density  $N_t(x, y)$  at time (a)  $t = 50$ , (b)  $t = 100$ , (c)  $t = 150$  and (d)  $t = 200$  respectively. Parameters are  $\alpha_N = 0.1, \alpha_P = 0.125, a = 6.0$  and  $b = 2.4$ . Initial conditions are given by (3.16)-(3.17).



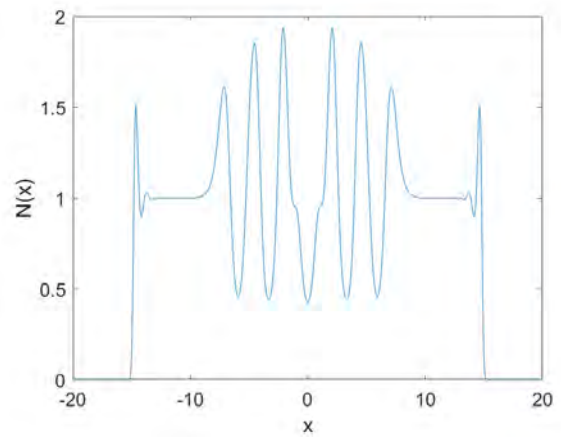
(a)



(b)



(c)



(d)

Figure 4.5: A cross-sectional view of Fig. 4.4 at  $x = 0$ .

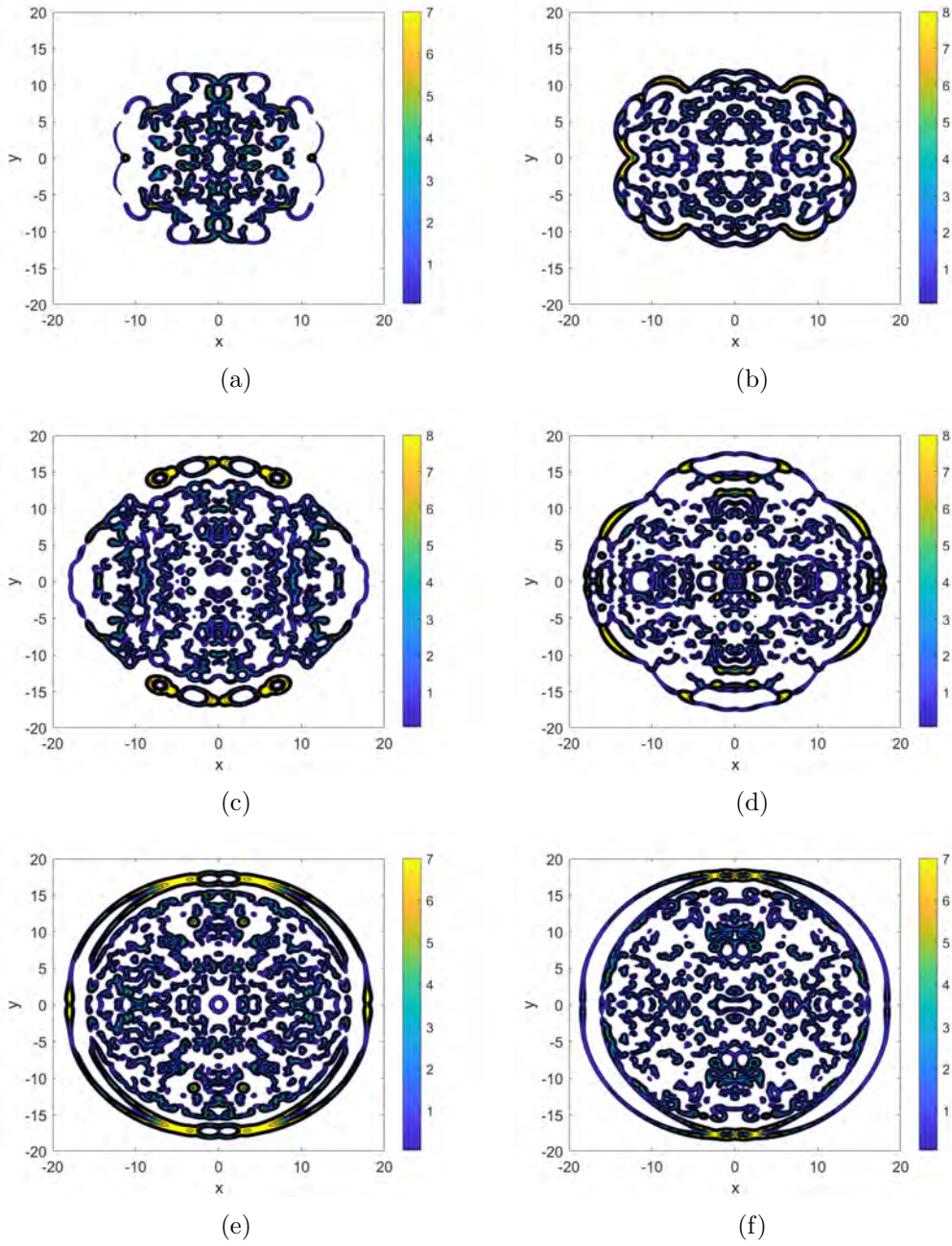


Figure 4.6: Examples of spatial distributions in a spatial domain where  $x \in [-20, 20]$  and  $y \in [-20, 20]$ . Contour plots of prey density  $N(x, y)$  generated at time  $t = 200$ , as obtained for the Gaussian kernel (3.11) and initial conditions (3.16)-(3.17). Parameters are  $\alpha_N = 0.1$ ,  $\alpha_P = 0.125$  and (a)  $a = 6.2$ ,  $b = 0.700$ ; (b)  $a = 6.2$ ,  $b = 0.704$ ; (c)  $a = 6.2$ ,  $b = 0.720$ ; (d)  $a = 6.2$ ,  $b = 0.724$ ; (e)  $a = 6.2$ ,  $b = 0.740$ ; (f)  $a = 6.2$ ,  $b = 0.750$ .

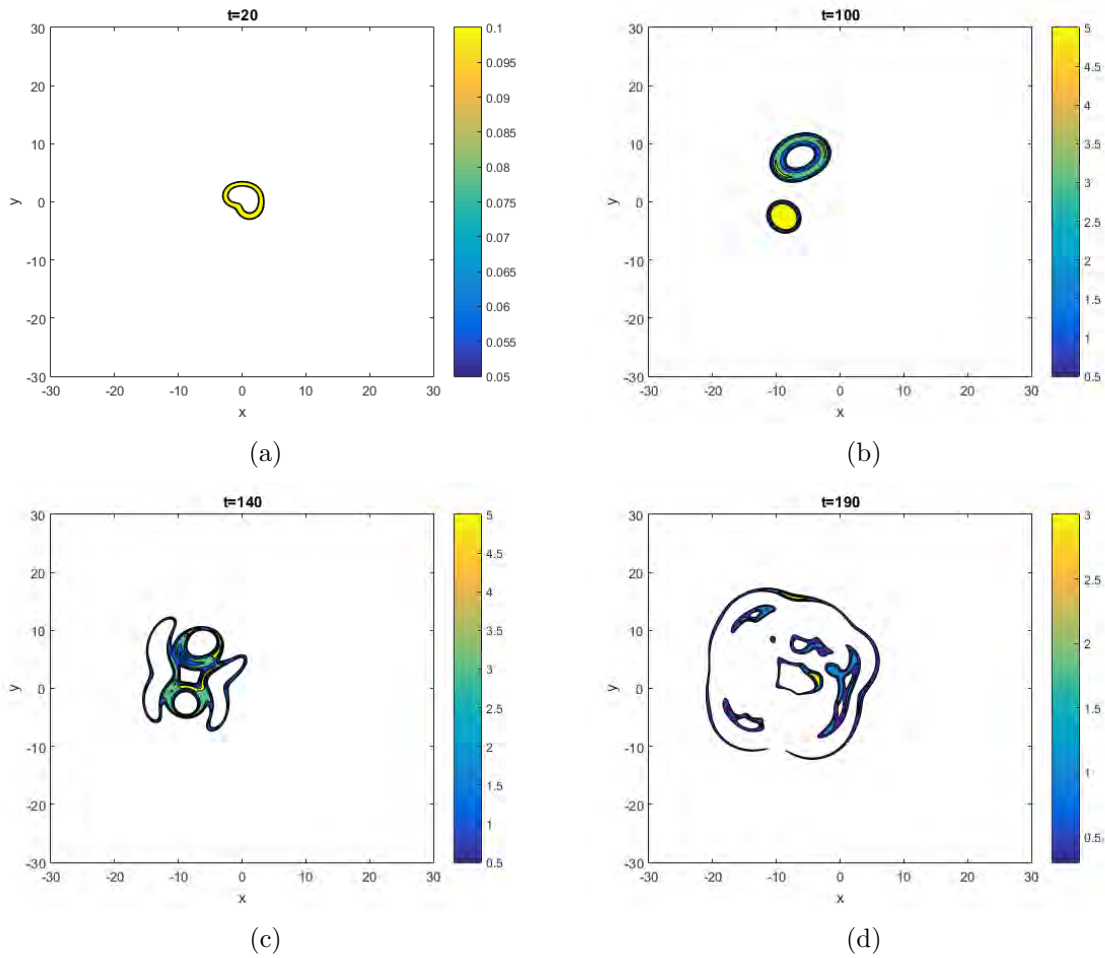


Figure 4.7: Contour plots of prey density  $N(x, y)$  at time (a)  $t = 20$ , (b)  $t = 100$ , (c)  $t = 140$  and  $t = 190$ , as obtained for Cauchy kernel and asymmetric initial conditions (3.18)-(3.19). Parameters are  $\beta_N = 0.0488$ ,  $\beta_P = 0.098$ ,  $a = 4.5$  and  $b = 0.68$ .

unusual scenario where there is no population front and the species are spreading into space through the dynamics of separate patches of high population density. This scenario has been called ‘the patchy invasion’ in [35] and in this chapter we confirm formation of separate patches when both Gaussian and Cauchy dispersal kernels are used in the model. It is important to distinguish between patchy distributions and distributions that have a continuous population front, as patchy distributions are much more challenging in monitoring the biological invasions.

## CHAPTER 5

# CLASSIFICATIONS OF SPATIAL PATTERNS

In chapter 4 we noticed a special invasion regime that does not have a continuous population front, which is called patchy invasion. Simulation results in Chapter 4 show that patchy invasion occurs inside a particular parameter domain (where the corresponding non-spatial population goes to extinction, cf. domain 3 in Fig. 2.5) but little is known about the fine structure of the parametric plane. However, identification of relevant parameters is very important for the purposes of monitoring and control. Therefore, the first goal of this chapter is to introduce a classification of spatial patterns and reveal the corresponding structure of the parameter space by performing extensive numerical simulations.

Another goal of this chapter is to distinguish between continuous-front spatial patterns and patchy spatial pattern, because agglomeration of separate patches located close to each other looks often like a continuous front spatial distribution and visual inspection of those patterns may easily result in a wrong conclusion about the type of biological invasion. Hence introduction of more reliable means of identification of spatial patterns is required and in this chapter we investigate several topological characteristics that can potentially help us to distinguish between continuous front and patchy spatial patterns. It will be shown that, among the other topological

quantities such as the fragmentation rate and the density of objects, the number of objects in the binary map of a spatial distribution remains the most reliable topological characteristics when it is required to conclude whether or not spatial pattern is a patchy structure.

## 5.1 Structure of parametric plane

In order to investigate the spatial patterns for various pairs of parameters  $a$  and  $b$  in the model (3.5)-(3.10), we performed numerical simulations for the parameters  $a$  and  $b$  in the range  $a \in [3.9, 6.5]$  and  $b \in [0.686, 0.766]$ , which is a sub-domain taken from domain 3 in Fig. 2.5. I varied parameters  $a$  and  $b$  in this sub-domain with an increment of  $\delta a = 0.1$  and  $\delta b = 0.002$ . The spatial patterns are examined for each pair of  $(b, a)$  at the moment  $t = 200$ . Our numerical simulations show that this time is sufficient for the spatial pattern to establish, i.e., the spatial pattern will not transform from patchy distribution to continuous front distribution at times  $t > 200$ .

In this chapter we first consider the symmetrical initial conditions given in equations (3.16)-(3.17) and the spatial patterns of each computation are summarised in Fig. 5.1. In this figure, the blue region indicates that populations become extinct for parameters located in this region. The green region means that patchy invasion occurs when the parameters are chosen from this range. The orange region shows that every distribution here has a concave continuous front. And the grey region indicates that a convex continuous front can be found for each distribution.

It can be concluded that for any  $a$  from Fig. 5.1, the population goes to extinction when  $b$  is less than  $b_1 = 0.688$  while the spatial pattern has a convex continuous front for  $b > b_2 = 0.752$ . But there are no threshold values that separate continuous-front spatial distributions from patchy spatial distributions. The spatial patterns between  $b_1$  and  $b_2$  are complicated. While



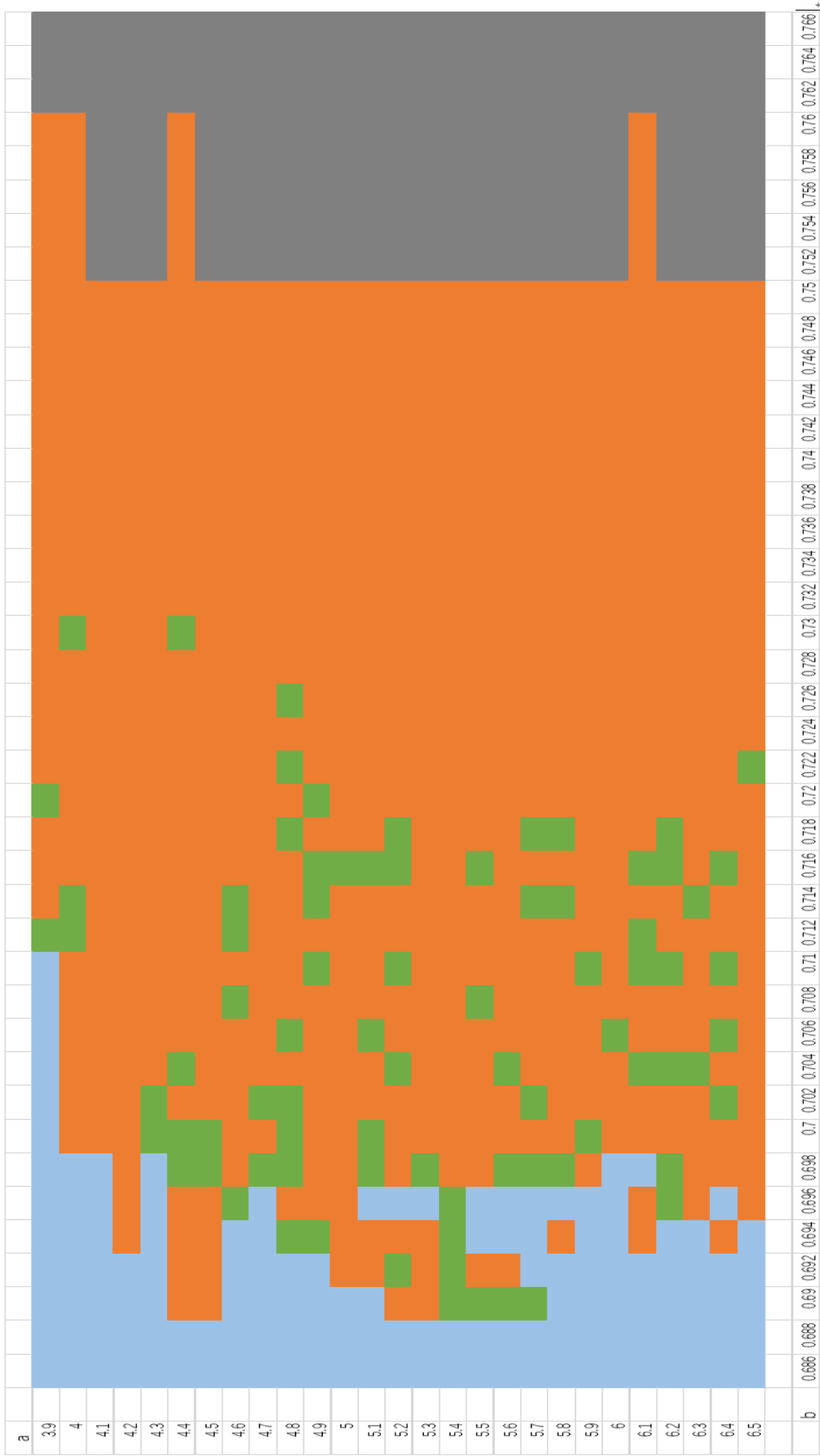


Figure 5.1: The spreadsheet of spatial density distributions in domain 3. For  $a \in [3.9, 6.5]$ ,  $b \in [0.686, 0.766]$ . The blue area corresponds to extinction. The green region represents patchy invasion. The orange area indicates there is a concave continuous front. The grey area indicates there exists a convex continuous front.

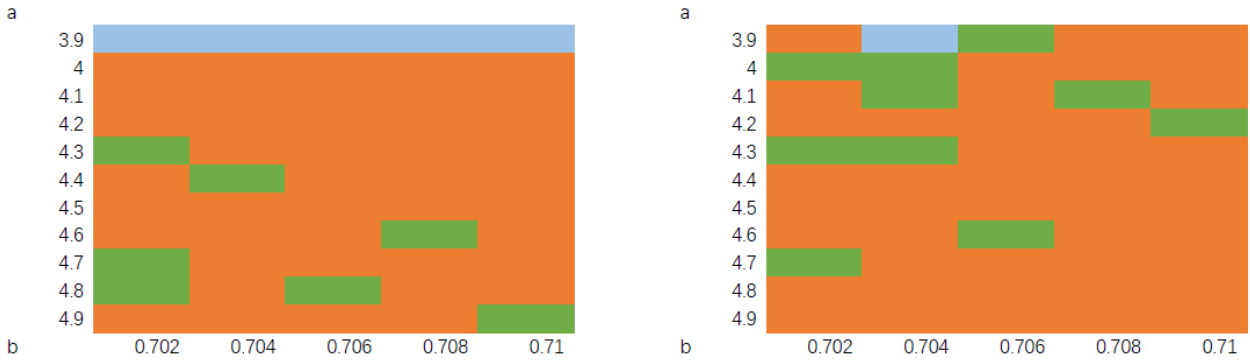


Figure 5.2: Comparison of spatial patterns under symmetrical initial conditions (3.16)-(3.17) (left), and asymmetrical initial conditions (3.18)-(3.19) (right). Parameters varies in  $a \in [3.9, 4.9]$ ,  $b \in [0.702, 0.71]$

the distribution with concave continuous front occurs in the range  $b \in [0.688, 0.752]$ , the patchy invasion only appears in a narrower range  $b \in [0.688, 0.732]$ .

The results in Fig. 5.1 are obtained with the symmetrical initial conditions (3.16)-(3.17). Then we are going to investigate the simulation results with the asymmetrical initial conditions (3.18)-(3.19). Fig. 5.2 shows the comparison between the results obtained with symmetrical and asymmetrical initial conditions; all of them were obtained at time  $t = 200$  and  $3.9 \leq a \leq 4.9$ ,  $0.702 \leq b \leq 0.710$ . It can be seen from the figure that the two maps are not the same. Thus it can be concluded that different initial conditions will result in different spatial patterns.

## 5.2 Topological indices

In this section, three topological indices are employed to classify the different kinds of spatial patterns. These indices are the number of objects, the fragmentation rate and the density of objects.

### 5.2.1 The number of objects

In the previous sections, spatial patterns were classified visually, which is not always reliable. A reliable technique was therefore developed to distinguish whether or not a spatial pattern is patchy. We define an object as a region of the non-zero density with a closed external boundary. A continuous front density distribution can be classified as a single object. The MATLAB code of this technique is given in Appendix. It can count the number of separate patches. In order to implement this technique, the original density distribution has to be converted to a binary matrix. Equation (5.1) illustrates how a matrix can be converted to a binary matrix.

$$\tilde{N}(x, y) = 1 \quad \text{for} \quad N(x, y) > C, \quad \text{and} \quad \tilde{N}(x, y) = 0 \quad \text{for} \quad N(x, y) \leq C \quad (5.1)$$

where  $C$  is the cut-off value.

Two examples of binary image are shown in Fig. 5.3. Both of them are obtained at the cutoff value  $C = 0.05$ . Fig. 5.3(a) shows a concave front distribution while Fig. 5.3(b) shows a patchy distribution. It is clear that Fig. 5.3(a) has a continuous front that indicates there is only one object in this graph; for Fig. 5.3(b), it can be seen that there are three objects in the graph.

Then we investigate the number of objects of spatial patterns for each pair of parameters  $(b, a)$  in the range  $a \in [3.9, 6.5]$  and  $b \in [6.90, 7.38]$  because we conclude from our previous numerical simulations that patchy distributions may appear for this range of parameters. The increment in parameter  $a$  is  $\delta a = 0.1$  and the increment in parameter  $b$  is  $\delta b = 0.002$  as before. All solutions were obtained at  $t = 200$  as well. The results are shown in Fig. 5.4. From the table,

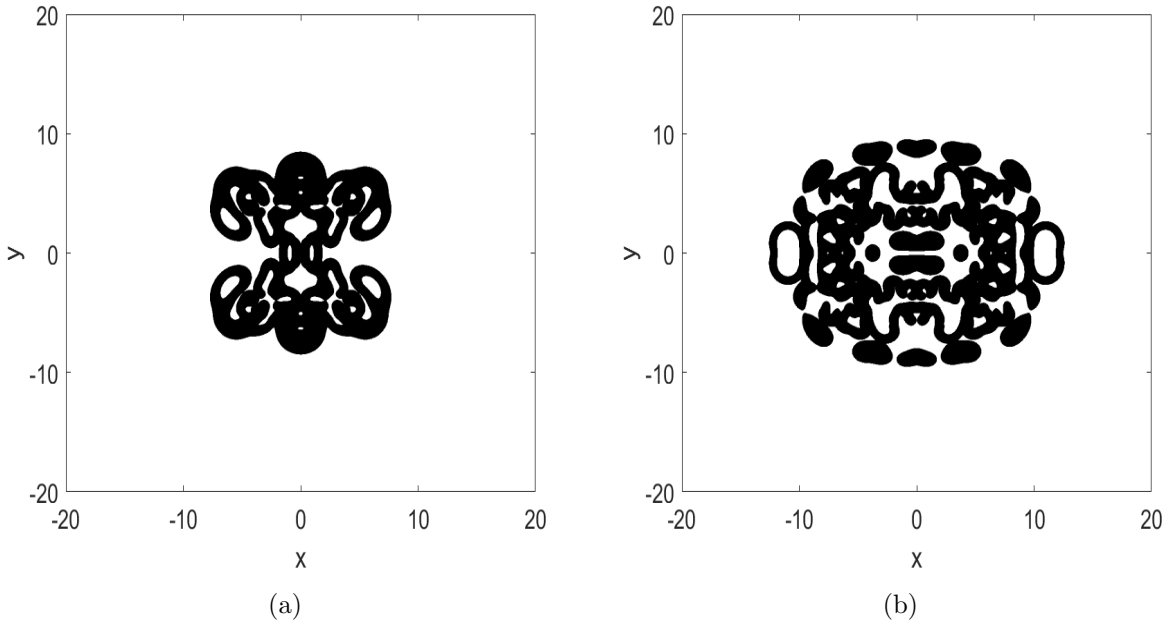


Figure 5.3: Examples of Binary images in a spatial domain where  $x \in [-20, 20]$  and  $y \in [-20, 20]$  obtained at  $C_0 = 0.05$  and  $t = 200$ . (a) A concave-front distribution obtained for parameters  $a = 4.1$  and  $b = 0.71$ . (b) A patchy distribution obtained for parameters  $a = 4.0$  and  $b = 0.73$ .

it can be concluded that no particular threshold exists that separates the patchy distributions from the continuous front patterns. Moreover, from Fig. 5.4 it can be seen that the spatial patterns are very sensitive to the parameters  $a$  and  $b$ . For instance, when  $a = 5.8$  and  $b = 0.710$  the solution is found to be patchy distribution at  $t = 200$ . However, if  $b$  is slightly increased or decreased by 0.002, the corresponding density distribution has a continuous front.

The result of Fig. 5.4 is obtained at the cut-off value  $C = 0.05$ , it would change when the cut-off value varies. However, we mention it here that, for those values of the number of objects that equal to 1 (i.e. the corresponding spatial pattern has a continuous population front), they remains 1 even at a relatively large cut off value (e.g.  $C = 0.2$ ); for those values of the number of objects that larger than 1 (i.e. the patchy distribution), the values will change if we slightly increase the cul-off value. The investigation on the sensitivity of the spatial patterns to the cut-off value will be discussed in Chapter 6.

| <b>a</b>    |     |      |      |      |      |    |      |      |      |      |     |      |      |      |      |     |      |      |      |      |     |      |      |      |      |
|-------------|-----|------|------|------|------|----|------|------|------|------|-----|------|------|------|------|-----|------|------|------|------|-----|------|------|------|------|
| 3.9         | 0   | 0    | 0    | 0    | 0    | 0  | 0    | 1    | 1    | 0    | 0   | 8    | 1    | 1    | 1    | 5   | 1    | 5    | 1    | 1    | 1   | 1    | 1    |      |      |
| 4           | 0   | 0    | 0    | 0    | 0    | 1  | 1    | 1    | 0    | 0    | 3   | 3    | 11   | 1    | 1    | 1   | 7    | 13   | 3    | 1    | 3   | 1    | 1    |      |      |
| 4.1         | 0   | 0    | 0    | 1    | 1    | 1  | 0    | 0    | 1    | 1    | 1   | 6    | 1    | 3    | 1    | 1   | 1    | 1    | 1    | 1    | 1   | 1    | 3    |      |      |
| 4.2         | 0   | 0    | 1    | 1    | 0    | 0  | 0    | 1    | 1    | 1    | 1   | 1    | 1    | 9    | 1    | 1   | 1    | 1    | 1    | 1    | 1   | 3    | 1    |      |      |
| 4.3         | 0   | 3    | 1    | 0    | 0    | 2  | 13   | 1    | 1    | 1    | 1   | 7    | 1    | 3    | 1    | 1   | 1    | 1    | 1    | 1    | 1   | 1    | 1    |      |      |
| 4.4         | 7   | 1    | 0    | 0    | 15   | 5  | 1    | 7    | 1    | 1    | 1   | 1    | 3    | 3    | 1    | 1   | 1    | 1    | 1    | 1    | 3   | 1    | 1    |      |      |
| 4.5         | 1   | 0    | 0    | 0    | 5    | 3  | 1    | 1    | 1    | 7    | 1   | 3    | 11   | 1    | 1    | 1   | 11   | 9    | 1    | 1    | 1   | 1    | 1    |      |      |
| 4.6         | 0   | 0    | 0    | 3    | 1    | 1  | 1    | 1    | 1    | 2    | 1   | 7    | 3    | 1    | 1    | 9   | 3    | 11   | 1    | 1    | 1   | 1    | 1    |      |      |
| 4.7         | 0   | 0    | 1    | 1    | 3    | 1  | 5    | 1    | 1    | 1    | 1   | 1    | 1    | 1    | 5    | 7   | 3    | 3    | 1    | 1    | 1   | 1    | 1    |      |      |
| 4.8         | 0   | 0    | 5    | 1    | 14   | 3  | 9    | 1    | 5    | 1    | 1   | 1    | 1    | 1    | 11   | 1   | 5    | 1    | 1    | 1    | 1   | 1    | 1    |      |      |
| 4.9         | 0   | 1    | 5    | 1    | 1    | 1  | 1    | 1    | 1    | 1    | 1   | 1    | 3    | 7    | 1    | 3   | 1    | 1    | 1    | 1    | 1   | 1    | 1    |      |      |
| 5           | 0   | 9    | 1    | 1    | 1    | 1  | 1    | 1    | 1    | 1    | 1   | 1    | 1    | 1    | 19   | 1   | 1    | 1    | 1    | 1    | 1   | 1    | 1    |      |      |
| 5.1         | 0   | 1    | 1    | 0    | 13   | 3  | 1    | 1    | 3    | 1    | 1   | 1    | 7    | 3    | 1    | 5   | 1    | 1    | 1    | 1    | 1   | 1    | 1    |      |      |
| 5.2         | 1   | 5    | 1    | 0    | 1    | 1  | 1    | 7    | 1    | 1    | 7   | 1    | 29   | 7    | 41   | 1   | 1    | 1    | 1    | 1    | 1   | 1    | 1    |      |      |
| 5.3         | 1   | 1    | 1    | 0    | 3    | 1  | 1    | 1    | 1    | 1    | 1   | 1    | 1    | 7    | 1    | 1   | 1    | 1    | 1    | 1    | 1   | 1    | 1    |      |      |
| 5.4         | 19  | 7    | 0    | 0    | 1    | 1  | 3    | 1    | 1    | 1    | 1   | 1    | 1    | 1    | 1    | 1   | 1    | 1    | 3    | 1    | 1   | 1    | 1    |      |      |
| 5.5         | 12  | 1    | 0    | 0    | 1    | 1  | 1    | 1    | 1    | 11   | 1   | 1    | 3    | 1    | 1    | 1   | 1    | 1    | 1    | 1    | 1   | 1    | 1    |      |      |
| 5.6         | 15  | 1    | 0    | 0    | 17   | 1  | 1    | 5    | 1    | 1    | 1   | 1    | 5    | 1    | 1    | 1   | 1    | 1    | 1    | 1    | 1   | 1    | 1    |      |      |
| 5.7         | 2   | 0    | 0    | 0    | 5    | 1  | 3    | 1    | 1    | 1    | 1   | 1    | 5    | 1    | 7    | 1   | 1    | 1    | 1    | 1    | 1   | 1    | 1    |      |      |
| 5.8         | 0   | 0    | 3    | 0    | 31   | 1  | 1    | 1    | 1    | 1    | 13  | 1    | 21   | 1    | 17   | 1   | 1    | 1    | 1    | 1    | 1   | 1    | 1    |      |      |
| 5.9         | 0   | 0    | 0    | 0    | 1    | 5  | 1    | 1    | 1    | 1    | 5   | 1    | 1    | 1    | 1    | 1   | 1    | 1    | 1    | 1    | 1   | 1    | 1    |      |      |
| 6           | 0   | 1    | 0    | 0    | 0    | 1  | 1    | 1    | 11   | 1    | 1   | 1    | 1    | 1    | 1    | 11  | 1    | 1    | 1    | 1    | 1   | 1    | 1    |      |      |
| 6.1         | 0   | 0    | 1    | 1    | 0    | 1  | 1    | 7    | 1    | 1    | 9   | 25   | 1    | 41   | 1    | 1   | 1    | 1    | 1    | 1    | 1   | 1    | 1    |      |      |
| 6.2         | 0   | 0    | 0    | 0    | 0    | 13 | 5    | 1    | 1    | 19   | 1   | 1    | 11   | 1    | 1    | 7   | 3    | 1    | 1    | 1    | 1   | 1    | 1    |      |      |
| 6.3         | 0   | 0    | 1    | 1    | 0    | 1  | 1    | 1    | 1    | 37   | 1   | 1    | 1    | 1    | 5    | 1   | 1    | 1    | 1    | 1    | 1   | 25   | 1    |      |      |
| 6.4         | 0   | 0    | 0    | 0    | 1    | 0  | 1    | 1    | 16   | 1    | 35  | 1    | 9    | 1    | 1    | 3   | 1    | 1    | 49   | 1    | 1   | 1    | 1    |      |      |
| 6.5         | 0   | 0    | 0    | 0    | 0    | 1  | 1    | 1    | 1    | 1    | 1   | 1    | 1    | 1    | 1    | 1   | 1    | 1    | 5    | 1    | 1   | 1    | 1    |      |      |
| <b>b*10</b> | 6.9 | 6.92 | 6.94 | 6.96 | 6.98 | 7  | 7.02 | 7.04 | 7.06 | 7.08 | 7.1 | 7.12 | 7.14 | 7.16 | 7.18 | 7.2 | 7.22 | 7.24 | 7.26 | 7.28 | 7.3 | 7.32 | 7.34 | 7.36 | 7.38 |

Figure 5.4: The number of objects in the spatial pattern as a function of parameters  $a$  and  $b$ . All solutions in this table is obtained at time  $t = 200$  and cut-off value  $C = 0.05$ .

### 5.2.2 The fragmentation rate and the density of objects

The number of objects is not enough to exhibit detailed information of a spatial pattern, so we introduce the fragmentation rate to measure the fragmented level of a spatial pattern. Consider, for example, two hypothetical spatial patterns shown in Fig. 5.5. The number of objects  $n = 3$  is the same in both patterns. Moreover, the total area of the objects is the same and is equal to 11 units where we consider the area of any square cell equal to one in the figure. However, the fragmentation rate is different. The fragmentation rate in Fig. 5.5a is equal to 0.2, while the fragmentation rate of Fig. 5.5 is 0.4.

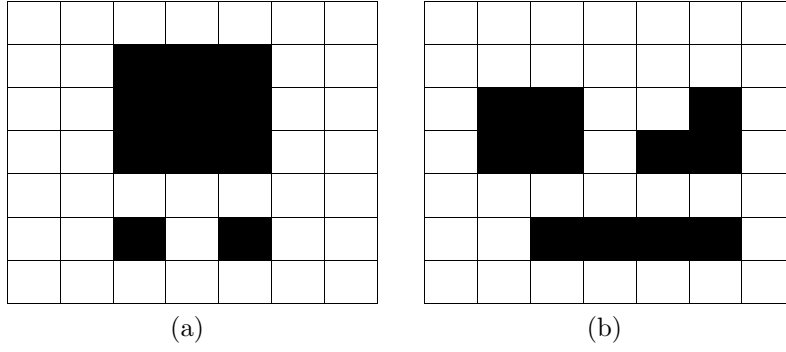


Figure 5.5: Spatial patterns in a hypothetical spatial domain are shown in black. The patterns have the same area of the non-zero density and the same number of objects but their fragmentation rate is different. (a) The fragmentation rate calculated is  $f_r = 0.2$  (b) the fragmentation rate is  $f_r = 0.4$ .

The computation of fragmentation rate is described by equations (5.2)–(5.6) which was developed by Harary [18].

We assume that function  $u(x, y)$  is defined on a square  $\Omega = [-L, L] \times [-L, L]$  and the square is divided into  $N \times N$  identical subsquares  $\Omega_i$ , we compute

$$p(u) = \frac{1}{N \times N} \int_{\Omega} u(x, y) dx dy, \quad (5.2)$$

$$s(u) = \frac{1}{2} \sum_{i=1}^{N^2} \sum_{u_j \in V(u_i)} \mathbb{1}\{u_i(x, y) = u_j(x, y) = 1\}, \quad (5.3)$$

where  $\mathbb{1}\{P\}$  is the indicator function, e.g.  $\mathbb{1}\{P\} = 1$  if  $P$  is true.  $V(u_i)$  is a four-neighbourhood system described by

$$V(u_{i,j}) = \{u_{i-1,j}, u_{i,j-1}, u_{i+1,j}, u_{i,j+1}\}. \quad (5.4)$$

$$B[p] := 2n_+ - \lceil 2\sqrt{n_+} \rceil, \quad (5.5)$$

where  $n_+ = p \times N^2$  and  $\lceil 2\sqrt{n_+} \rceil$  is the smallest integer that is larger than or equal to  $2\sqrt{n_+}$ .

$$fr(u) = 1 - \frac{s(u)}{B[p(u)]}. \quad (5.6)$$

We can think about equation (5.6) as follows. Let 1 in the equation be presented as  $s(u)/s(u)$ , then the second term gives us the measure of to what extent the pattern is uniform. The fragmentation rate (5.6) can range from 0 to 1. The larger the fragmentation rate is, the more fragmented the corresponding spatial pattern is. Fig. 5.5(a) and Fig. 5.5(b) have the same number of objects, population abundance  $p = \frac{11}{49}$ , but have different fragmentation rates. In this example,  $fr(a) < fr(b)$  implies that Fig. 5.5(a) is relatively more aggregated while Fig. 5.5(b) is more fragmented.

The fragmentation rates for all spatial patterns in Fig. 5.4 are summarised in Fig. 5.6 where blank spaces indicate that populations go to extinction for parameters taken from this region.

It can be concluded from the table that, while the fragmentation rate gives us information about the topological structure of a given spatial distribution, the fragmentation rate cannot help us to identify the topological structure of different spatial patterns. In other words, we cannot predict the value of the fragmentation rate if we give a small increment to the problem parameters. For instance, the spatial pattern obtained at  $a = 6.1$  and  $b = 0.712$  is a patchy distribution ( $n = 25$ ) with the fragmentation rate  $f_r = 0.0265$ . Meanwhile, spatial pattern obtained at  $a = 6.1$  and  $b = 0.714$  is a continuous-front distribution ( $n = 1$ ) with the same fragmentation rate  $f_r = 0.0265$ .

It is clear from the data in Fig. 5.6 that, similarly to the number of objects in the spatial pattern, we do not have any distinct continuous range of  $a$  and  $b$  where we can expect formation of patchy patterns only in spatial density distributions. Variations in the fragmentation rate may stem from the fact that a concave continuous front has a complex density distribution

| <b>a</b>    |            |             |             |             |             |          |             |             |             |             |            |             |             |             |             |            |             |             |             |             |            |             |             |             |             |  |  |  |
|-------------|------------|-------------|-------------|-------------|-------------|----------|-------------|-------------|-------------|-------------|------------|-------------|-------------|-------------|-------------|------------|-------------|-------------|-------------|-------------|------------|-------------|-------------|-------------|-------------|--|--|--|
| <b>3.9</b>  |            |             |             |             |             |          |             |             |             |             |            |             |             |             |             |            |             |             |             |             |            |             |             |             |             |  |  |  |
| <b>4</b>    |            |             |             |             |             |          |             |             |             |             |            |             |             |             |             |            |             |             |             |             |            |             |             |             |             |  |  |  |
| <b>4.1</b>  |            |             |             |             |             |          |             |             |             |             |            |             |             |             |             |            |             |             |             |             |            |             |             |             |             |  |  |  |
| <b>4.2</b>  |            |             |             |             |             |          |             |             |             |             |            |             |             |             |             |            |             |             |             |             |            |             |             |             |             |  |  |  |
| <b>4.3</b>  |            |             |             |             |             |          |             |             |             |             |            |             |             |             |             |            |             |             |             |             |            |             |             |             |             |  |  |  |
| <b>4.4</b>  |            |             |             |             |             |          |             |             |             |             |            |             |             |             |             |            |             |             |             |             |            |             |             |             |             |  |  |  |
| <b>4.5</b>  |            |             |             |             |             |          |             |             |             |             |            |             |             |             |             |            |             |             |             |             |            |             |             |             |             |  |  |  |
| <b>4.6</b>  |            |             |             |             |             |          |             |             |             |             |            |             |             |             |             |            |             |             |             |             |            |             |             |             |             |  |  |  |
| <b>4.7</b>  |            |             |             |             |             |          |             |             |             |             |            |             |             |             |             |            |             |             |             |             |            |             |             |             |             |  |  |  |
| <b>4.8</b>  |            |             |             |             |             |          |             |             |             |             |            |             |             |             |             |            |             |             |             |             |            |             |             |             |             |  |  |  |
| <b>4.9</b>  |            |             |             |             |             |          |             |             |             |             |            |             |             |             |             |            |             |             |             |             |            |             |             |             |             |  |  |  |
| <b>5</b>    |            |             |             |             |             |          |             |             |             |             |            |             |             |             |             |            |             |             |             |             |            |             |             |             |             |  |  |  |
| <b>5.1</b>  |            |             |             |             |             |          |             |             |             |             |            |             |             |             |             |            |             |             |             |             |            |             |             |             |             |  |  |  |
| <b>5.2</b>  |            |             |             |             |             |          |             |             |             |             |            |             |             |             |             |            |             |             |             |             |            |             |             |             |             |  |  |  |
| <b>5.3</b>  |            |             |             |             |             |          |             |             |             |             |            |             |             |             |             |            |             |             |             |             |            |             |             |             |             |  |  |  |
| <b>5.4</b>  |            |             |             |             |             |          |             |             |             |             |            |             |             |             |             |            |             |             |             |             |            |             |             |             |             |  |  |  |
| <b>5.5</b>  |            |             |             |             |             |          |             |             |             |             |            |             |             |             |             |            |             |             |             |             |            |             |             |             |             |  |  |  |
| <b>5.6</b>  |            |             |             |             |             |          |             |             |             |             |            |             |             |             |             |            |             |             |             |             |            |             |             |             |             |  |  |  |
| <b>5.7</b>  |            |             |             |             |             |          |             |             |             |             |            |             |             |             |             |            |             |             |             |             |            |             |             |             |             |  |  |  |
| <b>5.8</b>  |            |             |             |             |             |          |             |             |             |             |            |             |             |             |             |            |             |             |             |             |            |             |             |             |             |  |  |  |
| <b>5.9</b>  |            |             |             |             |             |          |             |             |             |             |            |             |             |             |             |            |             |             |             |             |            |             |             |             |             |  |  |  |
| <b>6</b>    |            |             |             |             |             |          |             |             |             |             |            |             |             |             |             |            |             |             |             |             |            |             |             |             |             |  |  |  |
| <b>6.1</b>  |            |             |             |             |             |          |             |             |             |             |            |             |             |             |             |            |             |             |             |             |            |             |             |             |             |  |  |  |
| <b>6.2</b>  |            |             |             |             |             |          |             |             |             |             |            |             |             |             |             |            |             |             |             |             |            |             |             |             |             |  |  |  |
| <b>6.3</b>  |            |             |             |             |             |          |             |             |             |             |            |             |             |             |             |            |             |             |             |             |            |             |             |             |             |  |  |  |
| <b>6.4</b>  |            |             |             |             |             |          |             |             |             |             |            |             |             |             |             |            |             |             |             |             |            |             |             |             |             |  |  |  |
| <b>6.5</b>  |            |             |             |             |             |          |             |             |             |             |            |             |             |             |             |            |             |             |             |             |            |             |             |             |             |  |  |  |
| <b>b*10</b> | <b>6.9</b> | <b>6.92</b> | <b>6.94</b> | <b>6.96</b> | <b>6.98</b> | <b>7</b> | <b>7.02</b> | <b>7.04</b> | <b>7.06</b> | <b>7.08</b> | <b>7.1</b> | <b>7.12</b> | <b>7.14</b> | <b>7.16</b> | <b>7.18</b> | <b>7.2</b> | <b>7.22</b> | <b>7.24</b> | <b>7.26</b> | <b>7.28</b> | <b>7.3</b> | <b>7.32</b> | <b>7.34</b> | <b>7.36</b> | <b>7.38</b> |  |  |  |

Figure 5.6: The fragmentation rate for spatial patterns whose classification is presented in Fig. 5.4. The values of fragmentation rate have been multiplied by 100. Blank spaces in the table correspond to the extinction regime (i.e. no objects in the spatial domain).

behind the front (cf. Fig. 5.7). We want therefore to introduce the density of objects to take the density distribution behind the front into account. We define the density of objects as

$$d = \frac{\tilde{n}}{A}, \tag{5.7}$$

where  $\tilde{n}$  is the number of objects (the definition of  $\tilde{n}$  is given in subsection 5.2.1) and  $A$  is the area occupied by those objects, i.e., the larger  $\tilde{n}$  is, the more objects we have in the same area. Remark: when we consider  $\tilde{n}$  for the continuous front patterns, the patches behind the



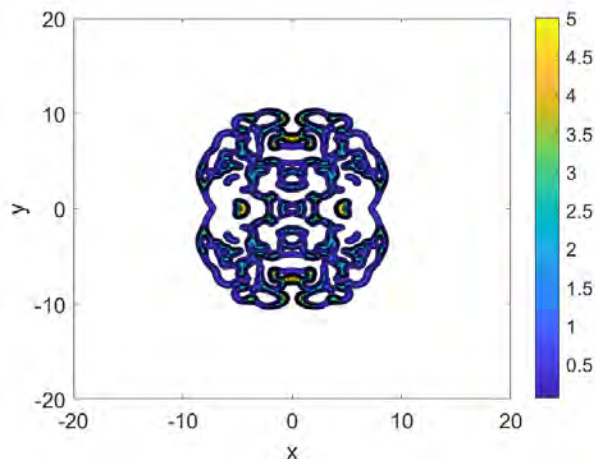


Figure 5.7: A example of spatial pattern that has a concave continuous front, which is obtained for parameters  $a = 4.0$  and  $b = 0.716$ .

continuous front are taken into account. Densities of objects for Fig. 5.4 are shown in Fig. 5.8.

It can be seen from Fig. 5.8 that the density of objects does not help us to distinguish between continuous and patchy distributions. Similarly to the fragmentation rate, we cannot see any distinct trend in the value of  $d$  when continuous front pattern transforms into patchy pattern and vice versa. Consider, for example, patchy spatial pattern obtained for  $a = 4.4$  and  $b = 0.698$ . The density of objects for that pattern is  $d = 0.138$ . This is a very high value in comparison with  $d = 0.0303$ , the density of objects we have for a continuous front spatial pattern obtained for the same  $a = 4.4$  and  $b = 0.702$ . However, we cannot conclude that the density of objects for patchy distributions is always distinctly higher than the density of objects for continuous front distributions. Continuous front spatial pattern obtained for  $a = 6.1$  and  $b = 0.7$  has the density of objects  $d = 0.1426$  while patchy pattern with  $a = 4.1$  and  $b = 0.738$  has  $d = 0.019$ .

In this chapter, we introduced some topological indices in order to distinguish between patchy spatial patterns with continuous-front spatial patterns. Clearly recognition of spatial pattern is particular important in the problem of biological invasion as accurate identification

of spatial pattern may help practitioners to apply better, more targeted, means of control to prevent an invasive species spreading into the space. Recognition of a spatial distribution as continuous front pattern often implies that the entire area behind the front will be considered for a control action (e.g. application of pesticide), while having a patchy spatial distribution may only require dealing with the areas occupied by patches of the invasive species.

Our study in this chapter reveals that continuous front and patchy spatial distributions may have a very similar topological structure behind the front and may therefore be easily confused with each other when simple visual inspection of those patterns is made. Moreover, the analysis

| <b>a</b>    |            |             |             |             |             |          |             |             |             |             |            |             |             |             |             |            |             |             |             |             |            |             |             |             |             |
|-------------|------------|-------------|-------------|-------------|-------------|----------|-------------|-------------|-------------|-------------|------------|-------------|-------------|-------------|-------------|------------|-------------|-------------|-------------|-------------|------------|-------------|-------------|-------------|-------------|
| <b>3.9</b>  | 0.00       | 0.00        | 0.00        | 0.00        | 0.00        | 0.00     | 0.00        | 2.72        | 0.84        | 0.00        | 0.00       | 8.69        | 0.55        | 2.71        | 1.65        | 3.36       | 1.38        | 2.70        | 3.77        | 1.44        | 0.40       | 4.86        | 2.32        | 2.51        | 1.85        |
| <b>4</b>    | 0.00       | 0.00        | 0.00        | 0.00        | 0.00        | 3.48     | 1.41        | 0.75        | 0.00        | 0.00        | 2.84       | 2.88        | 8.60        | 3.48        | 5.31        | 2.70       | 3.45        | 9.29        | 1.87        | 1.95        | 3.07       | 0.92        | 1.52        | 0.60        | 0.32        |
| <b>4.1</b>  | 0.00       | 0.00        | 0.00        | 6.72        | 4.74        | 0.56     | 0.00        | 0.00        | 3.22        | 1.49        | 0.68       | 2.89        | 0.44        | 1.30        | 0.37        | 0.28       | 0.79        | 1.58        | 0.40        | 1.21        | 0.26       | 1.69        | 0.93        | 1.54        | 0.85        |
| <b>4.2</b>  | 0.00       | 0.00        | 0.91        | 6.35        | 0.00        | 0.00     | 0.00        | 0.07        | 0.07        | 0.02        | 0.83       | 1.93        | 5.12        | 3.19        | 0.67        | 3.75       | 1.99        | 1.90        | 2.08        | 0.27        | 2.20       | 2.13        | 2.72        | 0.74        | 0.25        |
| <b>4.3</b>  | 0.00       | 5.56        | 5.86        | 0.00        | 0.00        | 11.37    | 8.59        | 4.43        | 0.60        | 1.29        | 1.78       | 3.57        | 2.87        | 4.55        | 4.45        | 1.64       | 3.03        | 2.36        | 1.52        | 2.03        | 1.71       | 0.79        | 0.74        | 2.95        | 0.84        |
| <b>4.4</b>  | 3.44       | 0.57        | 0.00        | 0.00        | 13.80       | 8.56     | 3.03        | 3.73        | 1.34        | 1.17        | 1.54       | 0.87        | 8.25        | 4.56        | 1.29        | 1.30       | 4.00        | 1.15        | 3.80        | 1.32        | 0.75       | 1.63        | 1.33        | 0.76        | 1.56        |
| <b>4.5</b>  | 10.63      | 0.00        | 0.00        | 0.00        | 4.26        | 2.85     | 2.74        | 5.58        | 1.45        | 4.12        | 6.59       | 5.57        | 4.60        | 0.67        | 0.72        | 3.54       | 4.58        | 2.81        | 4.13        | 0.25        | 1.97       | 2.66        | 2.44        | 5.46        | 2.99        |
| <b>4.6</b>  | 0.00       | 0.00        | 0.00        | 1.78        | 0.48        | 6.35     | 2.29        | 0.41        | 1.15        | 5.56        | 5.10       | 2.37        | 4.39        | 0.69        | 2.35        | 3.04       | 4.17        | 2.79        | 2.34        | 3.19        | 1.29       | 1.44        | 0.73        | 4.18        | 1.59        |
| <b>4.7</b>  | 0.00       | 0.00        | 3.14        | 6.97        | 1.46        | 1.31     | 3.66        | 0.31        | 5.06        | 4.27        | 0.40       | 3.19        | 1.63        | 1.97        | 3.45        | 2.70       | 1.64        | 2.66        | 1.94        | 5.21        | 0.23       | 2.50        | 1.62        | 1.10        | 2.42        |
| <b>4.8</b>  | 0.00       | 0.00        | 7.22        | 0.49        | 10.82       | 2.77     | 4.96        | 7.35        | 8.31        | 0.68        | 1.25       | 3.42        | 2.36        | 1.71        | 6.30        | 0.88       | 2.73        | 1.28        | 2.96        | 2.15        | 0.63       | 1.28        | 2.12        | 2.97        | 1.23        |
| <b>4.9</b>  | 0.00       | 3.09        | 8.20        | 0.70        | 0.63        | 4.32     | 3.31        | 4.00        | 1.44        | 5.54        | 0.74       | 6.72        | 4.42        | 2.83        | 4.39        | 1.78       | 0.66        | 2.88        | 3.66        | 1.93        | 1.02       | 0.58        | 4.14        | 3.68        | 3.06        |
| <b>5</b>    | 0.00       | 5.97        | 0.52        | 7.56        | 2.01        | 1.73     | 2.75        | 4.79        | 1.11        | 0.87        | 7.42       | 3.70        | 3.04        | 6.53        | 3.30        | 2.47       | 2.23        | 4.28        | 5.20        | 1.00        | 1.50       | 3.03        | 0.94        | 2.02        | 2.58        |
| <b>5.1</b>  | 0.00       | 6.12        | 0.58        | 0.00        | 12.23       | 4.34     | 2.42        | 1.01        | 2.76        | 0.94        | 3.77       | 1.90        | 3.81        | 3.12        | 3.82        | 1.15       | 1.15        | 4.03        | 2.96        | 3.99        | 1.90       | 2.16        | 1.69        | 1.16        | 5.04        |
| <b>5.2</b>  | 3.50       | 2.24        | 1.09        | 0.00        | 12.12       | 3.85     | 0.34        | 8.37        | 1.18        | 4.73        | 3.29       | 1.32        | 7.75        | 5.91        | 8.81        | 3.84       | 5.71        | 3.08        | 7.73        | 1.57        | 0.59       | 3.39        | 3.84        | 2.77        | 3.04        |
| <b>5.3</b>  | 0.80       | 5.82        | 1.00        | 0.00        | 2.86        | 4.54     | 7.02        | 2.35        | 1.69        | 8.78        | 1.88       | 4.24        | 2.55        | 3.97        | 1.97        | 2.47       | 3.68        | 1.81        | 2.55        | 3.15        | 1.03       | 3.00        | 2.63        | 4.24        | 2.21        |
| <b>5.4</b>  | 13.91      | 5.17        | 0.00        | 0.00        | 0.72        | 2.17     | 8.25        | 2.80        | 3.70        | 4.86        | 1.23       | 3.04        | 2.95        | 1.00        | 3.00        | 3.22       | 1.43        | 2.55        | 1.17        | 0.59        | 5.42       | 5.86        | 3.81        | 4.04        | 4.36        |
| <b>5.5</b>  | 7.78       | 4.94        | 0.00        | 0.00        | 1.56        | 1.93     | 2.61        | 0.67        | 1.41        | 5.47        | 5.84       | 1.18        | 2.97        | 3.10        | 3.71        | 3.78       | 1.78        | 4.25        | 7.00        | 3.95        | 5.14       | 3.07        | 1.31        | 4.29        | 6.99        |
| <b>5.6</b>  | 7.53       | 6.29        | 0.00        | 0.00        | 13.23       | 8.49     | 7.83        | 6.88        | 7.66        | 2.51        | 1.32       | 3.62        | 4.79        | 7.64        | 2.25        | 8.91       | 5.11        | 4.83        | 3.76        | 3.68        | 5.46       | 2.58        | 6.15        | 4.57        | 3.39        |
| <b>5.7</b>  | 13.77      | 0.00        | 0.00        | 0.00        | 1.52        | 9.78     | 4.33        | 11.23       | 6.27        | 3.00        | 4.89       | 5.66        | 7.44        | 6.63        | 2.38        | 1.58       | 3.15        | 2.11        | 4.20        | 2.10        | 4.46       | 3.92        | 6.73        | 6.96        | 3.30        |
| <b>5.8</b>  | 0.00       | 0.00        | 4.90        | 0.00        | 11.53       | 6.20     | 2.66        | 1.95        | 7.46        | 0.96        | 4.53       | 5.50        | 4.94        | 7.86        | 4.66        | 4.99       | 6.10        | 4.93        | 6.13        | 4.05        | 5.26       | 2.84        | 7.93        | 3.99        | 4.70        |
| <b>5.9</b>  | 0.00       | 0.00        | 0.00        | 0.00        | 4.32        | 4.39     | 3.60        | 4.54        | 0.88        | 4.28        | 5.35       | 4.09        | 4.61        | 4.05        | 5.35        | 5.46       | 3.51        | 0.57        | 6.95        | 2.28        | 8.04       | 4.31        | 6.95        | 4.19        | 7.78        |
| <b>6</b>    | 0.00       | 5.53        | 0.00        | 0.00        | 0.00        | 4.75     | 3.72        | 2.49        | 5.70        | 0.81        | 3.10       | 7.46        | 1.34        | 4.37        | 11.40       | 2.17       | 1.29        | 5.97        | 2.76        | 6.43        | 4.08       | 6.36        | 5.03        | 3.37        | 3.19        |
| <b>6.1</b>  | 0.00       | 0.00        | 5.10        | 1.17        | 0.00        | 14.26    | 8.95        | 9.31        | 4.85        | 2.92        | 6.12       | 6.44        | 10.97       | 9.63        | 3.25        | 5.26       | 5.94        | 7.30        | 8.32        | 10.46       | 2.67       | 2.76        | 3.19        | 4.06        | 6.74        |
| <b>6.2</b>  | 0.00       | 0.00        | 0.00        | 0.00        | 0.00        | 5.34     | 5.47        | 5.45        | 8.59        | 8.53        | 8.43       | 6.45        | 8.67        | 4.40        | 2.83        | 8.06       | 7.09        | 11.64       | 5.45        | 5.60        | 4.58       | 3.52        | 8.52        | 6.16        | 6.92        |
| <b>6.3</b>  | 0.00       | 0.00        | 2.01        | 6.34        | 0.00        | 2.76     | 3.88        | 6.34        | 10.04       | 13.84       | 3.55       | 1.90        | 10.42       | 7.99        | 6.93        | 3.78       | 4.26        | 5.31        | 1.93        | 2.56        | 1.50       | 1.24        | 5.38        | 3.01        | 8.59        |
| <b>6.4</b>  | 0.00       | 0.00        | 0.00        | 0.00        | 2.60        | 0.00     | 4.71        | 3.28        | 5.69        | 1.37        | 10.40      | 3.91        | 12.45       | 4.10        | 5.09        | 12.84      | 5.83        | 5.41        | 9.51        | 3.26        | 3.30       | 4.70        | 3.80        | 7.39        | 5.98        |
| <b>6.5</b>  | 0.00       | 0.00        | 0.00        | 0.00        | 0.00        | 9.04     | 7.64        | 13.17       | 4.65        | 1.57        | 4.36       | 2.82        | 3.97        | 7.72        | 4.09        | 1.71       | 2.34        | 9.85        | 4.87        | 6.06        | 6.61       | 9.03        | 6.11        | 2.48        | 6.66        |
| <b>b*10</b> | <b>6.9</b> | <b>6.92</b> | <b>6.94</b> | <b>6.96</b> | <b>6.98</b> | <b>7</b> | <b>7.02</b> | <b>7.04</b> | <b>7.06</b> | <b>7.08</b> | <b>7.1</b> | <b>7.12</b> | <b>7.14</b> | <b>7.16</b> | <b>7.18</b> | <b>7.2</b> | <b>7.22</b> | <b>7.24</b> | <b>7.26</b> | <b>7.28</b> | <b>7.3</b> | <b>7.32</b> | <b>7.34</b> | <b>7.36</b> | <b>7.38</b> |

Figure 5.8: The density of objects for spatial patterns whose classification is presented in Fig. 5.4. Density of objects  $d$  is multiplied by the factor of 100 for the sake of convenience

of the basic topological characteristics such as the number of objects, the fragmentation rate and the density of objects showed that the only reliable index of spatial distributions arising in the model is the number of objects in the pattern.

One important observation about the problem is that the number of objects in the visual image of the spatial distribution presents us with a very generic definition of patchy pattern. Indeed, every separate object in the visual image counts as a patch when the number of objects is analysed, no matter how large the size of the patch is and how large the density is within the patch. Furthermore, the definition of patch based on the number of objects implies that, in case we are allowed to neglect a complex spatial distribution behind the front, a continuous front spatial structure can be formally considered as a single large patch. Under more realistic conditions, however, the definition of patch may incorporate some additional restrictions. Indeed, practitioners may be interested just in identification of large patches with high population density and they may wish to neglect those patches where the population density in the patch and/or the patch size are relatively small. Hence the definition of patch will depend on additional parameters and different definitions of patch will then lead to different conclusions about spatial pattern. While we do not discuss this topic in more detail we notice that it requires further investigation when classification of spatial patterns is considered.

## CHAPTER 6

# SENSITIVITY OF SPATIAL PATTERNS TO THE PARAMETERS OF MONITORING PROTOCOL

It has been demonstrated in Chapter 5 that, for any of the topological characteristics we studied there, there are no threshold values that would separate continuous front spatial distributions from patchy spatial distributions. Furthermore, it is clearly seen from Fig. 5.4 that the solution to (3.5)-(3.10) is very sensitive to the choice of parameters and small variation in either parameter  $a$  or  $b$  may result in transformation of continuous front pattern into patchy pattern and vice versa. In the absence of a well defined boundary between continuous and patchy regimes in parametric plane  $(a, b)$  the question arises as to how strongly spatial patterns can be affected by the occasional loss of information about a spatial density distribution. In other words, how much information about the spatial distribution should we have in order to make a reliable conclusion about its topological characteristics? We further investigate the above question in this chapter.

### 6.1 Sensitivity of spatial patterns to the cutoff value

When collecting ecological data, it is often impossible to detect very small values of the

population density due to limitations of sampling/monitoring techniques, the minimum detectable density being called the “detection threshold”. Such a “detection threshold” we used in this thesis is known as cutoff value, denoted by  $C$

$$\tilde{N}(x, y) = 1 \quad \text{for} \quad N(x, y) > C, \quad \text{and} \quad \tilde{N}(x, y) = 0 \quad \text{for} \quad N(x, y) \leq C. \quad (6.1)$$

Using the equation (6.1) we are able to convert the original density distribution to a binary image. All of the results obtained in the previous chapter are under the assumption that the cut-off value  $C = 0.05$ . Consider the concave-front spatial pattern in Fig. 6.1(a). Its topological structure become a patchy pattern at a different cutoff value, see Fig. 6.1(b). Our investigation also shows that the number of objects in a patchy invasion will tend to increase when the cut-off value increases. Fig. 6.2(a) obtained at  $C = 0.05$  has three separate patches, the number of patches increased to nine at  $C = 0.130$  seen in Fig. 6.2(b).

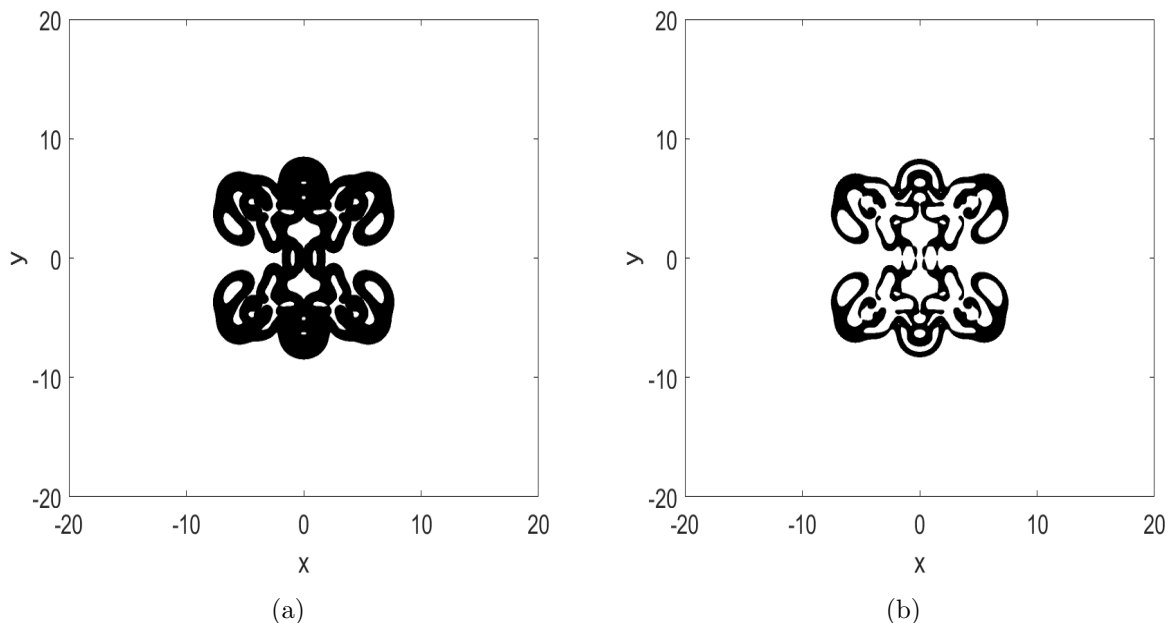


Figure 6.1: Examples of Binary images in Fig. 5.3(a) at cut-off (a)  $C = 0.05$ ; a concave continuous front pattern ( $n=1$ ) (b)  $C = 0.865$ ; patchy distribution with six separate patches

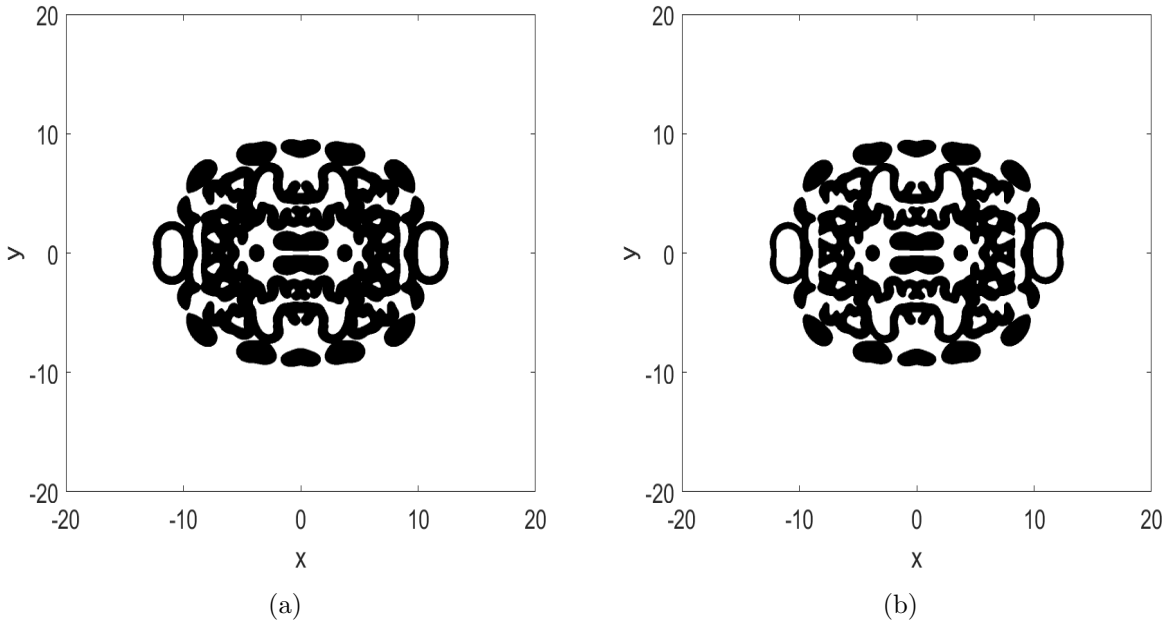


Figure 6.2: Examples of Binary images in Fig. 5.3(b) at cut-off (a)  $C = 0.05$ ; a patchy distribution with three separate patches (b)  $C = 0.130$ ; patchy distribution with nine separate patches

Consider the results presented in Fig. 6.3 and Fig. 6.4. The two figures shows the number of objects,  $n(C)$ , as a function of cutoff value,  $C$ . In Fig. 6.3, there are two functions of  $n(C)$  for two concave-front distributions while Fig. 6.4 give three functions of  $n(C)$  for three patchy distributions.

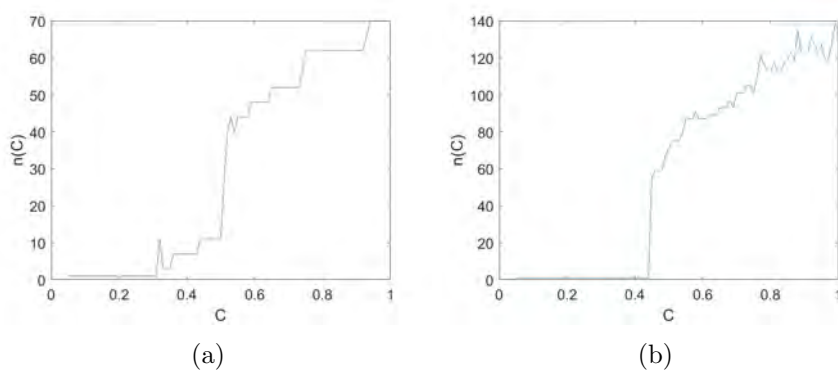


Figure 6.3: The number of objects  $n(C)$  as a function of the cut-off  $C$  for two concave-front distributions. Parameters of model (3.5)-(3.10) are (a)  $a = 6.0$ ,  $b = 0.710$  and (b)  $a = 5.7$ ,  $b = 0.711$ .

After comparing the behaviour of concave-front distributions and patchy distributions, it

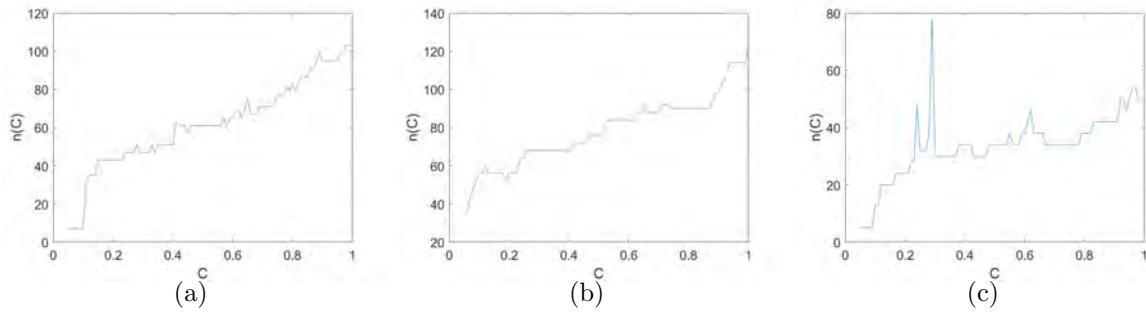


Figure 6.4: The number of objects  $n(C)$  as a function of the cut-off  $C$  for three patchy distributions. Parameters of model (3.5)-(3.10) are: (a)  $a = 5.2$ ,  $b = 0.71$ , (b)  $a = 6.4$ ,  $b = 0.71$  and (c)  $a = 5.9$  and  $b = 0.71$ .

can be seen that concave spatial patterns keep their topological structure as a single object in a wide range of cut-off values, e.g.,  $n(C) = 1$  for  $C \in [0.05, 0.32]$  in Fig. 6.3(a) and  $n(C) = 1$  for  $C \in [0.05, 0.47]$  in Fig. 6.3(b). However, for the spatial patterns in Fig. 6.3, a slight increase in cutoff value  $C$  from 0.05 to 0.12 will result in a sharp increase in the number of objects.

It is also observed in Fig. 6.3 and Fig. 6.4 that  $n(C)$  is not monotonous increasing. Let us have a look at Fig. 6.3(a) for example. When the cutoff value is increased from  $C = 0.511$  to  $C = 0.512$ . The number of objects decreases from 19 to 15. This is because some patches whose densities under 0.512 are removed from the spatial density distribution. Remark: this is just one example but in our other computations we have obtained similar results.

Let us also investigate the sensitivity of the other topological indices to the cut-off value. Consider two similar spatial patterns given in Fig. 6.5. Fig. 6.5(a) is a concave-front distribution while Fig. 6.5(b) is a patchy distribution. The corresponding topological quantities are shown as functions of the cutoff value in Fig. 6.6.

From Fig. 6.6(a), we can see the continuous front pattern Fig. 6.5(a) break into patchy pattern at a very high cut-off density, which is  $C = 0.4$ . Hence our chosen cutoff value  $C = 0.05$  is small enough to distinguish the continuous-front pattern and the patchy pattern.

However, the values of the fragmentation rate and the density of objects are similar to

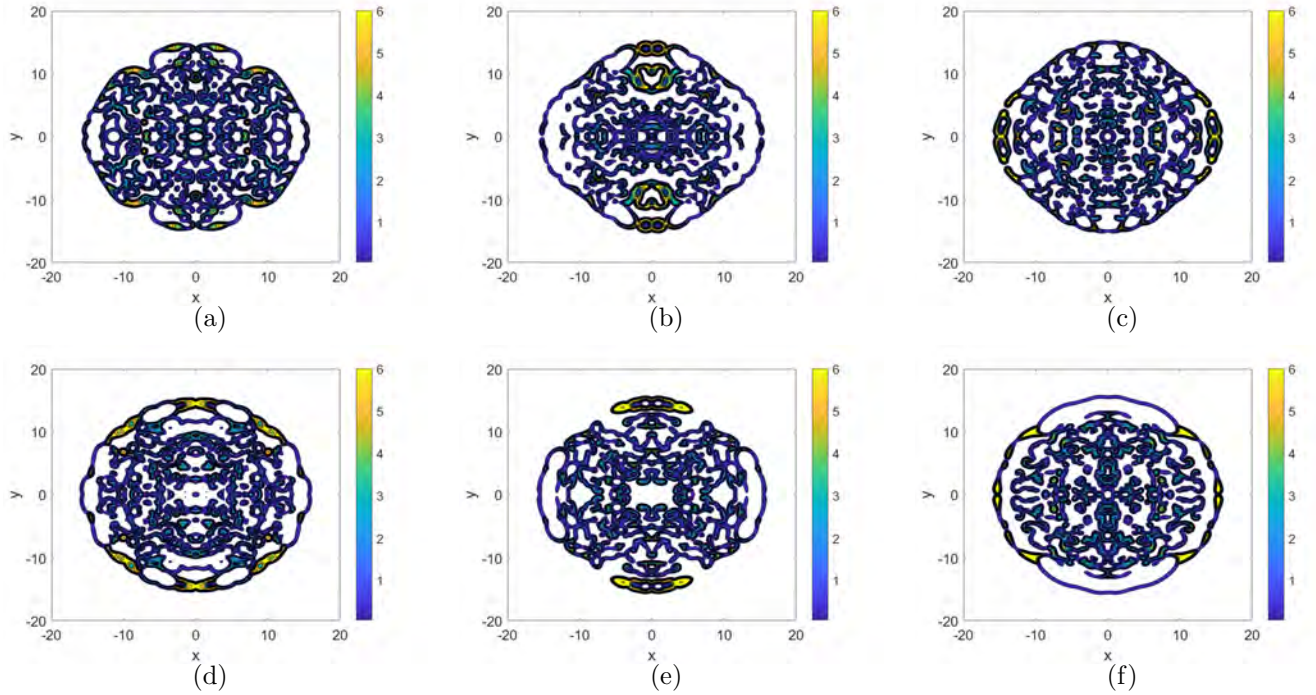


Figure 6.5: Sensitivity of spatial patterns. Snapshots of the spatial density distribution are shown at time  $t = 200$  for  $a = 5.1$ . A small variation in parameter  $b$  results in random transition between continuous front and patchy spatial patterns. (a), (d), (f) continuous front spatial distributions obtained for parameters  $b = 0.712$ ,  $b = 0.718$  and  $b = 0.722$  respectively; (b), (c), (e) patchy spatial patterns obtained for parameters  $b = 0.714$ ,  $b = 0.716$  and  $b = 0.720$  respectively

each other when we compute them for the continuous front pattern and patchy pattern in Fig. 6.5(a) and Fig. 6.5(b) respectively. The graphs in Fig. 6.6 demonstrate that those topological quantities alone cannot be used to distinguish between continuous front and patchy patterns appearing when we vary the cut-off value.

## 6.2 Reconstruction of spatial patterns from sparse data

We could see in the previous section that continuous and patchy spatial patterns are not sensitive to the loss of information about the population density related to increasing the cut-off parameter in the problem, i.e. the situation when small values of the population density are replaced by zero at spatial locations that belong to a computational grid. It is still possible



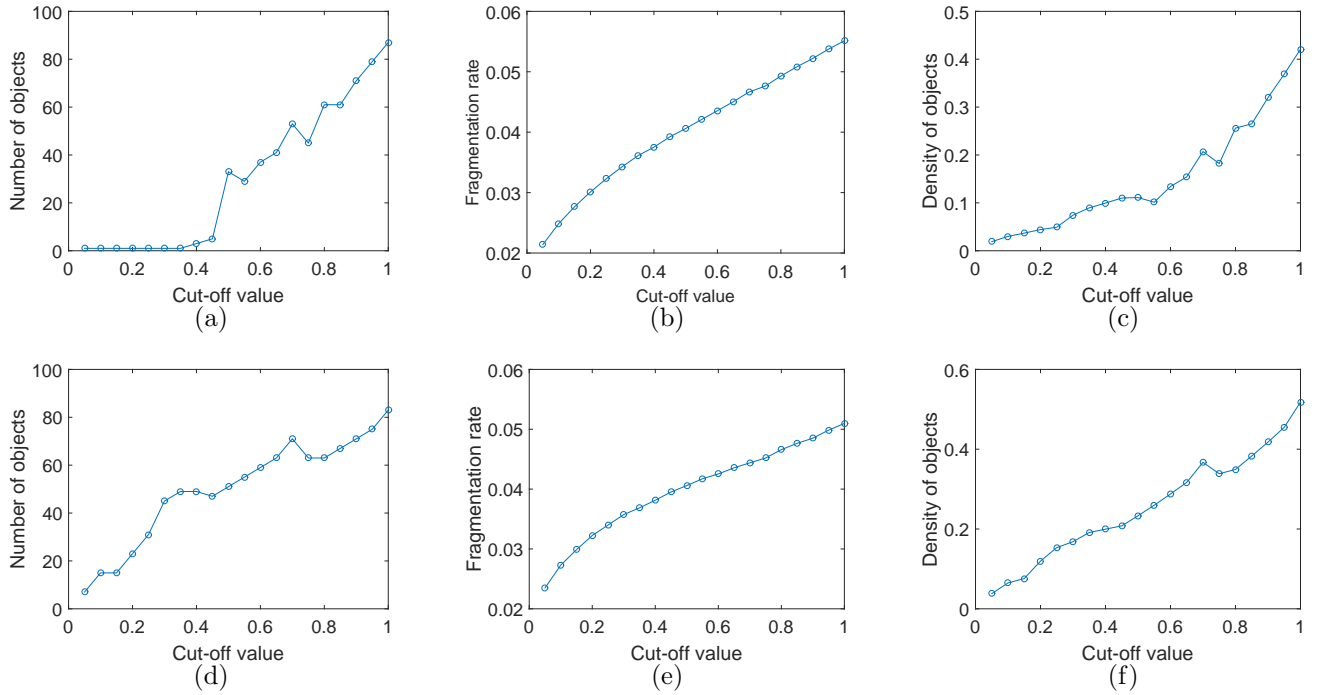


Figure 6.6: The topological characteristics of spatial pattern as a function of the the cutoff density  $C$  (a)–(c) The number of objects, the fragmentation rate, and the density of objects as functions of the cutoff value for the continuous front in Fig. 6.5(a); (d)–(f) The number of objects, the fragmentation rate, and the density of objects as functions of the cutoff value for the patchy distribution in Fig. 6.5(b)

to distinguish between spatial patterns of the two invasion regimes when an inadequately large cut-off parameter is employed (e.g.  $C = 0.5N_{max}$ , where  $N_{max}$  is the maximum density in the spatial domain) and some information about the population density is therefore lost. While the results of our computational experiment are preliminary and further investigation of a parametric plane is required we notice that variations in the cut-off parameter are not the main source of uncertainty when spatial pattern is reconstructed from data collected in the monitoring routine, the number of traps installed in the monitoring routine is also limited by the resource [42]. Below we discuss sensitivity of spatial patterns to the number  $N$  of sampling locations (i.e., the locations where traps are installed) which is crucial when a patchy distribution has to be distinguished from a continuous front distribution.

The images of spatial patterns we have analysed in the previous section have been generated

from the numerical solution of equations (3.5)–(3.6). That solution is defined at nodes of a computational grid where we have used a very fine grid of 1025 nodes in each direction to guarantee that the numerical solution has been computed with sufficient accuracy, this is confirmed in section 3.5. Hence, as a result of our computation, we have information about the population density at  $1025 \times 1025 = 1050625$  spatial locations (i.e. points  $(x, y)$  whose coordinates  $x$  and  $y$  are prescribed by the grid definition). That information allows us to reconstruct a spatial distribution with very good resolution and clearly distinguish between continuous front and patchy regimes.

Let us now assume for the sake of discussion that spatial distributions we have generated in our model exist in reality and we want to collect information about them. How much information about the population density is collected depends then on the number of sampling locations used in a monitoring routine. The grid of sampling locations must be fine enough to capture sufficient information about the population distribution in order to represent the spatial pattern adequately. Typically, we cannot use the same grid of 1050625 sampling locations and we have to employ a much coarser grid to make our simulation of the monitoring routine realistic. Furthermore, if we collect data about the population density on a coarse sampling grid then the spatial distribution we reconstruct from that data will be different from the original spatial distribution we have obtained on the grid of 1050625 nodes. One example illustrating the above statement is shown in Fig. 6.7 where we assume that the spatial density distribution in Fig. 6.5(b) exists in reality and we want to collect data on the population density by installing a regular ‘sampling grid’ of  $N \times N$  locations in the domain. We simulate installation of the sampling grid in the domain by considering our original grid and taking every  $i$ th node from it. Let us choose  $N = 65$  and take every 16th node from the original grid. As a result we have

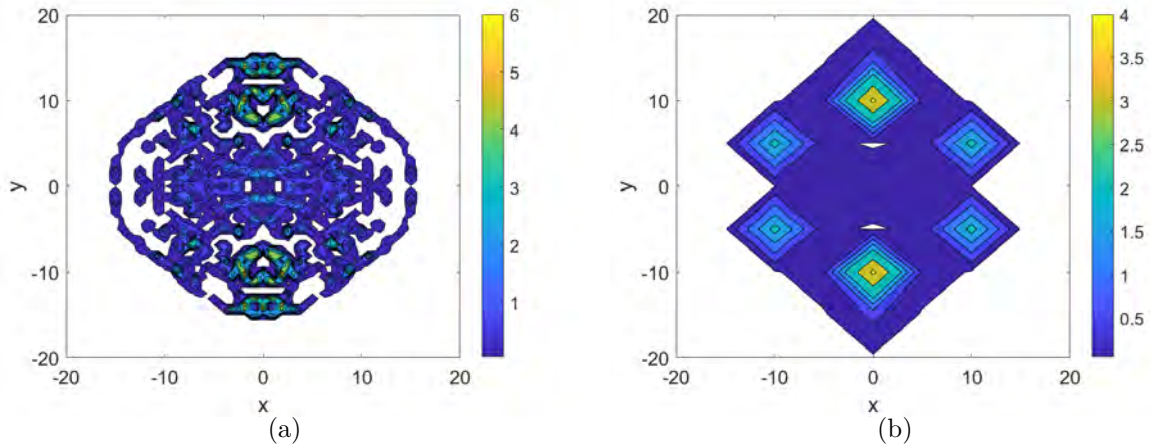


Figure 6.7: Examples of spatial pattern reconstruction on **(a)** coarse ( $N = 65$ ) and **(b)** very coarse ( $N = 9$ ) regular Cartesian grids, where  $N$  is the number of grid nodes at each direction. The original spatial distribution has been obtained on a fine grid with  $N = 1025$  for parameters  $a = 5.1$  and  $b = 0.714$ ; see Fig. 6.5b. The population density values are taken at every 16th node and 128th node of the original grid to simulate the density distribution on the coarse grid and the very coarse grid respectively

4225 spatial locations where information about the population density is available as opposed to 1050625 points on the original grid. We then reconstruct a spatial distribution from the information we have collected in our ‘sampling routine’ where the result is shown in Fig. 6.7(a). It can be seen from the figure that spatial pattern reconstructed from the information we have at 4225 sampling locations differs from the pattern reconstructed on the original grid yet it remains patchy. We then choose  $N = 9$  to generate a very coarse grid of 81 sampling points and reconstruct spatial pattern on that grid as shown in Fig. 6.7(b). It is clear from the figure that we now have a continuous front density distribution, so the information we collect about the population density on a grid with  $N = 9$  is not sufficient to recognise the type of spatial pattern correctly.

Hence, we want to understand to what extent any conclusion about spatial pattern can be affected by the number of sampling locations used to collect information and reconstruct a spatial distribution. We first numerically solve system (3.5)–(3.6) on very fine computational

grid  $G$  that has  $N = 2^m + 1$  grid nodes at each direction. We choose  $m = 10$  in our computation and consider the result obtained on that fine grid as the ‘true’ spatial density distribution. We then pretend that the spatial distribution is monitored and information about it can be collected at nodes of regular ‘sampling’ grid  $G_s$  only. Those ‘sampling’ grids  $G_s$  are generated from original grid  $G$  by taking the number of nodes at each direction as  $N = 2^s + 1$ ,  $1 \leq s \leq 9$ . As in our previous example, if we want to consider a ‘sampling’ grid with  $N = 2^6 + 1 = 65$  nodes at each direction we choose  $s = 6$  and take every  $2^{m-s}$ th node from the original fine grid. It is clear that information about the population density is readily available at nodes of any coarse ‘sampling’ grid we consider in our procedure because those nodes also belong to original grid  $G$ . Hence we can easily make our ‘sampling’ grid as coarse (fine) as we want by removing (adding) grid nodes, which is difficult in empirical field studies. Correspondingly, we can investigate how the type of spatial pattern we reconstruct from the data collected on a given sampling grid depends on the number of grid nodes.

Consider continuous front pattern shown in Fig. 6.5(a) and let us analyse information we have about the pattern on a sequence of ‘sampling’ grids obtained from the original grid as described above. We first reconstruct it on a grid of  $2^9 + 1$  nodes at each direction where the resulting pattern is visually identical to the pattern we have on the original grid. The same can be said when we have spatial pattern reconstructed on the grid of  $2^8 + 1$  nodes at each direction. That pattern still appears as a continuous front and the number of objects  $n$  in the image is therefore  $n = 1$ . We go on with this procedure and coarsen our sampling grid to see whether continuous front pattern breaks into several isolated patches for some threshold number  $N_t$  of grid nodes on a sampling grid. The results are shown in Fig. 6.8(a) where we generate the number of objects  $n$  in the image of spatial pattern as a function of the number of grid points

$N$  on a grid where the pattern is reconstructed. Clearly, the number of objects is  $n = 1$  when the number of grid nodes is very large. When we decrease the number  $N$  of grid points the pattern transforms as we lose information about it and the image appears as a collection of  $n = 23$  isolated objects when the number of grid points is  $N = 65$  at each direction. Hence the threshold number  $N_t$  is identified in this example as  $N_t = 65$ . A further decrease in the number of grid points results in an increase in the number of objects and we have  $n = 35$  objects when the pattern is reconstructed on a grid with  $N = 33$  nodes at each direction. However, the number of objects is again  $n = 1$  on a coarser grid of  $N = 17$  nodes. This happens because all information about relatively small patches is now lost on a coarse ‘sampling’ grid and the image appears again as a continuous front spatial structure. We further investigate this problem for continuous fronts in Fig. 6.5(d) and Fig. 6.5(f). It can be seen from Fig. 6.8(d) and Fig. 6.8(f) respectively that the threshold number remains  $N_t = 65$  and on sampling grids with a larger number of grid nodes a continuous front density distribution is always recognised correctly as a single object.

Consider now patchy pattern shown in Fig. 6.5(b) and let us repeat the analysis above. We are now interested in the threshold number  $N_t$  when the patchy distribution is reconstructed as a continuous front based on data taken from a sampling grid of  $N_t$  points at each direction. The results are shown in Fig. 6.8(b). It can be concluded from the graph that a patchy spatial pattern is not sensitive to the loss of information as it remains patchy until the grid is coarsened to  $N_t = 9$  nodes at each direction. The other patchy patterns shown in Fig. 6.5(c) and Fig. 6.5(e) demonstrate similar properties. It follows from the analysis of graphs in Fig. 6.8(c) and Fig. 6.8(e) that the spatial distributions remain patchy until an extremely coarse grid of  $N = 3$  points is considered.

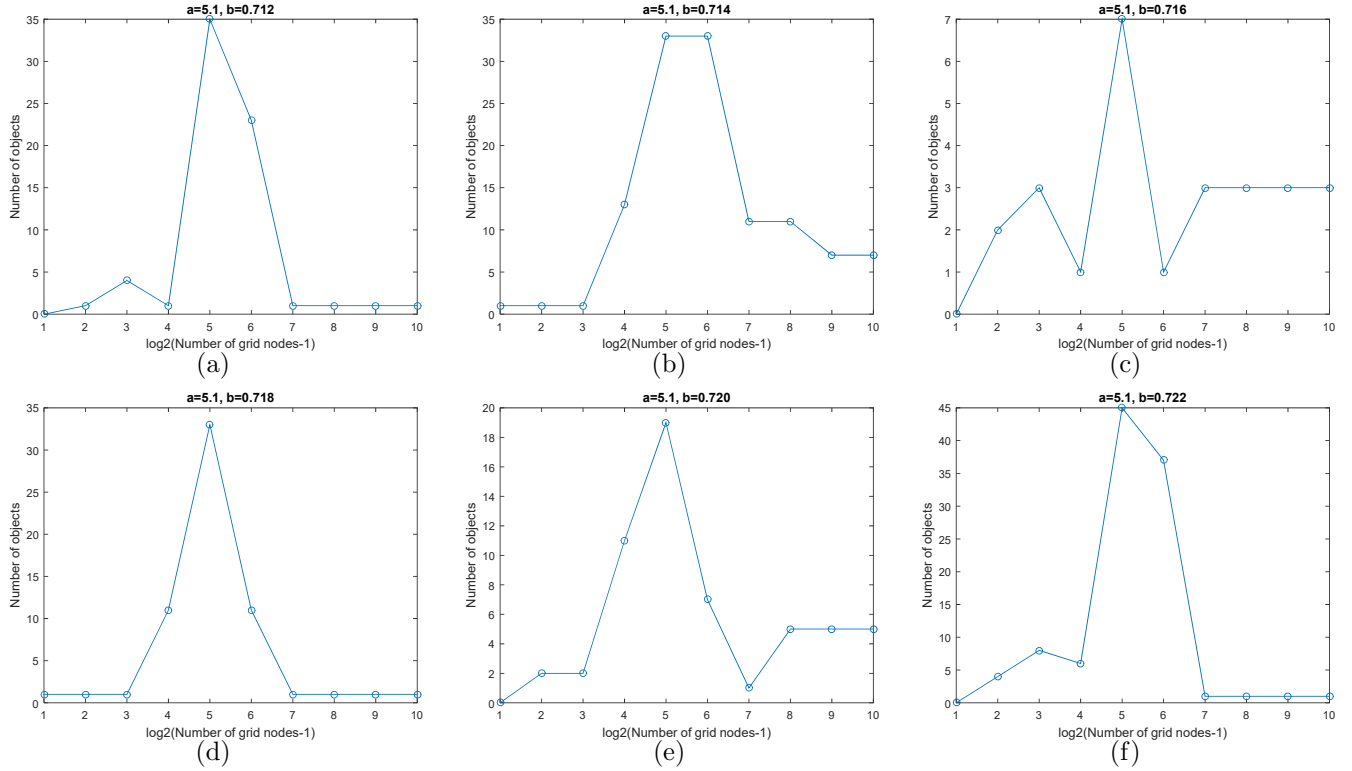


Figure 6.8: The number of objects as a function of the number of grid points in a sampling grid used to reconstruct the visual image of spatial pattern. Graphs (a)–(f) in the figure have been obtained when spatial patterns in Fig. 6.5 (a)–(f) are reconstructed on a sequence of sampling grids. The number of grid points is shown on the logarithmic scale

In this chapter we have studied the sensitivity of spatial patterns to variations in the cutoff density and the number of grid points used to reconstruct the density distribution in the domain.

In section 6.1 we have shown that the spatial patterns resulting from the continuous front propagation and from the patchy invasion respond differently to cutoff value. In both cases, the number of disconnected patches increases along with an increase in the cutoff value, such an increase starts when the cutoff value exceeds a certain critical value. However, the critical value of the cutoff value is consistently several times larger for the continuous-front pattern than for the patchy-invasion pattern, even when visually the patterns may have similar properties.

It has been demonstrated in section 6.2 that patchy spatial patterns are very robust and

their topology can still be recognised when a lot of information about the population density is missed, that is when we either increase the cutoff value or decrease the number of grid nodes. In particular, we have demonstrated in all our numerical test cases that patchy spatial patterns are present until the density values are collected on a very coarse sampling grid. While this result is model specific it gives us some useful insight into the accuracy of measurements required to recognise the type of spatial pattern.

## CHAPTER 7

# SPATIAL PATTERNS ARISING IN REACTION-DIFFUSION MODELS

In Chapters 3-6 we have studied spatial patterns in integro-difference models. In this chapter we employ an alternative model to simulate spatio-temporal dynamics and see if we still have the wealth of spatial patterns of biological invasion.

This chapter will consider a mathematical model of biological invasion given by two coupled diffusion-reaction PDEs. The model has been previously introduced in [24] where basic classification of spatial patterns has been done. The model allows for generating spatial distributions that are visually very similar to each other, yet some of those distributions are continuous fronts while the others are patchy spatial patterns. The ultimate goal of our study is to understand whether reliable criteria for classification and comparison can be elaborated for spatial patterns arising in the model. Hence basic topological indices of spatial pattern (the number of objects, the fragmentation rate, etc.) have been analysed for a variety of spatial distributions arising in the model to see if the spatial pattern type can be recognised correctly by using any of the quantities above.

It will be shown that a slight increment in the model parameters results in slight increment



in topological indices (i.e. production of spatial patterns with similar topological properties) when topology of continuous front that has no patches behind the front is considered. The above, however, is not true when we analyse continuous front density distributions that have patchy patterns behind the front and, most of all, spatial distributions consisting of separate patches. In the latter case a slight change in the model parameters results in random fluctuations of topological indices as spatial pattern with very different topology may appear. The ‘random’ behaviour of patchy patterns is further studied to understand whether or not patchy spatial structure can transform itself into a continuous front spatial distribution as time progresses. It will be argued in this chapter that information about spatial pattern alone is not sufficient to conclude about the type of spatial distribution (i.e. patchy pattern vs. continuous front) and spatio-temporal dynamics must be taken into account when formation and propagation of patchy structures is considered.

## 7.1 Model

The model is formulated as follows:

$$\frac{\partial U(X, Y, T)}{\partial T} = D_1 \left( \frac{\partial^2 U}{\partial X^2} + \frac{\partial^2 U}{\partial Y^2} \right) + P(U) - E(U, V), \quad (7.1)$$

$$\frac{\partial V(X, Y, T)}{\partial T} = D_2 \left( \frac{\partial^2 V}{\partial X^2} + \frac{\partial^2 V}{\partial Y^2} \right) + E(U, V) - MV. \quad (7.2)$$

Here  $U$  and  $V$  in (7.1)-(7.2) are the densities of susceptible population and infected population, respectively, at time  $T(T > 0)$  and location  $(X, Y)$ . Coefficients  $D_1$  and  $D_2$  describe species diffusivity due to the movement of the individuals and below we assume that

$D_1 = D_2 = D$  for the sake of simplicity. The function  $E(U, V)$  describes disease transmission,  $P(U)$  describes the local population growth where infected individuals do not contribute to the growth rate (as the disease is terminal) and  $M$  is the mortality rate for the infected population. The growth rate  $P$  is selected as to incorporate the strong Allee effect into the model (e.g. see [9, 44]):

$$P(U) = \left( \frac{4\nu}{(K - U_0)^2} \right) U(U - U_0)(K - U), \quad (7.3)$$

where parameter  $K$  is the carrying capacity of the susceptible population,  $U_0$  is the Allee threshold density ( $0 < U_0 < K$ ),  $\nu$  is the maximum per capita growth rate. The transmission function  $E$  is considered in the form of the mass-action law

$$E(U, V) = AUV, \quad (7.4)$$

where  $A$  is the rate of infection transmission.

In order to obtain the population distributions, the system (7.1)–(7.2) is solved numerically by a finite difference method. For convenience, we first introduce dimensionless variables. The carrying capacity  $K$  makes a convenient scale for the population density,  $u = U/K$  and  $v = V/K$ . We also introduce parameter  $a = AK$  to make the coordinates  $x = X(a/D)^{1/2}$  and  $y = Y(a/D)^{1/2}$  and the dimensionless time is  $t = aT$ . Equations (7.1)–(7.2) then take the following form:

$$\frac{\partial u(x, y, t)}{\partial t} = \frac{\partial^2 u}{\partial x^2} + \frac{\partial^2 u}{\partial y^2} + \gamma u(u - \beta)(1 - u) - uv, \quad (7.5)$$

$$\frac{\partial v(x, y, t)}{\partial t} = \frac{\partial^2 v}{\partial x^2} + \frac{\partial^2 v}{\partial y^2} + uv - mv. \quad (7.6)$$

where  $\beta = U_0/K < 1$ ,  $\gamma = 4\nu K(A(K - U_0))^2$ ,  $m = M/a$  are dimensionless parameters.

Species  $u$  and  $v$  are considered to propagate in a square domain  $\Omega$ . The domain size of  $\Omega$  is  $[0, L] \times [0, L]$ . In our model we consider no flux boundary conditions.

As for the initial conditions, we assume both species are located in the centre of the domain  $\Omega$ . The population density is uniform in a square subdomain at time  $t = 0$ . The domain occupied by species  $u$  is a square whose length is 10. And the domain taken by species  $v$  is also a square whose length is equal to 5. The initial conditions can be described as below:

$$u_0(x, y) = \begin{cases} 0.5, & \text{for } |x - \frac{L}{2}| < 10 \text{ and } |y - \frac{L}{2}| < 10, \\ 0, & \text{otherwise,} \end{cases} \quad (7.7)$$

$$v_0(x, y) = \begin{cases} 0.5, & \text{for } |x - \frac{L}{2}| < 5 \text{ and } |y - \frac{L}{2}| < 5, \\ 0, & \text{otherwise.} \end{cases} \quad (7.8)$$

These initial conditions simulate the original distribution of the invasive species when it is located in a subdomain whose size is small in comparison with the size of the entire domain.

## 7.2 Numerical approach

We will use the explicit finite difference method (FDM) to solve the problem (7.5)–(7.6).

We choose  $\delta t = 0.01$  and  $\delta x = \delta y = 1$ . The length and width of the domain is  $L = 600$  so there are  $601 \times 601$  grid nodes in total. The x and y coordinates are

$$x_i = (i - 1)\delta x = i - 1, i = 1, 2, \dots, 601, \quad (7.9)$$

$$y_j = (j - 1)\delta y = j - 1, j = 1, 2, \dots, 601. \quad (7.10)$$

Applying explicit FDM method, we can approximate  $\frac{\partial u}{\partial t}$  and  $\frac{\partial^2 u}{\partial x^2} + \frac{\partial^2 u}{\partial y^2}$  numerically:

$$\frac{\partial u}{\partial t} = \frac{u_{t+1}(x_i, y_j) - u_t(x_i, y_j)}{\delta t}, \quad (7.11)$$

$$\frac{\partial^2 u}{\partial x^2} + \frac{\partial^2 u}{\partial y^2} = u_t(x_{i-1}, y_j) + u_t(x_{i+1}, y_j) + u_t(x_i, y_{j+1}) + u_t(x_i, y_{j-1}) - 4u_t(x_i, y_j). \quad (7.12)$$

So the equations (7.5)–(7.6) can be approximated by

$$\begin{aligned} \frac{u_{t+1}(x_i, y_j) - u_t(x_i, y_j)}{\delta t} &= (u_t(x_{i-1}, y_j) + u_t(x_{i+1}, y_j) + u_t(x_i, y_{j+1}) + u_t(x_i, y_{j-1}) - 4u_t(x_i, y_j)) \\ &\quad + \gamma u_t(x_i, y_j)(u_t(x_i, y_j) - \beta)(1 - u_t(x_i, y_j) - u_t(x_i, y_j)v_t(x_i, y_j)), \end{aligned} \quad (7.13)$$

$$\frac{v_{t+1}(x_i, y_j) - v_t(x_i, y_j)}{\delta t} = u_t(x_i, y_j)v_t(x_i, y_j) - mv_t(x_i, y_j). \quad (7.14)$$

The computational implementation of the FDM to solve problem (7.5)–(7.6) on MATLAB is shown in the Appendix.

### 7.3 Stability analysis

In Chapter 3-6, we have studied the integro-difference model and found that patchy invasion only occurs in the parameter range where the extinction state is the only stable solution of the non-spatial system, see Fig. 5.1. So in this section we are going to investigate which factors will lead to the appearance of patchy invasions.

The corresponding non-spatial model of system (7.5)-(7.6) is given by

$$\frac{du(t)}{dt} = \gamma u(u - \beta)(1 - u) - uv, \quad (7.15)$$

$$\frac{dv(t)}{dt} = uv - mv. \quad (7.16)$$

The stability analysis of system (7.5)-(7.6) has been demonstrated in section 2.1.3. The structure of the parameter plane  $(m, \beta)$  is shown in Fig. 7.1(a).

We now go back to the spatio-temporal problem (7.5)-(7.6). For any fixed value of  $\gamma$ , the parameter  $m$  is varied along the line  $\beta = \text{const}$  where we focus our attention at the ‘transitional’ zone between the extinction state (the region  $\beta > m$ ) and the stable coexistence state (the region  $\beta < 2m - 1$ ). A fragment of the parametric plane  $(m, \beta)$  along with the solution type obtained for every pair  $(m, \beta)$  at time  $t = 600$  for  $\gamma = 6.0$  is shown in Fig. 7.1(b). Pairs  $(m, \beta)$  in the parametric plane resulting in different spatial patterns are colour-coded in the figure as blue stars for the extinction, red triangles for patchy invasion (no continuous front), green circles for continuous front spatial distributions. We note that Fig. 7.1 (b) only shows the distribution of the types of spatial patterns over the parametric plane at the time  $t=600$  and that distribution will be different if we consider a different moment of time. The temporal dynamics is further

discussed in Section 7.5 where we introduce the concept of topological stability.

Let us fix the value of  $\beta$  and decrease parameter  $m$  as we move along the line  $\beta = \text{const}$  in the parametric plane of Fig. 7.1(b). Typical examples of spatial distributions obtained in numerical solution of model (7.5-7.6) when  $m$  is varied are shown in Fig. 7.2. All spatial patterns in the figure have been generated for  $\beta = 0.21$  and  $\gamma = 6.0$  at time  $t = 600$ . The size of computational domain has been varied under the requirement that the invasive species must not approach the domain boundary at  $t = 600$ , i.e., the domain must be large enough (areas with zero population density are shown in white in the figure). The above requirement resulted in computations with the domain size of  $L = 600$  in some cases while in other computations we have used  $L = 800$  or  $1200$ . A convex continuous front in Fig. 7.2(a) obtained for  $m = 0.60$  presents the simplest pattern from a topological viewpoint and we should expect similar spatial distributions for  $m > 0.60$ . Meanwhile, as we slightly decrease  $m$  to  $m = 0.59$  regular oscillations appear in the front wake; see Fig. 7.2(b). Further decrease in  $m$  results in

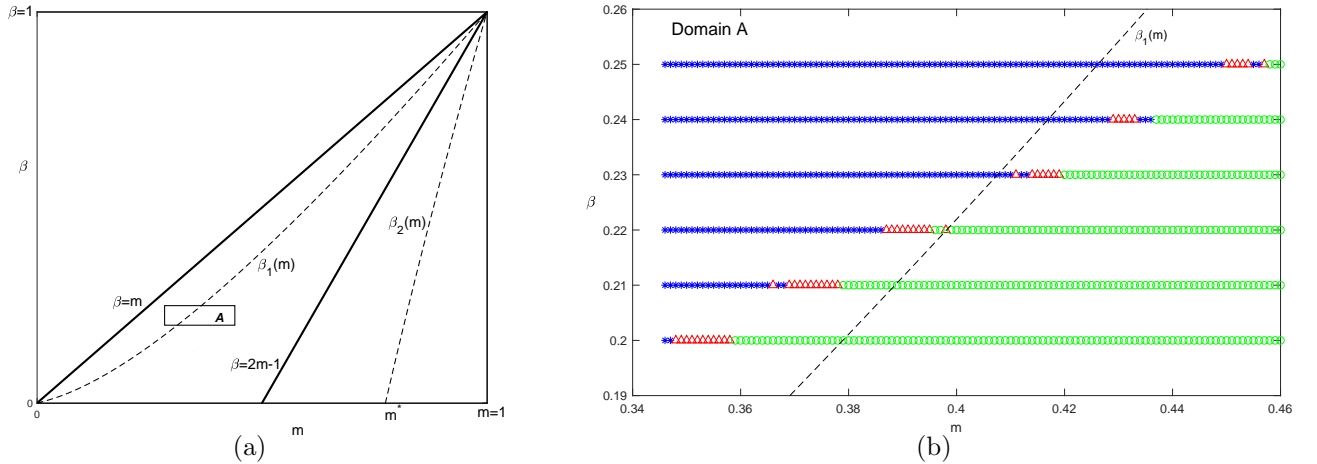


Figure 7.1: (a) The parametric plane  $(m, \beta)$  for non-spatial equations (7.15-7.16) (See section 2.1.3 for the stability analysis of the system (7.15-7.16)). (b) Various spatial patterns obtained in numerical solution of the spatial system (7.5-7.6) at time  $t = 600$ . Parameters  $m$  and  $\beta$  are taken in Domain A (see Fig. 7.1a) of the parametric plane and are varied with a small increment, parameter  $\gamma = 6.0$ . Pairs  $(m, \beta)$  in the parametric plane resulting in different spatial patterns are color-coded as follows: blue stars for extinction, red triangles for patchy invasion (no continuous front), green circles for continuous front spatial distributions.

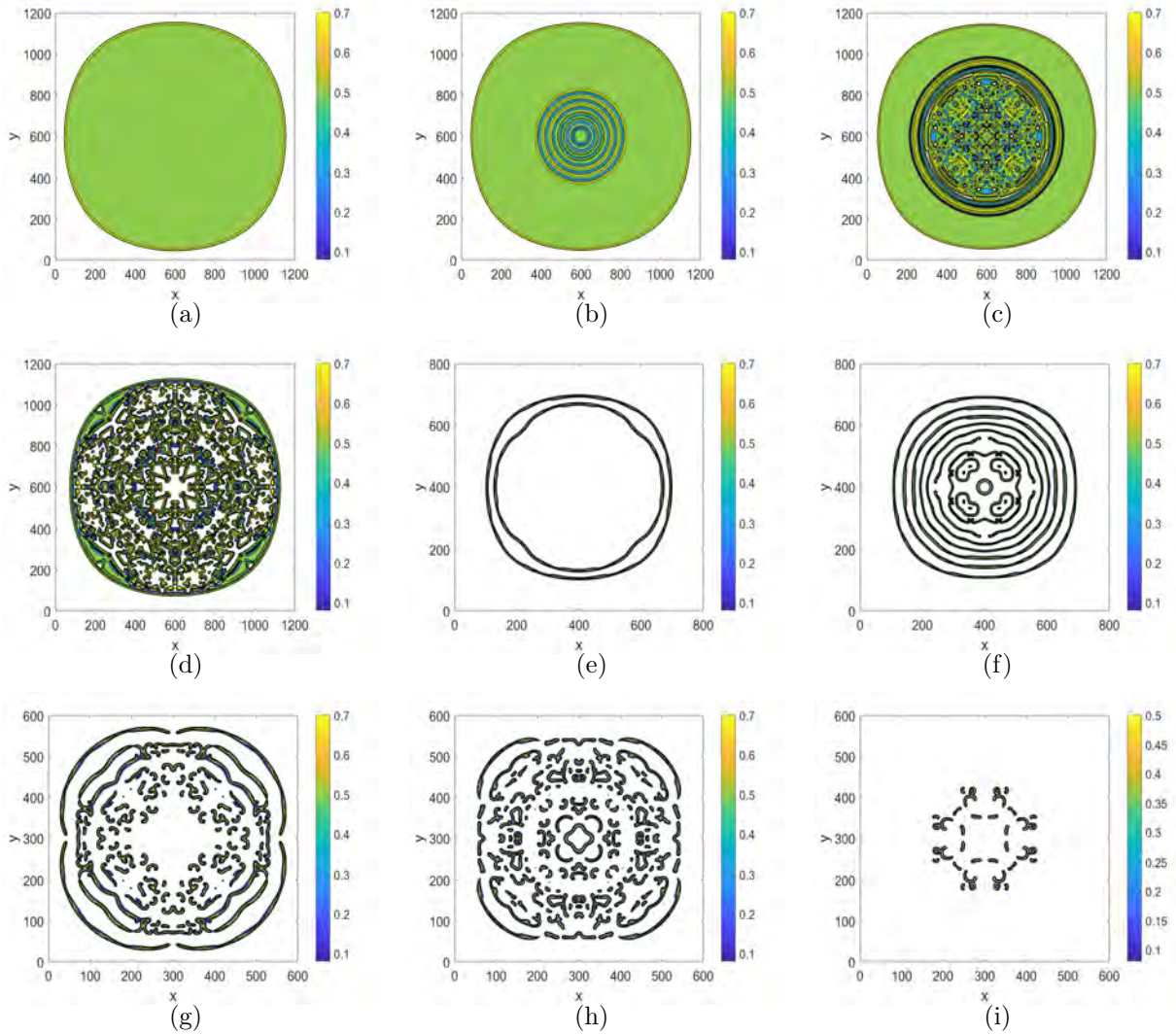


Figure 7.2: Typical examples of spatial distributions arising in the model (7.5)-(7.6) (see also Fig. 7.1(b)). Snapshots of the spatial density distribution obtained for various values of parameter  $m$  at time  $t = 600$ . The other problem parameters are  $\beta = 0.21$  and  $\gamma = 6.0$ . The white colour in each panel corresponds to zero population density (not shown in the figure legend). (a)  $m = 0.600$ : continuous front with no oscillations in the front wake; (b)  $m = 0.59$ : continuous front with regular oscillations in the front wake; (c)  $m = 0.57$ : continuous front with irregular oscillations in the wake; (d)  $m = 0.53$ : irregular oscillations become more distinct in the wake; (e)  $m = 0.38675$ : irregular oscillations in the wake are located in a narrow domain close to the front; (f)  $m = 0.3860$ : continuous front with patchy pattern formation in the wake; (g)  $m = 0.379$ : patchy pattern in the wake of continuous front becomes more distinct as  $m$  decreases; (h)  $m = 0.378$ : continuous front breaks down as  $m$  further decreases; (i)  $m = 0.366$ : patchy pattern consisting of few separate patches appears before the population extinctions at smaller values of parameter  $m$ .

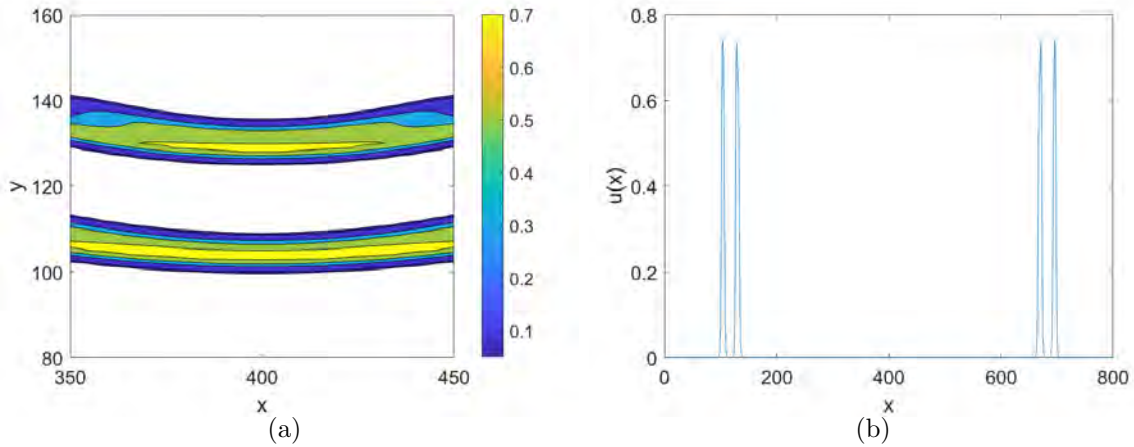


Figure 7.3: The spatial distribution of Fig. 7.2(e). (a) Zooming in the spatial density distribution in a subdomain where  $x \in [350, 450]$  and  $y \in [80, 160]$ . (b) A cross section of the spatial distribution along the line  $y=400$ .

irregular oscillations in the wake as shown in Fig. 7.2(c) obtained for  $m = 0.57$ . Those irregular oscillations can be seen in a larger domain behind the front at smaller values of parameter  $m$ ; see Fig. 7.2(d) with  $m = 0.53$ . For smaller values of  $m$  the topology of spatial pattern changes again as all oscillations are now located at a narrow ring-shaped spatial domain close to the front as shown in Fig. 7.2(e) obtained for  $m = 0.38675$  (see Fig. 7.3 for a zoom-in view of Fig. 7.2(e)). The spatial distribution in the wake then breaks down as  $m$  decreases and formation of patches occurs behind the front as shown in Fig. 7.2(f) with  $m = 0.3860$ . The patchy pattern in the wake of continuous front includes more small patches as  $m$  decreases; see Fig. 7.2(g) obtained for  $m = 0.379$ . If we further decrease the value of  $m$  a continuous front breaks down and the topology of the spatial pattern undergo another significant change as spatial patterns will appear as a collection of separate patches of non-zero density. One example of patchy spatial distribution is shown in Fig. 7.2(h) for  $m = 0.378$  (cf. Fig. 7.1(b)). Further evolution of a patchy pattern as  $m$  decreases can be seen in Fig. 7.2(i) where the spatial pattern obtained for  $m = 0.366$  now consists of few separate patches with no resemblance to



continuous fronts in Figs. 7.2(a)–7.2(e). Finally, the population extincts when  $m < 0.365$ ; cf. the results in Fig. 7.1(b).

To better distinguish spatial patterns, we will analyse those results with topological indices in the next section.

## 7.4 Topological indices of spatial patterns

### 7.4.1 Number of objects and density of objects

Now we fix  $\gamma = 6.0$  and  $\beta = 0.21$  and have a look at how the number of objects  $n$  changes as a function of parameter  $m$ . The function  $n(m)$  is given in Fig. 7.4a. It can be seen from the figure that patchy invasion occurs in the region  $m \in [0.365, 0.379]$ . The corresponding density of objects  $d(m)$  changes rapidly in this region as well (see Fig. 7.4b).

$$n(m) = 0, \text{ if the corresponding density distribution is an extinction state,} \quad (7.17)$$

$$n(m) = 1, \text{ if the corresponding density distribution has a continuous front,} \quad (7.18)$$

$$n(m) > 1, \text{ if the corresponding density distribution is a patchy spatial pattern.} \quad (7.19)$$

### 7.4.2 The Morisita index and the fragmentation rate

We could see in Chapter 5 that the fragmentation rate is not a reliable topological index when we want to make any prediction about location of patchy and continuous front spatial distributions on the parametric plane. Thus, in this section we introduce another topological

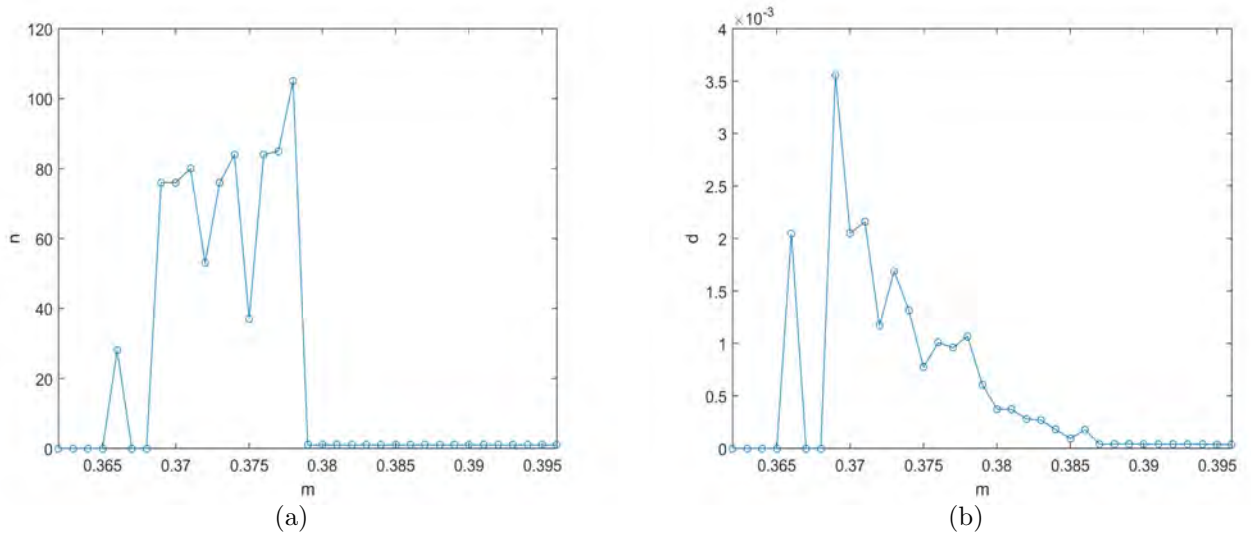


Figure 7.4: Topological indices of spatial patterns as a function of parameter  $m$  in the model (7.5)–(7.6) with the initial conditions (7.7)–(7.8) and parameters  $\beta = 0.21$ ,  $\gamma = 6.0$ . The spatial distributions have been obtained for various  $m$  at time  $t = 600$ . (a) the number of objects,  $n(m)$ ; (b) the density of objects,  $d(m)$ .

index to see whether it may be more reliable in comparison with the fragmentation rate when different spatial patterns are analysed.

The Morisita index [52] is defined as

$$I_M = Q \frac{\sum_{k=1}^Q n_k(n_k - 1)}{N(N - 1)}, \quad (7.20)$$

where  $N$  is the total number of ‘population units’,  $Q$  is the number of quadrats (i.e. the number of auxiliary sub-domains used to count the ‘population units’) and  $n_k$  is the number of ‘population units’ in the  $k$ th quadrat. The Morisita index provides a measure of how likely it is that two randomly selected individuals in a given distribution are found within the same quadrat compared to that of a uniform random distribution. Given two distributions, the clustered one has smaller Morisita Index  $I_M$  [27]. For example, both Fig. 7.5(a) and Fig. 7.5(b) have 12 ‘population units’ distributed in a  $8 \times 8$  units domain. We have the cell populated if it

is shown in black with the population density equal to 1. Unpopulated cells are shown in white with the population density equal to zero. Then we divide the entire domain into 4 quadrats to compute their Morisita Indices respectively. Fig. 7.5(a) is more dispersed so it has a smaller Morisita Index  $I_M = 0.73$ . Therefore Fig. 7.5(b) has a greater Morisita Index  $I_M = 1.82$ .

We now go back to problem (7.5)-(7.6) and compute Morisita index  $I_M$  as a function of  $m$ . The population units are now defined as grid cells on our computational grid used for numerical solution of problem (7.5)-(7.6). and we choose number of quadrants  $Q = 18$ . The graph  $I_M(m)$  is shown in Fig. 7.6(a). The analysis of  $I_M$  reveals that the Morisita index allows one to distinguish between topologically different patterns: a sharp jump in the Morisita index at  $m = 0.386$  corresponds to topological transition from continuous front patterns with no patches ( $m > 0.386$ ) and a high degree of aggregation to formation of separate patches behind the front ( $m \leq 0.386$ ) that results in less spatially aggregated patterns; cf. Fig. 7.2(e) and Fig. 7.2(g). The Morisita index then becomes almost constant ( $I_M \approx 2.1$ ) at  $m \in [0.379, 0.386]$

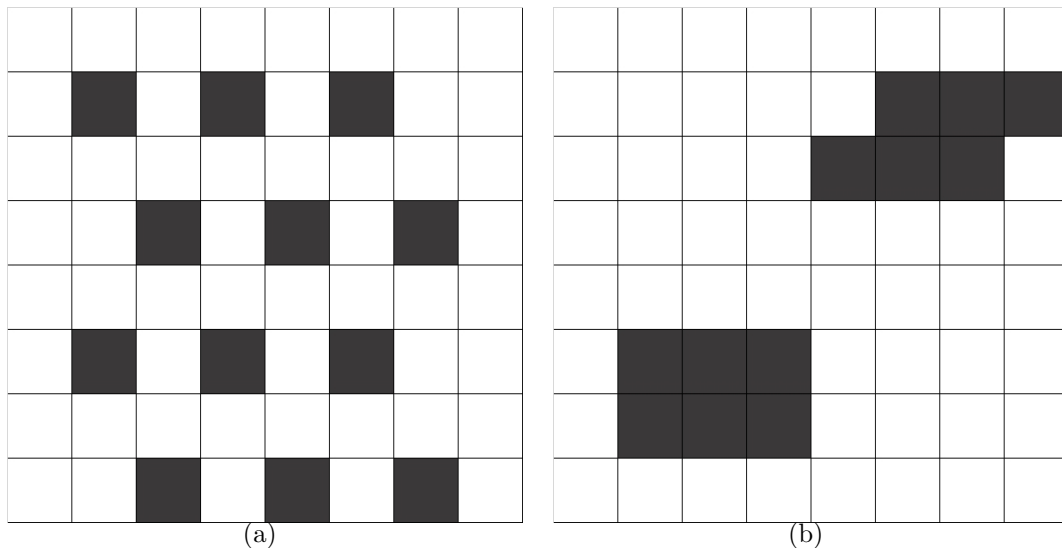


Figure 7.5: Hypothetical spatial patterns with different topological indices. (a)-(b) The degree of spatial aggregation in the two patterns measured by the Morisita index is different: (a) quasi-uniform density distribution,  $I_M = 0.73$ ; (b) highly aggregated density distribution with the same area of the non-zero density  $I_M = 1.82$ ;

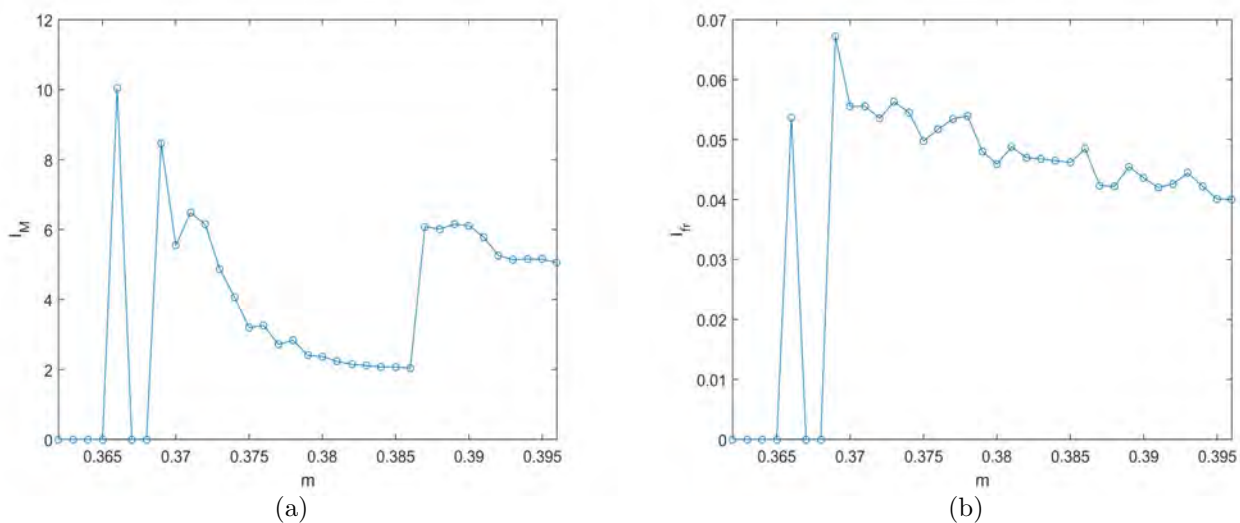


Figure 7.6: Topological indices of spatial patterns as a function of parameter  $m$  in the model (7.5)–(7.6) with the initial conditions (7.7)–(7.8) and parameters  $\beta = 0.21$ ,  $\gamma = 6.0$ . The topological indices are computed at time  $t = 600$ . (a) the Morisita index,  $I_M(m)$ ; (b) the fragmentation rate,  $I_{fr}(m)$ .

where spatial patterns are continuous fronts with patches behind the front. Meanwhile  $I_M$  starts increasing when transition from continuous front to patchy spatial distributions occurs at  $m = 0.379$ . The spatial pattern appearing at  $m = 0.366$  before the transition to the extinction sub-domain  $m \leq 0.365$  has the highest Morisita index  $I_M = 10.1$  as the image consists of a small number of patches (cf. Fig. 7.2(i)) which is considered as a high degree of aggregation according to definition (7.20). However, despite the Morisita index showing a trend to grow as  $m$  decreases in the ‘patchy’ parametric sub-domain, we notice several occasional jumps in  $I_M$  when  $m$  varies in the ‘patchy’ range. We hypothesize that those jumps occur because the number of spatial patches changes randomly when we give a small increment to the parameter  $m$ .

The graph  $I_{fr}(m)$  is shown in Fig. 7.6(b) where  $I_{fr} = 0$  corresponds to the extinction regime (i.e. no objects in the spatial domain) by the definition of the fragmentation rate. It is seen from the graph that the fragmentation rate increases when we decrease parameter

$m$  and patchy structures become more distinct. However, although the topological index  $I_{fr}$  has been employed to distinguish between various fine spatial structures of patchy patterns, it does not even define accurately the range of parameter  $m$  where patchy spatial patterns appear. Random variations in the fragmentation rate may stem from the fact that continuous front spatial patterns have a complex density distribution behind the front (cf. Fig. 7.2(g) and Fig. 7.2(h)) and therefore images of continuous front patterns and patchy patterns may have a similar fragmentation rate.

To conclude this section we notice that topological indices allow one to distinguish between various continuous front topological regimes yet we cannot rely upon the topological indices when we want to compare two patchy spatial distributions to each other. Patchy patterns obtained for close values of parameter  $m$  (while the other problem parameters remain the same) may have very different topological structures. Our study of graphs in Fig. 7.4 and Fig. 7.6 reveals that we cannot predict what transformation the spatial pattern will undergo when we give a small increment to  $m$  in the parametric sub-domain corresponding to formation of patchy spatial distributions.

## 7.5 Topological stability

In our study of spatial patterns we have identified two basic topological structures: a continuous front and a patchy spatial distribution. If a spatial pattern stops changing to another topological structure as time increases (e.g. patchy pattern to continuous front pattern or vice versa), then we say this spatial pattern is topologically stable. Let us define transition time  $t^*$  as a time over which transition from the initial condition to the topologically stable spatial distribution occurs, i.e. if a spatial pattern has a certain topological structure (continuous front

or patchy distribution) at time  $t^*$ , then the same type of topological structure will remain at later time  $t > t^*$ . A continuous front spatial structure at small times can evolve into patchy spatial pattern over time interval  $t \in [0, t^*]$  and it will then remain patchy at  $t > t^*$ . However, the evolution from a continuous spatial structure to a patchy one is not monotone, as multiple switches between continuous front and patchy spatial patterns can be observed at  $t < t^*$ . Furthermore, spatial structures that are classified as continuous fronts after the transition time show similar behaviour with multiple transformations back and forth to patchy distributions before the end of the transient regime.

Consider, for example, line  $\beta = 0.22$  in the parametric plane of Fig. 7.1(b). One simple illustration of transient spatio-temporal dynamics is shown in Table 7.1 where we compare spatial patterns that appear at time  $t = 300$  and  $t = 600$ . It is seen from the table that the spatial pattern we have at time  $t = 300$  is not topologically stable: a patchy spatial structure observed at time  $t = 300$  for  $m = 0.399$  evolves into a continuous front at  $t = 600$ , while a continuous front at  $t = 300$  for  $m = 0.398$  becomes a patchy spatial distribution at  $t = 600$ . Our numerical tests reveal that similar transient dynamics is observed for other values of  $m$  and  $\beta$  in the parametric plane.

| m           | $\leq 0.386$ | $0.387 \leq m \leq 0.395$ | 0.396    | 0.397    | 0.398    | 0.399    | $\geq 0.400$ |
|-------------|--------------|---------------------------|----------|----------|----------|----------|--------------|
| $N_{t=300}$ | <i>e</i>     | <i>p</i>                  | <i>p</i> | <i>c</i> | <i>c</i> | <i>p</i> | <i>c</i>     |
| $N_{t=600}$ | <i>e</i>     | <i>p</i>                  | <i>c</i> | <i>c</i> | <i>p</i> | <i>c</i> | <i>c</i>     |

Table 7.1: Comparison of spatial patterns for  $\beta = 0.22$ ,  $\gamma = 6.0$  and various  $m$  at times  $t = 300$  and  $t = 600$ . The legend in the table is as follows: *e* - extinction, *p* - patchy spatial distribution, *c* - continuous front spatial distribution; see also Fig. 7.1(b). Spatial distributions are not topologically stable as switches between continuous front and patchy structures are observed.

Given the volatile spatio-temporal dynamics in the table, our next goal is to evaluate time  $t^*$  in order to conclude about topological stability of given spatial pattern. In a computational

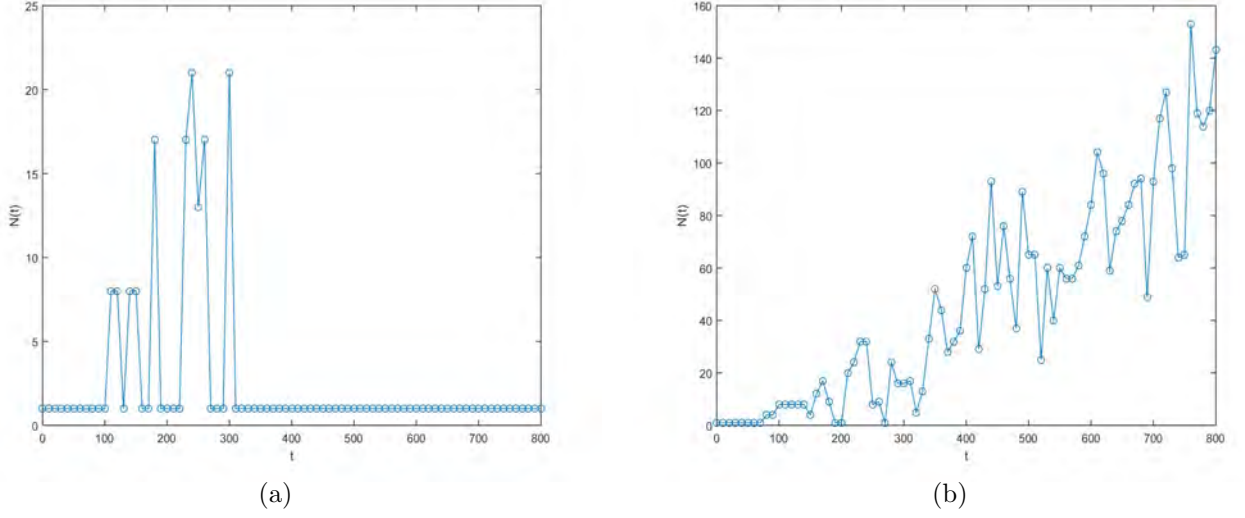


Figure 7.7: The number of objects  $n$  as a function of time  $t$  for spatio-temporal dynamics with  $\beta = 0.21$  and  $\gamma = 6.0$ : (a)  $m = 0.381$ : convergence to continuous front spatio-temporal dynamics,  $n(t) = 1$  at any time  $t > t^* = 310$  (b)  $m = 0.374$ : convergence to patchy spatio-temporal dynamics;  $n(t) > 1$  at any time  $t > t^* = 280$ .

routine we employ for this purpose the spatio-temporal dynamics is traced over time  $T$ , where we require that  $T \gg t^*$ , and the number of objects  $n$  is recorded at every time  $t_{k+1} = t_k + \Delta t$ ,  $k = 1, \dots, K-1$  to form the dataset  $n(t_k)$  (see Fig. 7.7). The total time  $T$  is defined empirically in our computation, i.e. we have repeated each computation several times with increasing value of  $T$  to check that all conditions of our computational tests are satisfied.

We define a simple topological index  $I_t$  of the spatial distribution at given time  $t_k$ ,  $k = 1, \dots, K$  as  $I_t = 0$  if we are in the extinction regime at time  $t_k$  (i.e.  $n(t_k) = 0$ ). We also define  $I_t = 1$  for continuous front pattern ( $n(t_k) = 1$ ) and  $I_t = 2$  for patchy pattern ( $n(t_k) > 1$ ). The number of objects in the dataset  $n(t_k)$  is then replaced by index  $I_t(k)$ . The most straightforward way to define transition time  $t^*$  is to find number  $k^*$  that satisfies condition  $i(k) = i(K)$  for any  $k > k^*$ . Given  $k^*$ , the transition time  $t^*$  is evaluated as  $t^* = k^* \Delta t$ .

Consider Fig. 7.7 where the number of objects is shown as a function of time for spatio-temporal dynamics defined by parameters  $\beta = 0.21$ ,  $\gamma = 6.0$  and we have  $m = 0.381$  in

Fig. 7.7(a) and  $m = 0.374$  in Fig. 7.7(b). It is readily seen from the graph in Fig. 7.7(a) that spatial pattern appears as a continuous front ( $n = 1$ ) at any time  $t > t^* = 310$ , while spatial patterns are not topologically stable (i.e. the number of objects varies) at times  $t < t^*$ . Examples of topologically different spatial distributions before transition time  $t^*$  are shown in

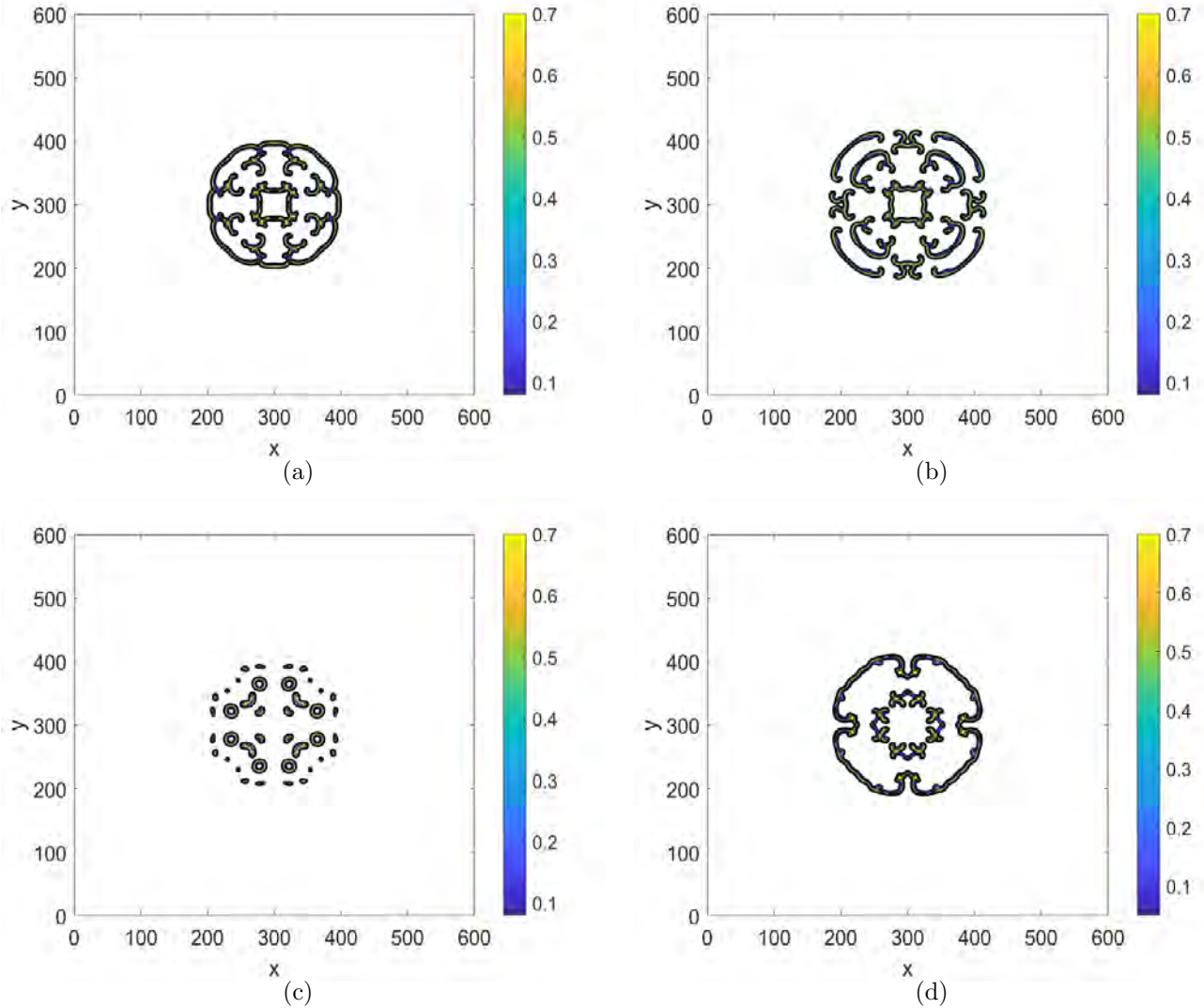


Figure 7.8: Examples of occasional switches between patchy and continuous front spatial distributions over transition period  $0 < t < t^*$ . The system parameters are as in Fig. 7.7. (a)-(b) The spatio-temporal dynamics of Fig. 7.7a, the transition time to continuous front spatial pattern is  $t^* = 310$ . (a) continuous front pattern at time  $t_1 = 200 < t^*$ , (b) patchy pattern at time  $t_2 = 250$  where  $t_1 < t_2 < t^*$ ; (c)-(d) The spatio-temporal dynamics of Fig. 7.7b, the transition time to patchy spatial pattern is  $t^* = 280$ . (c) patchy pattern at time  $t_1 = 230 < t^*$ , (d) continuous front pattern at time  $t_2 = 270$  where  $t_1 < t_2 < t^*$ ;



Fig. 7.8a and Fig. 7.8(b). Similarly, the analysis of Fig. 7.7(b) reveals that it is always patchy spatial pattern for time  $t > t^* = 280$  while occasional transitions to a continuous front appear at  $t < t^*$ ; see also examples of spatial distributions in Fig. 7.8(c) and Fig. 7.8(d). We would like to emphasise here that both continuous front and patchy spatio-temporal dynamics may experience switches between the two regimes when time  $t < t^*$ ; this is contrary to conclusion in [24] where it was suggested that only a continuous front regime may exhibit topological instability at  $t < t^*$ .

## 7.6 Topological stability of invasion regimes

It immediately follows from the example of Fig. 7.7 that transition time  $t^*$  depends on the system parameters  $m$ ,  $\beta$  and  $\gamma$ . Hence, in line with our approach in the previous section we now investigate how time  $t^*$  varies when we vary parameter  $m$  for  $\beta = 0.21$  and  $\gamma = 6.0$ . The graph  $t^*(m)$  is shown as a solid curve in Fig. 7.9. Every point on curve  $t^*(m)$  in the figure presents transition time  $t^*$  evaluated according to the procedure described in Section 7.5 for spatio-temporal dynamics obtained from the evolution of initial condition (7.7) with given value of  $m$ . Open circles on the curve correspond to transition to the spatio-temporal dynamics of propagating continuous front after  $t^*$  while closed circles correspond to spatio-temporal dynamics resulting in propagation of patchy spatial patterns after  $t^*$ . The analysis of the graph reveals that the following classification of spatial patterns appearing in the system when  $m$  is varied can be made for  $t > t^*$ : the invasive population extinctions for  $m < 0.365$  (extinction happens at  $t^* \approx 50$  for that range of parameter  $m$  and the range of  $m$  leading to extinction is not shown in the figure for the sake of convenience), the invasive population spreads into the space as a collection of separate density patches for  $m \in [0.365, 0.379]$ , the invasive species

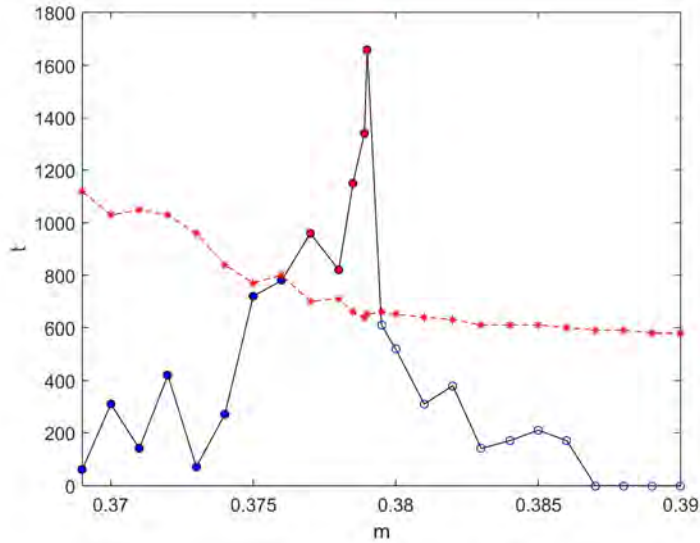


Figure 7.9: The transient dynamics of model (7.5–7.6) with initial conditions (7.7–7.8) and parameters  $\beta = 0.21$ ,  $\gamma = 6.0$ . Transition time  $t^*$  (solid blue curve, open and closed circles) and time  $t^D$  required for the invasive species to spread over square domain  $D$  of linear size  $L = 600$  (dashed red curve, red stars) are shown as functions of the parameter  $m$ . Open circles on graph  $t^*(m)$  show time  $t^*$  required for transition to continuous front spatio-temporal dynamics, while closed blue and red circles correspond to spatio-temporal dynamics resulting in patchy patterns after  $t^*$ . For  $m < 0.365$  transition to extinction happens at  $t^* \approx 50$  (not shown in the figure). For  $m > 0.386$  the initial ‘continuous front’ density distribution given by (7.7–7.8) never experiences switches to patchy spatial pattern, i.e.  $t^* = 0$ . Closed blue circles on graph  $t^*(m)$  show topologically stable spatio-temporal dynamics in domain  $D$ , while closed red circles show topologically unstable dynamics in  $D$  (see further explanation on the domain size in the text).

propagates as a continuous front with oscillations in the wake for  $m \in [0.380, 0.386]$ , and the propagating continuous front has no oscillations in the wake for  $m > 0.386$  (cf. Fig. 7.2).

An essential feature of graph  $t^*(m)$  is that the range of transition time  $t^*$  is much larger when  $m$  is taken from ‘patchy’ topological zone  $m \in [0.365, 0.379]$ . While time  $t^*$  is in good agreement with the estimate made in [24] for spatio-temporal dynamics of continuous fronts arising when  $m$  is selected not very close to the boundary of the ‘patchy’ range (i.e. we have  $t^* < 300$  for  $m > 0.382$ ), the maximum transition time we have observed in our computation of patchy spatio-temporal dynamics is  $t^* = 1750 \gg 300$  obtained for  $m = 0.379$ . It also is worth

noticing here that for the above-mentioned ‘patchy’ range of  $m$  the number of random switches between patchy and continuous front patterns registered at  $t < t^*$  does not decrease as time increases and gets closer to  $t^*$ . One example is shown in Fig. 7.10a where we have recorded all switches between patchy (number of objects  $n > 1$ ) and continuous front ( $n = 1$ ) regimes over time interval  $t \in [0, 1500]$  for  $m = 0.379$  (we recall that  $t^* = 1750$ ). It is seen from the figure that time  $t = 600$  can be erroneously thought of as transition time  $t^*$  as there are no switches at time  $t \in [600, 950]$ . However, after  $t = 950$  random jumps between patchy and continuous front regimes resume. The transitional dynamics is further presented in Fig. 7.10b where the number of switches  $s$  over the same time interval  $t \in [0, 1500]$  is shown as a function of  $m$ . It is seen from the figure that indeed the largest number of switches occurs when  $m$  belongs to the ‘patchy’ range,  $m \in [0.365, 0.379]$ .

One important observation about time  $t^*$  is that in practical consideration it has to be

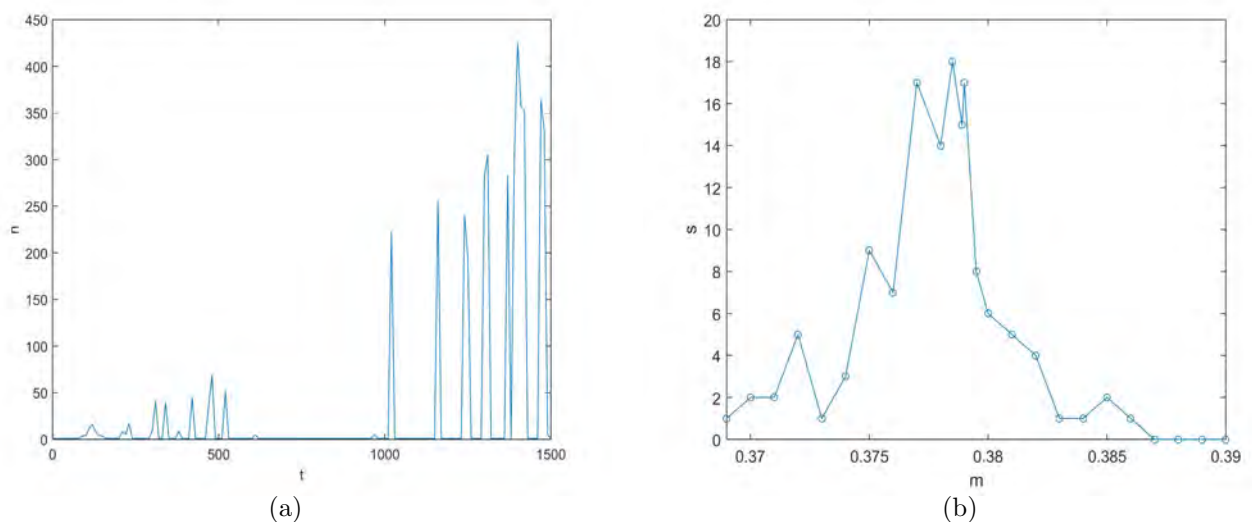


Figure 7.10: (a) Example of multiple random switches between continuous front and patchy spatial distributions. The number of objects  $n$  is shown as a function of time  $t \in [0, 1500]$  for  $m = 0.379$ ,  $\beta = 0.21$ ,  $\gamma = 6.0$ . Parameter  $m = 0.379$  presents the boundary between patchy and continuous front topological zones. (b) The number of switches  $s$  between patchy and continuous front regimes over time  $t = 1500$  as a function of parameter  $m$ . The time increment in the graphs is  $\Delta t = 10$ .

compared to time  $t^D$  required for invasive species to spread over spatial domain  $D$  where the species is monitored. Indeed, if we want to identify the invasion regime (continuous vs. patchy) in some spatial domain  $D$  to make an adequate control decision on the invasion prevention, we have to collect reliable information about spatial pattern before domain  $D$  will be fully invaded. Hence if  $t^* > t^D$  then we cannot give any recommendation on invasion control based on the type of spatial pattern. In other words, we will still have a transient regime at time  $t^D$  where we cannot say for sure what spatial pattern we deal with in domain  $D$ , while the domain is already completely invaded at  $t = t^D$  and it therefore is too late to make a control decision.

Time  $t^D$  required for invasive species in model (7.5-7.6) to spread over square domain  $D$  with linear size  $L$  is shown as a function of parameter  $m$  for  $L = 600$  in Fig. 7.9; see a dashed red line in the figure. In all cases presented in the figure computation has been performed in a larger spatial domain where the square domain  $D$  has been considered as a sub-domain placed at the center of the computational domain. We do not show time  $t^D$  in the graph for extinction regime  $m < 0.365$  because extinction of the invasive species happens at  $t^* \approx 50$ , i.e. well before domain  $D$  becomes fully invaded. It is seen from the figure that for continuous front regimes with  $m > 0.379$  the transition time is always  $t^* < t^D$ . The conclusion about relationship between  $t^*$  and  $t^D$  is, however, different when we consider the range of parameter  $m \in [0.365, 0.379]$  resulting in patchy spatio-temporal dynamics. We have  $t^* > t^D$  for several values of  $m$  in the figure. Moreover, transition time  $t^*(m)$  is not a monotone function over the interval  $m \in [0.365, 0.379]$  and we cannot therefore predict what happens to the transition time if  $m$  is slightly changed. Thus, if we take an arbitrary value of  $m$  from the above interval it is likely that the invasion type cannot not be determined in spatial domain  $D$  where we are interested in the control of invasive species.

Consider now arbitrary spatial domain  $D$  and let us introduce the ratio

$$r(m) = t^*(m)/t^D(m), \quad (7.21)$$

where times  $t^*(m)$  and  $t^D(m)$  are defined as above. For any given value of  $m$ , we will say that spatial pattern is topologically stable in domain  $D$  if ratio  $r$  obtained for that  $m$  is  $r < 1$  and the pattern is topologically unstable in  $D$  if  $r \geq 1$ . Clearly,  $r$  depends on domain size  $L$  and we have  $r \rightarrow 0$  as  $L \rightarrow \infty$ . Meanwhile, another case resulting in  $r = 0$  is when transition time is  $t^* = 0$ , i.e. when the spatio-temporal dynamics does not undergo any switches between patchy and continuous states. We will call the latter topological type of spatio-temporal dynamics unconditionally stable.

Let us apply the above classification to the spatio-temporal dynamics of Fig. 7.9. The range  $m \in [0.365, 0.379]$  resulting in patchy spatio-temporal dynamics can be subdivided as follows: we have topologically stable patchy patterns in domain  $D$  for  $m \in [0.365, 0.376]$  and topologically unstable ‘quasi-patchy’ patterns in  $D$  for  $m \in (0.376, 0.379]$ . Meanwhile all continuous front patterns remain topologically stable in  $D$ , all of them being unconditionally stable for  $m > 0.386$ . Hence, we cannot make any conclusion about the topology of spatial pattern in domain  $D$  when spatio-temporal dynamics is induced by the demographic parameter  $m \in [0.365, 0.376]$ , while the topological classification of spatio-temporal patterns obtained for all other values of  $m$  can be decided upon before spatial domain  $D$  is fully invaded.

The transition time  $t^*$  has to be taken into account when the topological indices introduced in Section 7.4 are analysed. Consider, for example, the graphs of Fig. 7.4 and Fig. 7.6. We recall that all topological indices presented in those figures have been computed for time  $\tilde{t} = 600$ . Once the transition time has been defined for every spatial pattern whose topological indices are

computed, we have  $\tilde{t} > t^*$  for continuous front distributions generated when  $m > 0.379$ . Those spatial patterns are topologically stable (most of them are unconditionally stable) in a spatial domain where computation has been made and a small increment in parameter  $m$  results in a relatively small change of topological properties, i.e. spatial distributions generated for similar values of  $m$  will look similar. However, most spatial patterns obtained at time  $\tilde{t} = 600$  with  $m$  taken from the ‘patchy’ range have  $\tilde{t} < t^*$  and the topology of spatial pattern is not well defined at  $t = \tilde{t}$ . Hence our next step is to check whether the presence of random oscillations in topological indices is an inherent feature of patchy spatial patterns and those oscillations will not disappear when patchy spatial patterns are analysed at time  $t > t^*$ .

Several values of parameter  $m$  taken with a small increment from the ‘patchy’ range are shown in Table 7.2. For each  $m$  in the table the transition time has been defined and we have then selected the maximum value  $t_{max}^*$  from the range of transition times. In our computation we had  $t_{max}^* = 790$  and spatial patterns have therefore been analysed at time  $t = 810 > t_{max}^*$  to ensure that all spatial patterns obtained at that time are already topologically stable. The topological indices of spatial patterns generated at time  $t = 810$  are compared to the topological indices calculated for the same range of  $m$  at time  $t = 600$  in the table.

## 7.7 Topological indices of field data: gypsy moth in the United States

What we have discussed in the previous sections are theoretical models that are subject to symmetrical initial conditions. However, in reality when we noticed invasive species in an area, they have already established and spread. The individuals are usually distributed asymmetrically. In addition, the local ecosystem can be very complex and there might be more than

| m                                | 0.3750 | 0.3752 | 0.3754 | 0.3756 | 0.3758 | 0.3760 |
|----------------------------------|--------|--------|--------|--------|--------|--------|
| $n, t = 600$                     | 37     | 1      | 89     | 105    | 89     | 84     |
| $n, t = 810$                     | 181    | 115    | 133    | 152    | 142    | 193    |
| $d \times 10^{-4}, t = 600$      | 8.0    | 7.0    | 10.0   | 15.0   | 12.0   | 10.0   |
| $d \times 10^{-4}, t = 810$      | 12.0   | 9.0    | 10.0   | 11.0   | 12.0   | 15.0   |
| $I_{fr} \times 10^{-2}, t = 600$ | 4.97   | 4.83   | 5.08   | 5.62   | 5.52   | 5.18   |
| $I_{fr} \times 10^{-2}, t = 810$ | 5.17   | 5.27   | 5.15   | 5.37   | 5.30   | 5.77   |
| $I_M, t = 600$                   | 3.20   | 3.36   | 3.20   | 3.25   | 3.45   | 3.26   |
| $I_M, t = 810$                   | 1.78   | 2.25   | 2.23   | 1.97   | 2.03   | 2.06   |

Table 7.2: Topological indices of spatial patterns as a function of parameter  $m$  in the model (7.5)–(7.6) with the initial conditions (7.7)–(7.8) and parameters  $\beta = 0.21$ ,  $\gamma = 6.0$ . The values of  $m$  taken with a small increment at the interval  $m \in [0.375, 0.376]$  result in patchy spatio-temporal dynamics after transition time  $t^*$ . The number of objects  $n$ , the density of objects  $d$ , the Morisita index  $I_M$ , and the fragmentation rate  $I_{fr}$  are compared at time  $t = 600 < t^*$  and  $t = 810 > t^*$ .

two interacting species which means that it is difficult to construct an accurate mathematical model to simulate biological invasion in the real world. However, we can use mathematical techniques to analyse their spatial patterns which might be helpful for the management of the invasive species.

The gypsy moth eats the leaves of over 500 species of plants, trees and shrubs and is generally regarded as pest that is destructive to the local ecosystem. The gypsy moth (Fig. 7.11) was introduced into Medford, Massachusetts from Europe in 1869 and by 2007, it had invaded Michigan, Minnesota, Virginia, West Virginia, Illinois, and Wisconsin. In this section, we will investigate the spatial patterns of the gypsy moth in the United States. Data are collected by the ‘Slow the Spread’ program.

It was discovered that the pheromone could be extracted from adult females and used as baits in traps [80]. In order to collect data, the ‘Slow the Spread’ program place 70,000 to 90,000 baited traps in the areas infested by the the gypsy moth. The data is composed of 3 columns: the index of each trap, the number of individuals in each trap and the location of each trap.



Figure 7.11: (a) Adult gypsy moth and (b) gypsy moth caterpillar

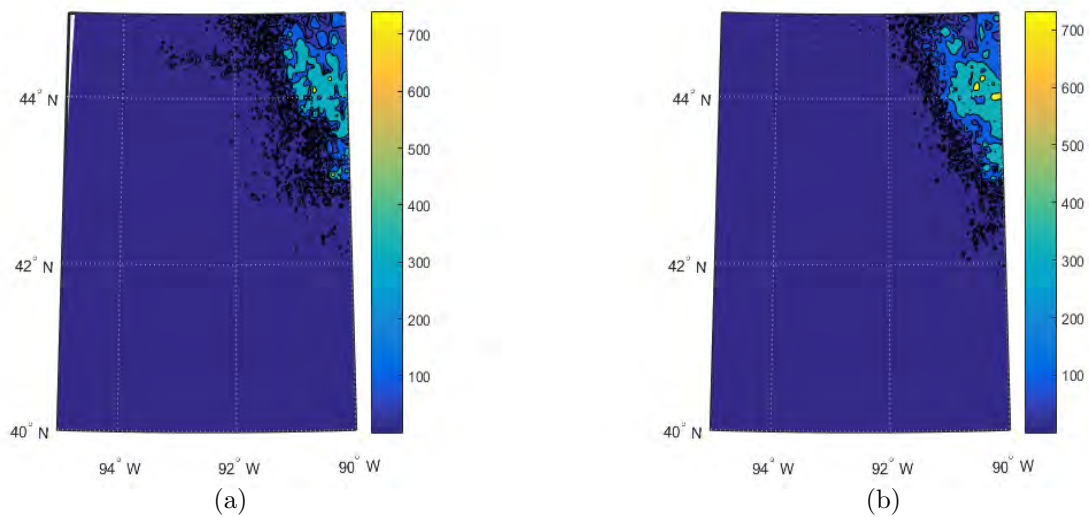


Figure 7.12: interpolated density distribution of gypsy moth in (a) year 2015; (b) year 2016

Now let us consider the spatial density distribution of gypsy moth in the region  $\Omega = [-95^\circ\text{W}, -90^\circ\text{W}] \times [40^\circ\text{N}, 45^\circ\text{N}]$  which is shown in Fig. 7.12. Fig. 7.12 (a) is the distribution of gypsy moth in year 2015 and Fig. 7.12 (b) is its distribution in year 2016. In this region we can find many isolated colonies and a clear continuous front is not apparent. Compared to 2015, many remote colonies had been eradicated by 2016.

We compute the number of objects and fragmentation rate of the gypsy moth in year 2015



and 2016 and obtain:  $N_{2015} = 208$ ,  $fr_{2015} = 0.0292$ ,  $N_{2016} = 163$ ,  $fr_{2016} = 0.0171$ . The number of objects decreased and the spatial pattern became more clustered, which means that the efforts made to control the spread of gypsy moth in this area were successful in this year.

The results above are obtained at cutoff value  $C = 1$  and the number of grid nodes installed is  $1025 \times 1025$ . Then let us investigate how will the topological indices of the spatial patterns in Fig. 7.12 (a) change when the cutoff value and number of grid nodes change. From Fig. 7.13, it can be seen that the number of objects decreases as the cutoff values increases. Meanwhile, the fragmentation rate will decrease at first before increasing.

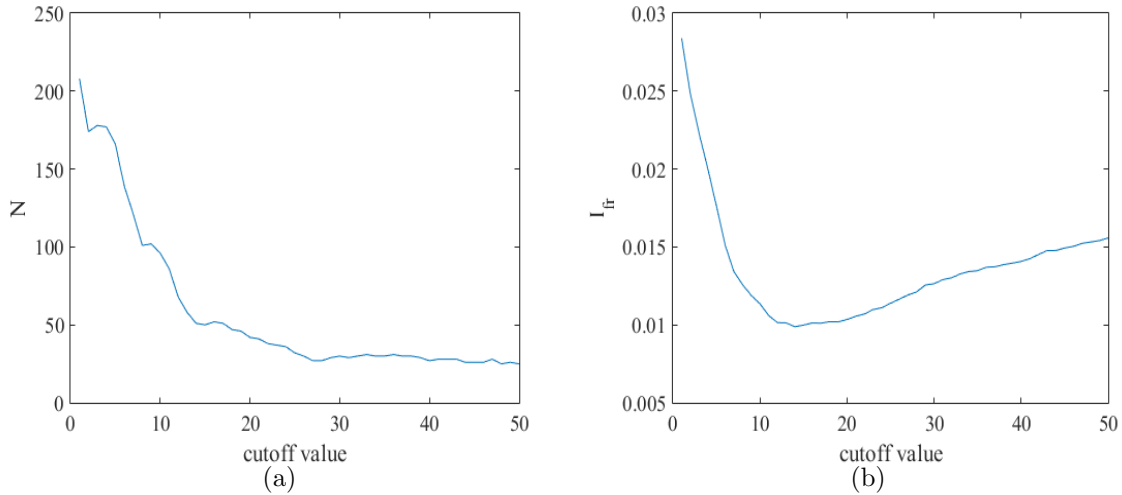


Figure 7.13: (a) The number of objects as a function of the cut-off value for Fig. 7.12a (b)The fragmentation rate as a function of the cut-off value for Fig. 7.12a

The Fig. 7.14 shows the the topological indices as a function of the number of grid nodes. When the number of grid nodes decreases from 1025 to 513, both topological indices change slightly. However, if the number of grid nodes keeps decreasing, the topological indices will change significantly. In conclusion, the traps installed in the region  $\Omega = [-95^\circ\text{W}, -90^\circ\text{W}] \times [40^\circ\text{N}, 45^\circ\text{W}]$  should be greater than  $513 \times 513$  to preserve as much information as possible.

The next step is to compare spatial patterns between three neighbouring region taken from

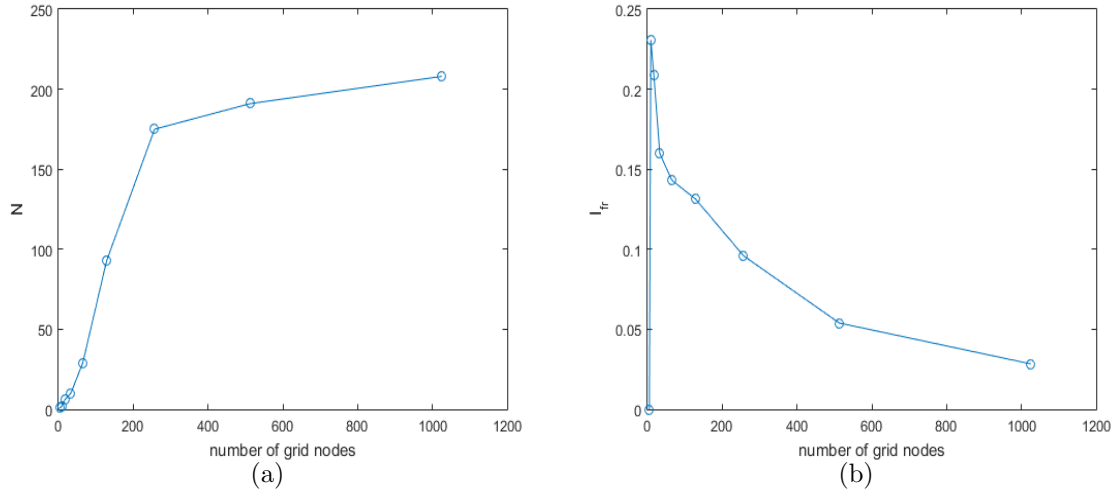


Figure 7.14: (a) The number of objects as a function of the number of grid nodes for Fig. 7.12a (b)The fragmentation rate as a function of the number of grid nodes for Fig. 7.12a

$[-95^{\circ}\text{W}, -90^{\circ}\text{W}] \times [40^{\circ}\text{N}, 45^{\circ}\text{W}]$ ; these are  $\Omega_1 = [-93, -92] \times [44, 45]$ ,  $\Omega_2 = [-92, -91] \times [44, 45]$  and highly infested region  $\Omega_3 = [-91, -90] \times [44, 45]$ . Spatial patterns are given in Fig. 7.15. The population in  $\Omega_1$  is significantly low with a maximum density less than 10, while the maximum density in  $\Omega_2$  is 488 and that in  $\Omega_3$  is 783. Then we calculate the number of objects and fragmentation rate for them. Those indices are  $N_1 = 42$ ,  $fr_1 = 0.1064$ ,  $N_2 = 35$ ,  $fr_1 = 0.0393$ ,  $N_3 = 1$ ,  $fr_3 = 0.0003$ .

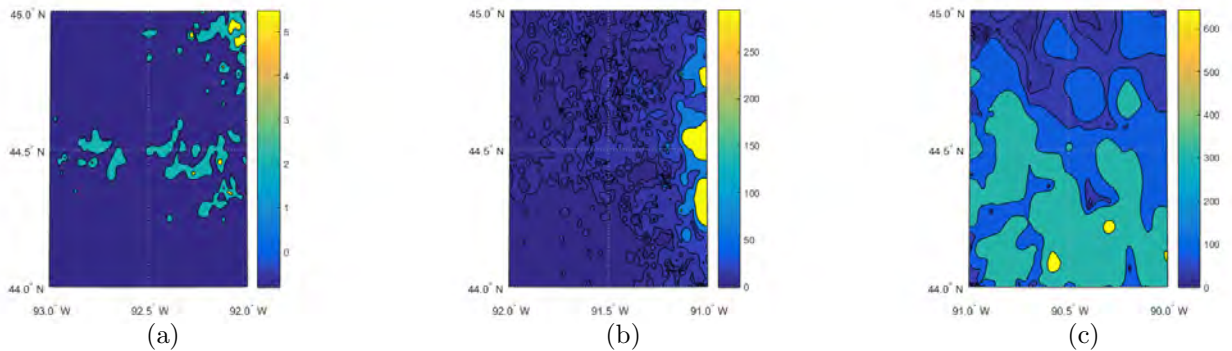


Figure 7.15: interpolated density distribution of gypsy moth in region (a)  $\Omega_1 = [-93, -92] \times [44, 45]$ ; (b)  $\Omega_2 = [-92, -91] \times [44, 45]$  and (c)  $\Omega_3 = [-91, -90] \times [44, 45]$

Our study of spatial patterns has been based on results of a mathematical model which

is capable of producing a great variety of spatial density distributions depending on the model parameters. Basic topological characteristics of spatial pattern such as the number of objects, the density of objects, the degree of aggregation (as given by the Morisita index), and the fragmentation rate have been employed to analyse spatial distributions arising in the model. We have checked whether the spatial pattern type can be recognised correctly and two spatial patterns can be compared to each other by using the topological indices above. It has been shown in the chapter that close values of the model parameters generate spatial patterns with similar topological indices when simple topology of continuous front is considered. The conclusion, however, is different when we deal with complex topological structures such as continuous front density distributions with patches behind the front or patchy distributions that do not form a continuous propagation front. In particular, transition from continuous front spatial patterns to patchy spatial distributions as model parameters vary does not result in any distinct and predictable change in the density of objects, the Morisita index, and the fragmentation rate, although the number of objects does identify correctly the topological type of spatial pattern.

In our attempt to explain variations in topological indices observed when close values of the system parameters are considered we have investigated spatio-temporal dynamics of the invasive species to see whether those fluctuations will disappear as time progresses. Our study of temporal evolution of spatial patterns resulted in the conclusion that, along with the topological indices, transition time  $t^*$  required for ‘topological stabilisation’ of spatial pattern must be taken into account. If spatial pattern is considered at time  $t < t^*$  its topological properties may significantly change with time, i.e. continuous front spatial pattern may transform itself into patchy pattern and vice versa. Thus, spatial patterns can only be identified after transition time  $t^*$  and it appears that the transition time can be much greater for patchy invasion regimes

than for continuous front regimes. Moreover, it has been found in the chapter that for spatio-temporal dynamics resulting in formation of patchy patterns the transition time can also be much greater than time  $t^D$  required for the invasive species to spread over some spatial domain  $D$  where invasive species is monitored. The latter case is true for most patchy regimes considered in the chapter and those regimes have been labelled as ‘topologically unstable’ in domain  $D$ . By the definition of topologically unstable patterns their topological type cannot not be determined in domain  $D$  where we want to control the spread of invasive species.

Our study reveals that propagation of patchy density distributions present the most difficult case of the spatio-temporal dynamics of invasive species when topological properties of spatial distribution have to be determined. It has been argued in the chapter that patchy spatial patterns obtained for closed values of system parameters may have very different topological structure even after the transition time and we therefore cannot rely upon the topological indices if two patchy spatial distributions are compared to each other.

Finally, we would like to emphasise here that, according to the results in Section 7.5 and 7.6, registration of separate patches at any time  $t < t^*$  cannot serve as a reliable indicator of patchy invasion as separate patches can be transformed into a continuous front after the transition time. Thus, another conclusion of our study is that timely recognition of patchy invasion regimes may be a challenging issue that may require allocation of additional monitoring resource and therefore determination of reliable ‘early signs’ of patchiness should consist another topic of future work.

## CHAPTER 8

# CONCLUSION AND DISCUSSION

The spread of invasive species has been in the focus of ecological research in recent decades. Propagation of a population front was a paradigm of biological invasion for several decades [14, 32, 87]. More recently, however, there has been a growing understanding that the invading species can proliferate into space by creating isolated patches or colonies but without forming any continuous population front [67, 86]. Patchy invasion has been observed in several field studies [8, 40, 42, 46] and in a variety of different mathematical models [37, 50, 86] including PDEs [24, 53] and, recently, integral-difference equations [77].

Patchy invasion can be attributed to several factors, one of which is that it can occur in particular landscapes such as small islands [98]. Moreover, it can also occur as a result of the influence of predators [50, 67], pathogens [24, 68, 69], or multi-species interactions [8, 54].

In this thesis, we have studied two models of biological invasion. The first one is an integro-difference system simulating the predator-prey system influenced by the strong Allee effect, both prey and predator are stage-structured species. The second one is a reaction diffusion model simulating predator-prey system influenced by the strong Allee effect, both species have overlapping generations in this model.

In Chapters 3,4,5 and 6 we have studied the stage-structured model simulating the predator-prey system influenced by the strong Allee effect. This model is formed of two integro-difference equations that can take into account the effect of both short-distance and long-distance dispersal. We have observed patchy spatial distribution in the model with short distance and long distance dispersal to confirm preliminary conclusions made in [76, 77]. Furthermore, we have investigated how formation of patchy patterns depend on the parameter range used in the problem. In addition, we have investigated several topological characteristics of the spatial pattern that can be employed to distinguish between continuous and discontinuous spatial distributions.

From the discussion in Chapter 4, we know the propagation rates for spatial patterns obtained for the parameters from domain for parameters from domains that correspond to stable temporal dynamics in the non-spatial problem are constants (cf. domain 1 and 2 in Fig. 2.5). In this case, the location of the population front of a spatial pattern is predictable. For those parameters where we have unstable equilibrium in the non-spatial problem (cf. domain 3 in Fig. 2.5), pattern formation in the spatial problem is complicated and difficult to predict, and the propagation rate is not constant. Therefore, a comprehensive recognition of the spatial patterns that arise in biological invasion is important for the management and control of invasive species. Once a spatial pattern has been recognised, a continuous front distribution only requires addressing the area behind the population front to eradicate the invasive species. Meanwhile, having a collection of separate patches in a spatial domain requires having a more carefully designed control protocol from the practitioner.

Based on the simulation results in Chapter 5, we found that the spatial distribution is sensitive to the choice of problem parameters. Our results show that patchy spatial distribu-

tions and concave-front spatial distributions occur on the edge of extinction, yet concave-front distributions occur within a broader parameter range. We have also investigated the case of asymmetric initial conditions to confirm that it still results to formation of various (i.e., patchy and continuous front) spatial patterns yet patchy patterns correspond to different choice of problem parameters. In this chapter, we developed some topological characteristics to assist with the classification of the spatial patterns and reveal the properties of a spatial pattern. These characteristics include the number of objects, the fragmentation rate, the density of objects and the Morisita Index. The number of objects can help to distinguish whether a spatial pattern has a continuous front. We have demonstrated that, some simulation results may have very similar spatial patterns, yet some of them should be classified as patchy distributions while the others are continuous front distributions. We have shown in our work that the number of objects is the only reliable topological index to distinguish between these two types of distribution. The remaining characteristics, that is the fragmentation rate, the density of objects and the Morisita index, do not show any significant difference between patchy distribution and continuous-front distribution.

In chapter 6, we simulated the data collection routine in the field study of biological invasion. A practitioner might neglect the patches with low densities. In this case, we vary the cut-off values in the simulation results to investigate the changes. On the other hand, a practitioner may collect data on a very coarse grid, which implies some smaller patches will be neglected. We have investigated how topology of spatial patterns changes when we change the conditions under which information about the spatial pattern is collected. It has been demonstrated in Chapter 6 that patchy spatial patterns are very robust and their topology can still be recognised when a lot of information about the population density is missed. In

particular, the numerical test cases in this thesis have demonstrated that patchy spatial patterns are present until the density values are collected on a very coarse sampling grid (see Fig. 6.8 in Chapter 6). While this result is model specific it gives us some useful insight into the accuracy of measurements required to recognise the type of spatial pattern.

This thesis has mainly focused on the spatial patterns of short-distance dispersal species. While we have briefly investigated spatial patterns arising as a result of long-distance dispersal to confirm that patchy spatial distribution may appear when Cauchy dispersal kernels are considered. While it has been confirmed in the thesis that long distance dispersal may result in patchy spatial patterns the influence of parameters on those patterns is still unclear and future work is required. Whether patchy invasion is more or less likely to occur in long-distance than short-distance dispersal species is a question we need to investigate in the future work.

The second model we studied in chapter 7 is the reaction-diffusion model, this model is proposed by [24] where basic classification of spatial patterns has been done. The model allows for generating spatial distributions that are visually very close to each other, yet some of those distributions are continuous fronts while the others are patchy spatial patterns. The ultimate goal of our study has been to understand whether reliable criteria for classification and comparison can be elaborated for spatial patterns arising in the model. Hence basic topological indices of spatial pattern (the number of objects, the fragmentation rate, etc.) have been analysed for a variety of spatial distributions arising in the model to see if the spatial pattern type can be recognised correctly by using any of the quantities above.

It has been shown in the Chapter 7 that a slight increment in the model parameters results in slight increment in topological indices (i.e. production of spatial patterns with similar topological properties) when topology of continuous front that has no patches behind the front is



considered. The above, however, is not true when we analyse continuous front density distributions that have patchy patterns behind the front and, most of all, spatial distributions consisting of separate patches. In the latter case a slight change in the model parameters results in random fluctuations of topological indices as spatial pattern with very different topology may appear. In our attempt to explain random fluctuations of topological indices observed when close values of the system parameters are considered we have investigated spatio-temporal dynamics of the invasive species to see whether those fluctuations will disappear as time progresses. Our study of temporal evolution of spatial patterns resulted in the conclusion that, along with the topological indices, transition time  $t^*$  required for ‘topological stabilisation’ of spatial pattern must be taken into account. If spatial pattern is considered at time  $t < t^*$  its topological properties may significantly change with time, i.e. continuous front spatial pattern may transform itself into patchy pattern and vice versa. Thus, spatial patterns can only be identified after transition time  $t^*$  and it appears that the transition time can be much greater for patchy invasion regimes than for continuous front regimes. Moreover, it has been found in the thesis that for spatio-temporal dynamics resulting in formation of patchy patterns the transition time can also be much greater than time  $t^D$  required for the invasive species to spread over some spatial domain  $D$  where invasive species is monitored. The latter case is true for most patchy regimes considered in the thesis and those regimes have been labelled as ‘topologically unstable’ in domain  $D$ . By the definition of topologically unstable patterns their topological type cannot be determined in domain  $D$  where we want to control the spread of invasive species.

Chapter 7 also investigated the example of spatial distribution of gypsy moth in the US in the years 2015 and 2016, showing that the dispersal of the gypsy moth in the US is a patchy invasion. In order to slow the spread of the gypsy moth, a pest management strategy called

‘Slow the Spread’ program was developed. We analysed the data collected in a ‘transition zone’ between the infested area and uninfested area to give a suggestion about the minimum number of traps required to resolve a spatial pattern and determine accurately its topological type.

## APPENDIX

### MATLAB CODES

#### FFT method

The codes below solves the problem (3.5)–(3.6) using the fast Fourier transform (FFT).

```
1 function [n] = FFTGaussian(a,b,t)
2
3 n=2049; alphaN=0.1; alphaP=0.125;
4 L=40; h=2*L/(n-1); n_old=zeros(n,n); p_old=zeros(n,n);
5 x=zeros(1,n); y=zeros(1,n); kP=zeros(n,n); kN=zeros(n,n);
6 ff=zeros(2*n-1,2*n-1); gf=zeros(2*n-1,2*n-1);
7 knf=zeros(2*n-1,2*n-1); kpf=zeros(2*n-1,2*n-1);
8
9 for i=1:n
10     x(i)=-L+(i-1)*h;
11     for j=1:n
12         y(j)=-L+(j-1)*h;
13
14         if (x(i)>-1)&&(x(i)<1)&&(y(j)>-1)&&(y(j)<1)
15             n_old(i,j)=(a+sqrt(a^2-4*b))/(2*b);
16
17         end
18         if (x(i)>-0.1)&&(x(i)<0.1)&&(y(j)>-1)&&(y(j)<1)
19             p_old(i,j)=log(a/(b+1));
```

```

20
21     end
22
23
24     kN(i,j)=exp(-(x(i)^2+y(j)^2)/(2*alphaN.^2))/(2*pi*alphaN.^2);
25     kP(i,j)=exp(-(x(i)^2+y(j)^2)/(2*alphaP.^2))/(2*pi*alphaP.^2);
26
27     end
28 end
29
30     n_old=gpuArray(n_old); p_old=gpuArray(p_old);
31 kN=gpuArray(kN); kP=gpuArray(kP);
32 ff=gpuArray(ff); gf=gpuArray(gf);
33 knf=gpuArray(knf); kpf=gpuArray(kpf);
34
35     for j=1:t
36
37         f=exp(-p_old).*(a*n_old.^2)./(1+b*n_old.^2);
38         g=n_old.*p_old;
39         ff(1:n,1:n)=f; gf(1:n,1:n)=g;
40         knf(1:n,1:n)=kN;
41         kpf(1:n,1:n)=kP;
42         z1=ifft2(fft2(ff).*fft2(knf))*h*h;
43         z2=ifft2(fft2(gf).*fft2(kpf))*h*h;
44         z1=real(z1); z2=real(z2);
45         n_old(513:1537,513:1537)=z1(1537:2561,1537:2561);
46         p_old(513:1537,513:1537)=z2(1537:2561,1537:2561);
47
48     end
49
50 n=real(n_old);

```

# Finite difference method

The codes below solves the partial differential equations (7.5)-(7.6) with finite difference method.

```
1 function [u] = FDM(tmax,beta,gamma,m)
2
3 dt=0.01; d=1; L=600; h=1;
4 N=L/h+1;
5 % initial conditions
6 u0=zeros(N,N);
7 v0=zeros(N,N);
8 x=linspace(0,L,N);
9 y=linspace(0,L,N);
10 for i=1:N
11     for j=1:N
12         if (x(i)>295)&&(x(i)<305)&&(y(j)>295)&&(y(j)<305)
13             v0(i,j)=0.5;
14         end
15         if (x(i)>290)&&(x(i)<310)&&(y(j)>290)&&(y(j)<310)
16             u0(i,j)=1-v0(i,j);
17         end
18     end
19 end
20
21 % boundary conditions
22 u=zeros(N,N); v=zeros(N,N);
23
24 % explicit method
25 u_old=u0; v_old=v0;
26 u_old=gpuArray(u_old);
27 v_old=gpuArray(v_old);
28 u=gpuArray(u);
29 v=gpuArray(v);
30 for t=0:dt:tmax-dt
```

```

31
32         F1=d*(u_old(3:N,2:N-1)-4*u_old(2:N-1,2:N-1)+u_old(1:N-2,2:N-1)+
u_old(2:N-1,3:N)+u_old(2:N-1,1:N-2))/(h^2)+gamma*u_old(2:N-1,2:N-1).*(
u_old(2:N-1,2:N-1)-beta*ones(N-2,N-2)).*(ones(N-2,N-2)-u_old(2:N-1,2:N-1)
)-u_old(2:N-1,2:N-1).*v_old(2:N-1,2:N-1);
33
34         u(2:N-1,2:N-1)=u_old(2:N-1,2:N-1)+dt*F1;
35
36         F2=d*(v_old(3:N,2:N-1)-4*v_old(2:N-1,2:N-1)+v_old(1:N-2,2:N-1)+
v_old(2:N-1,3:N)+v_old(2:N-1,1:N-2))/(h^2)+u_old(2:N-1,2:N-1).*v_old(2:N
-1,2:N-1)-m*v_old(2:N-1,2:N-1);
37
38         v(2:N-1,2:N-1)=v_old(2:N-1,2:N-1)+dt*F2;
39
40         u(1,:)=u(2,:);
41         u(N,:)=u(N-1,:);
42         u(:,1)=u(:,2);
43         u(:,N)=u(:,N-1);
44
45         v(1,:)=v(2,:);
46         v(N,:)=v(N-1,:);
47         v(:,1)=v(:,2);
48         v(:,N)=v(:,N-1);
49
50         u_old=u;
51         v_old=v;
52
53     end

```

## Number of objects

The codes below count the number of objects in a binary image. Remark: the objects behind the population front are neglected.

```
1 function [N]=objects6(BM)
2 [B,L,N]=bwboundaries(BM,4,'noholes');
3 n=length(B);
4 count=0;
5
6 for i=1:length(B)
7     value=0;
8     for j=1:length(B)
9         if i==j
10            break;
11        else
12            B1=B{i}; B2=B{j};
13        end
14
15        x1=B1(:,1)'; y1=B1(:,2)';
16        x2=B2(:,1)'; y2=B2(:,2)';
17        in = inpolygon(x1,y1,x2,y2);
18        value=value+sum(in);
19    end
20    if value==0
21        count=count+1;
22    end
23 end
24
25 N=count;
```

## LIST OF REFERENCES

- [1] Allee, W. C., & Bowen, E. S. (1932) Studies in animal aggregations: mass protection against colloidal silver among goldfishes. *Journal of Experimental Zoology*, 61(2), 185-207.
- [2] Allen, L.J.S. (2007) *An introduction to Mathematical Biology*, Pearson Prentice Hall.
- [3] Amaral, M.K., Pellico Netto, S., Lingnau, C., Figueiredo Filho, A. (2015) Evaluation of the Morisita index for determination of the spatial distribution of species in a fragment of araucaria forest. *Appl. Ecol. Environm. Res.* 13(2):361-372
- [4] Andersen, M. (1991). Properties of some density-dependent integrodifference equation population models. *Math. Biosci.* 104, 135–157.
- [5] Andow, D.A., Kareiva, P.M., Levin, S.A., Okubo, A. (1990) Spread of invading organisms. *Landsc. Ecol.* 4(23), 177-188.
- [6] Atkinson, Kendall E. (1989) *An Introduction to Numerical Analysis*. J. Wiley.
- [7] Bengfort M, Malchow H, Hilker FM. (2016) The Fokker–Planck law of diffusion and pattern formation in heterogeneous environments. *J Math Biol* 73:683-704.
- [8] M.B. Davis, R.R. Calcote, S. Sugita & H. Takahara (1998) Patchy invasion and the origin of a Hemlock-Hardwoods forest mosaic. *Ecology* 79: 2641-2659.
- [9] Dennis, B. (1989) Allee effects: population growth, critical density, and the chance of extinction. *Natural Resources Modeling*, 3:481–53
- [10] Dwyer, G. (1992). On the spatial spread of insect pathogens: theory and experiment. *Ecology*, 73(2), 479-494.
- [11] Editorial: Japanese beetle ravages. *Reading Eagle* (July 22), 26 (1923)



- [12] Ellis, J.R., Petrovskaya, N.B., & Petrovskii, S.V. (2019) Effect of density-dependent individual movement on emerging spatial population distribution: Brownian motion vs Levy flights. *Journal of Theoretical Biology*, 464:159–178
- [13] Fasham M (1978) The statistical and mathematical analysis of plankton patchiness. *Oceanogr Mar Biol Ann Rev* 16:43-79.
- [14] Fisher, R.A. (1937) The wave of advance of advantageous genes. *Ann. Eugen.* 7, 355-369.
- [15] Garnier, G., Roques, L., & Hamel, F. (2012) Success rate of a biological invasion in terms of the spatial distribution of the founding population. *Bull. Math. Biol.*, 74:453-473
- [16] Grimm, V. (1994) Mathematical models and understanding in ecology. *Ecol. Model.*, 75/76:641–651
- [17] Grünbaum D. (2012) The logic of ecological patchiness. *Interface Focus* 2:150-155.
- [18] Harary, F. & Harborth, H. (1976) Extremal animals. *Journal of Combinatorics, Information and System Sciences* 1:1–8
- [19] Hargis, C.D., Bissonette, J.A., & David, J.L. (1998) The behavior of landscape metrics commonly used in the study of habitat fragmentation. *Landscape Ecology*, 13:167–186
- [20] Hastings A, Harisson S, McCann K. (1997) Unexpected spatial patterns in an insect outbreak match a predator diffusion model. *Proc R Soc Lond B* 264:1837-1840.
- [21] Hayes, J.J., Castillo, O. (2017) A new approach for interpreting the Morisita index of aggregation through quadrat size. *Int. J. Geo-Inf.* 6, 296; doi:10.3390/ijgi6100296
- [22] Hengeveld, R. (1989). *Dynamics of Biological Invasion*. London: Chapman and Hall.
- [23] Hutchinson, G.E. (1953) The concept of pattern in ecology. *Proceedings of the Academy of Natural Sciences of Philadelphia*, 105:1-12
- [24] Jankovic, M., & Petrovskii, S.V. (2013) Gypsy moth invasion in North America: a simulation study of the spatial pattern and the rate of spread. *Ecol. Compl.* 14, 132-144.

- [25] Jankovic M, Petrovskii SV, Banerjee M. (2016) Delay driven spatiotemporal chaos in single species population dynamics models. *Theor Popul Biol* 110:51-62.
- [26] D.M. Johnson, A.M. Liebhold, P.C. Tobin & O.N. Bjørnstad (2006) Allee effects and pulsed invasion by the gypsy moth. *Nature* 444: 361-363.
- [27] Kanevski, M. (2004) *Analysis and Modelling of Spatial Environmental Data*. EPFL Press: Lausanne, Switzerland.
- [28] Kareiva PM. (1990) Population dynamics in spatially complex environments: theory and data. *Philos Trans R Soc Lond B* 330:175-190.
- [29] Keddy, P. A. (2010). *Wetland ecology: principles and conservation*. Cambridge University Press.
- [30] Kierstead, H., & Slobodkin, L. B. (1953). The size of water masses containing plankton blooms. *J. mar. Res*, 12(1), 141-147.
- [31] Klafter, J., & Sokolov, I. M. (2005). Anomalous diffusion spreads its wings. *Physics world*, 18(8), 29.
- [32] Kolmogorov, A.N., Petrovskiy, I.G., Piskunov, N.S. (1937) A study of the diffusion equation with increase in the quantity of matter, and its application to a biological problem. *Bull. Moscow Univ. Math. Ser. A* 1:1-25
- [33] Kot, M., and W.M. Schaffer (1986) Discrete-time growth-dispersal models, *Math. Biosci.* 80, 109-136.
- [34] Kot, M. (2001). *Elements of mathematical ecology*. Cambridge University Press.
- [35] Levin S. 1994 Patchiness in marine and terrestrial systems: from individuals to populations. *Phil. Trans. R. Soc. B* 343, 99-103.
- [36] S.A. Levin, T.M. Powell, and J.H. Steele, eds. (1993), *Patch Dynamics*, Lecture Notes in Biomath. 96, Springer-Verlag, Berlin.
- [37] M.A. Lewis & S. Pacala (2000) Modeling and analysis of stochastic invasion processes. *J. Math. Biol.* 41: 387-429.

- [38] Lewis, M.A., Kareiva, P. (1993) Allee dynamics and the spread of invading organisms. *Theoretical Population Biology* 43:141–158
- [39] Lewis, M.A., Petrovskii, S.V., & Potts, J. (2016) *The Mathematics Behind Biological Invasions*. *Interdisciplinary Applied Mathematics*, Vol. 44. Springer.
- [40] Liebhold, A.M., Halverson, J.A. & Elmes, G.A. (1992) Gypsy moth invasion in North America: a quantitative analysis. *J. Biogeogr.* 19, 513-520.
- [41] Liebhold, A.M., Elmes, G.A., Hawerson, J.A., Quimby, J. (1994) Landscape characterization of forest susceptibility to gypsy moth defoliation. *Forest Science* 40:18–29
- [42] Liebhold A.M. et al. (1996) *Gypsy moth in the United States: An atlas*. US Department of Agriculture, General Technical Report NE-233.
- [43] Liebhold, A.M., Gurevitch, J. (2002) Integrating the statistical analysis of spatial data in ecology. *Ecography* 25:553–557
- [44] Liebhold, A.M., Bascompte, J. (2003) The Allee effect, stochastic dynamics and the eradication of alien species. *Ecology Letters* 6:133–140
- [45] Lutscher, F. & Petrovskii, S.V. (2008) The importance of census times in discrete-time growth-dispersal models. *Journal of Biological Dynamics* 2, 55-63.
- [46] Mack R.N. (1981) Invasion in *Bromus tectorum* L. into western North America: an ecological chronicle. *Agro-Ecosystems* 7, 145-165.
- [47] Mack, R. N., & Erneberg, M. (2002). The United States naturalized flora: largely the product of deliberate introductions. *Annals of the Missouri Botanical Garden*, 176-189.
- [48] Malchow, H., Petrovskii, S.V., & Venturino, E. (2008) *Spatiotemporal Patterns in Ecology and Epidemiology: Theory, Models, Simulations*, Chapman & Hall / CRC Press.
- [49] <https://uk.mathworks.com/help/images/index.html>
- [50] Mistro, D.C., Rodrigues, L.A.D. & Petrovskii, S.V. (2012) Spatiotemporal complexity of biological invasion in a space- and time-discrete predator–prey system with the strong Allee effect. *Ecol. Compl.* 9:16–32

- [51] Mohr, E., & Hollister, M. P. (1933). The Muskrat, *Ondatra zibethica* (Linnaeus), in Europe. *Journal of Mammalogy*, 14(1), 58-63.
- [52] Morisita, M. (1959) Measuring of the dispersion of individuals and analysis of the distributional patterns. *Mem. Fac. Sci. Kyushu Univ. Ser. E* 3:65–80
- [53] Morozov, A.Y., Petrovskii, S.V. & Li, B.L. (2006) Spatiotemporal complexity of patchy invasion in a predator-prey system with the Allee effect. *J. Theor. Biol.* 238:18–35
- [54] Morozov, A., Ruan, S., & Li, B. L. (2008). Patterns of patchy spread in multi-species reaction–diffusion models. *ecological complexity*, 5(4), 313-328.
- [55] Nagumo, J., Arimoto, S., & Yoshizawa, S. (1962). An active pulse transmission line simulating nerve axon. *Proceedings of the IRE*, 50(10), 2061-2070.
- [56] Nayfeh, A.H., Balachandran, B. (1995) *Applied Nonlinear Dynamics*. New York: Wiley.
- [57] Neubert, M. G., Kot, M., & Lewis, M. A. (1995). Dispersal and pattern formation in a discrete-time predator-prey model. *Theoretical Population Biology*, 48(1), 7-43.
- [58] Nowak, R. M., & Walker, E. P. (1999). *Walker’s Mammals of the World* (Vol. 1). JHU press.
- [59] Oppenheim, A. V., Schaffer, R. W., & Buck, J.R. (1999) *Discrete-Time Signal Processing*. Upper Saddle River, NJ: Prentice-Hall.
- [60] I.M. Parker (2004) Mating patterns and rates of biological invasion. *PNAS* 101: 13695–13696.
- [61] Petrou, M. M., & Petrou, C. (2010). *Image processing: the fundamentals*. John Wiley & Sons.
- [62] Petrovskaya, N.B., Petrovskii, S.V. (2010) The coarse-grid problem in ecological monitoring. *Proceedings of the Royal Society A* 466:2933–2953
- [63] Petrovskaya, N.B., Embleton, N.L. (2013) Evaluation of peak functions on ultra-coarse grids. *Proceedings of the Royal Society A* 469: 20120665 doi: 10.1098/rspa.2012.0665

- [64] Petrovskaya, N.B., Petrovskii, S.V. & Zhang, W. (2017) Patchy, not patchy, or how much patchy? Classification of spatial patterns appearing in a model of biological invasion. *Math. Model. Nat. Phenom.*, 12:208-225
- [65] Petrovskaya, N., & Zhang, W. (2020). Accurate Recognition of Spatial Patterns Arising in Spatio-Temporal Dynamics of Invasive Species. In *Current Trends in Dynamical Systems in Biology and Natural Sciences* (pp. 19-41). Springer, Cham.
- [66] Petrovskaya, N., & Zhang, W. (2020). When seeing is not believing: Comparative study of various spatial distributions of invasive species. *Journal of theoretical biology*, 488, 110141.
- [67] S.V. Petrovskii, A.Y. Morozov, & E. Venturino (2002) Allee effect makes possible patchy invasion in a prey-predator system. *Ecol. Lett.* 5: 3450-352.
- [68] S.V. Petrovskii, H. Malchow, F.M.Hilker & E. Venturino (2005) Patterns of patchy spread in deterministic and stochastic models of biological invasion and biological control. *Biological Invasions* 7: 771-793.
- [69] S.V. Petrovskii, & K. McKay (2010) *Biological invasion and biological control: A case study of the gypsy moth spread*. *Aspects of Applied Biology* 104: 37-48.
- [70] Petrovskii, S.V., Bearup, D., Ahmed, D.A., Blackshaw, R. (2012) Estimating insect population density from trap counts. *Ecol. Compl.* 10, 69-82.
- [71] S.V. Petrovskii, N.B. Petrovskaya & D. Bearup (2014) Multiscale approach to pest insect monitoring: random walks, pattern formation, synchronization, and networks. *Physics of Life Reviews* 11: 467-525.
- [72] Petrovskii, S.V. (2016) Pattern, process, scale, and model's sensitivity. *Physics of Life Reviews* 19, 131-134.
- [73] Pimentel, D. (2002). *Biological Invasions: Economic and Environmental Costs of Alien Plant, Animal and Microbe Species*. New York: CRC Press.
- [74] Press, W. H., Teukolsky, S. A., Vetterling, W. T., & Flannery, B. P. (2007). *Numerical recipes 3rd edition: The art of scientific computing*. Cambridge university press.
- [75] Powell, T., 1995. Physical and biological scales of variability in lakes, estuaries and the coastal ocean. In: Powell, T., Steele, J. (Eds.), *Ecological Time Series*. Chapman & Hall, New York, pp. 119-138.

- [76] Rodrigues, L.A.D., Mistro, D.C. & Petrovskii, S.V. (2012) Pattern formation in a space- and time-discrete predator–prey system with a strong Allee effect. *Theor. Ecol.* 5:341-362
- [77] Rodrigues, L.A.D., Mistro, D.C., Petrovskaya, N.B. & Petrovskii, S.V.(2015) Patchy invasion of stage-structured alien species with short-distance and long-distance dispersal. *Bulletin of Mathematical Biology*, 77:1583-1619
- [78] Rosenberg, M. & Anderson, C. (2016) *Spatial Pattern Analysis*. In: *Oxford Bibliographies in Ecology* (ed David Gibson). New York: Oxford University Press
- [79] Sakai, A.K., Allendorf, F.W., Holt, J.S., Lodge, D.M., Molofsky, J., With, K.A., Baughman, S., Cabin, R.J., Cohen, J.E., Ellstrand, N.C., McCauley, D.E., O’Neil, P., Parker, I.M., Thompson, J.N., & Weller, S.G. (2001). The population biology of invasive species. *Ann. Rev. Ecol. Syst.* 32, 305–332.
- [80] Schwalbe, C.P., Disparlure-baited traps for survey and detection. In: Doane, C.C.; McManus, M.L., eds. *The gypsy moth: research toward integrated pest management*. Number 1584. US Department of Agriculture, 1981.
- [81] Segel, L.A., Jackson, J.L., 1972. Dissipative structure: An explanation and an ecological example. *J. Theor. Biol.* 37, 545-559.
- [82] Sharov, A.A., Liebhold, A.M., Roberts, E.A., 1997. Correlation of counts of gypsy 959 moths (Lepidoptera: Lymantriidae) in pheromone traps with landscape characteristics. *Forest Science* 43 (3), 483-490.
- [83] J.A. Sherratt, M.A. Lewis & A.C. Fowler (1995) Ecological chaos in the wake of invasion. *Proc. Natl. Acad. Sci. USA* 92: 2524-2528.
- [84] J.A. Sherratt, B.T. Eagan & M.A. Lewis (1997) Oscillations and chaos behind predator-prey invasion: mathematical artifact or ecological reality? *Phil. Trans. R. Soc. Lond. B* 352: 21-38.
- [85] N. Shigesada & K. Kawasaki (1997) *Biological Invasions: Theory and Practice*. Oxford: Oxford University Press.
- [86] Shigesada, N., Kawasaki, K. & Takeda, Y. (1995) Modeling stratified diffusion in biological invasions. *Am. Nat.* 146(2), 229-251.

- [87] Skellam, J.G. (1951) Random dispersal in theoretical populations. *Biometrika* 38:196-218
- [88] Strogatz, S.H. (2000) *Nonlinear Dynamics and Chaos: With Applications to Physics, Biology, Chemistry and Engineering*. Reading MA: Perseus Books.
- [89] Thomas CFG, Parkinson L, Marshall EJP. (1998) Isolating the components of activity-density for the carabid beetle *Pterostichus lanarius* in farmland. *Oecologia* 116:103-112.
- [90] U.S. Congress, Office of Technology Assessment (1993). *Harmful Non-Indigenous Species in the United States*. OTA-F-565. Washington DC: U.S. Government Printing Office.
- [91] USDA, A. (1998). *Managing the Japanese beetle: a homeowner's handbook*. Program Aid, (1599).
- [92] Viswanathan, G. M., Da Luz, M. G., Raposo, E. P., & Stanley, H. E. (2011). *The physics of foraging: an introduction to random searches and biological encounters*. Cambridge University Press.
- [93] Vitousek, P.M., D'Antonio, C.M., Loope, L.L., & Westbrooks, R. (1996). Biological invasions as global environmental change. *American Scientist* 84, 468–478.
- [94] Volpert, V., Petrovskii, S.V. (2009) Reaction-diffusion waves in biology. *Physics of Life Reviews* 6, 267-310.
- [95] X. Wang, F.G. Blanchet & N. Koper (2014) Measuring habitat fragmentation: An evaluation of landscape pattern metrics. *Methods in Ecology and Evolution* 5, 634-646.
- [96] Williamson, M.H. (1996). *Biological invasions*. London: Chapman & Hall.
- [97] Williamson, M., & Fitter, A. (1996). The varying success of invaders. *Ecology*, 77(6), 1661-1666.
- [98] With, K. A. (2002). The landscape ecology of invasive spread. *Conservation Biology*, 16(5), 1192-1203.